# Open–Ocean Convection in the Labrador and Greenland Seas: Plume Scales and Interannual Variability

Dissertation
zur Erlangung des Doktorgrades
der Mathematisch–Naturwissenschaftlichen Fakultät
der Christian–Albrechts–Universität
zu Kiel

vorgelegt von
Christian Mertens

*Kiel*
*2000*

Referent: . . . . . .
Korreferent: . . . . . .
Tag der mündlichen Prüfung: . . . . . .
Zum Druck genehmigt: Kiel, den . . . . . .

Der Dekan

# ZUSAMMENFASSUNG

In dieser Arbeit wurden Beobachtungen aus den Konvektionsgebieten der Labrador- und der Grönlandsee analysiert. Dabei standen zwei Aspekte besonders im Vordergrund: Zum Einen die zwischenjährliche Variabilität der Konvektionstätigkeit und deren Abhängigkeit von Änderungen der hydrographischen und meteorologischen Bedingungen sowie von der Eisbedeckung. Zum Anderen die räumlichen Skalen und Vertikalgeschwindigkeiten in einzelnen Konvektionszellen (Plumes) im Vergleich zu existierenden Skalierungen aus numerischen und Tankexperimenten. Die Beobachtungen umfassen in der Labradorsee den Zeitraum von 1996 bis 1999, in der Grönlandsee den von 1989 bis 1995. Während dieser Zeit wurde die Entwicklung von Temperatur und Salzgehalt sowie Horizontal- und Vertikalgeschwindingkeiten mit verankerten Geräten erfaßt. Zusätzlich wurden die Meßreihen mit früheren Daten von 1994/95 (Labradorsee) und 1988/89 (Grönlandsee) verglichen.

Die beobachtete Konvektionsaktivität in der Labrador- und Grönlandsee zeigt erhebliche zwischenjährliche Variabilität. Im Beobachtungszeitraum konnte jedoch kein mit dem Nordatlantischen Oszillationsindex (NAO) korreliertes Dipolverhalten in Auftreten und Stärke der Konvektion festgestellt werden. In der zentralen Labradorsee nahm die maximale Konvektionstiefe zwischen 1995 und 1999 von 1800 m auf 600 m ab. Das neugebildete Wasser wurde zunehmend wärmer und salzärmer. In den oberen 2000 m der Wassersäule wurde eine generelle Erwärmung mit einem entsprechenden Wärmefluß von 34 W $m^{-2}$ festgestellt. Verankerungen im Randstrom der Labradorsee zeigten weder in den Vertikalgeschwindigkeitsmessungen noch in der Temperaturentwicklung Anzeichen von winterlicher Konvektion. Die Situation in der Grönlandsee war aufgrund der Wechselwirkung mit Eisbildung komplexer. Konvektion trat nur unregelmäßig und auch nur bis in mittlere Tiefen auf, wobei der Antrieb teilweise rein atmosphärisch, teilweise durch Salzanreicherung aufgrund von Eisbildung bestimmt war.

Die Messungen der Vertikalgeschwindigkeiten wurden auf das Auftreten von Plumes hin untersucht. Die Plumes in der Grönlandsee lagen im Durchmesser zwischen 200 und 600 m, in der Labradorsee wurden 200 bis 1200 m beobachtet. Die abwärtsgerichteten Vertikalgeschwindigkeiten lagen zwischen 3 und 9 cm $s^{-1}$, wobei in der Labradorsee häufiger hohe Werte registriert wurden. Während Perioden von starker Konvektion war es in der Labradorsee möglich, den vertikalen Wärmefluß direkt aus den Messungen zu bestimmen. Die beobachteten Geschwindigkeiten skalieren sich mit dem Oberflächenauftriebsfluß und der Tiefe der durchmischten Schicht. Sie werden nicht von der Erdrotation beeinflußt.

# ABSTRACT

Observations from the Labrador and Greenland Seas, sites known for open ocean convection to occur, are analyzed under two major aspects: the interannual variability of convection and its relation to variability of the hydrographic, meteorological, and ice conditions, and the spatial and velocity scales of individual convective plumes compared to existing scaling arguments derived from numerical and laboratory experiments. The observations were carried out in the Labrador Sea between 1996 and 1999 and in the Greenland Sea between 1989 and 1995. There, moored stations were deployed, measuring the temperature and salinity evolution and the three–dimensional flow field over the winter periods. Further, the measurements are compared to earlier observations from the Labrador Sea in 1994/95 and from the Greenland Sea in 1988/89.

The convection activity observed in the central Labrador and Greenland Seas showed considerable interannual variability throughout the observational period, but no seesaw behavior correlated with the North Atlantic Oscillation index. In the Labrador Sea, the maximum depth of convection decreased from about 1800 m in 1995 to only 600 m in 1999. The water mass properties of the winter mixed layer shifted towards warmer and less saline conditions. A general warming of the upper 2000 m was observed, corresponding to a heat flux of 34 W $m^{-2}$. Observations were also carried out in the Labrador Sea boundary current region to register eventually happening convection, but both the vertical velocity measurements as well as the temperature development showed no evidence of convection activity at the mooring locations. In the Greenland Sea, the situation was more complex because of the interaction with sea ice. Convection occurred irregularly to intermediate depths, either purely driven by the atmosphere or with additional buoyancy forcing by ice formation.

The three–dimensional current measurements were analyzed for individual events of convective plumes. The plumes in the Greenland Sea showed horizontal scales of 200 – 600 m and in the Labrador Sea diameters of 200 – 1200 m were diagnosed. The downward velocities were of 3 – 9 cm $s^{-1}$ with more events of strong downward motion in the Labrador Sea. During periods of intense convection activity in the Labrador Sea, it was possible to directly measure the vertical heat flux. The observed velocity scales were found to be a function of the surface buoyancy flux and the mixed layer depth and not controlled by the Earth's rotation.

CONTENTS

# 1. INTRODUCTION

Two distinct types of deep water formation occur in the world ocean. The first is the descending of dense water along a continental slope which is found around the Arctic and Antarctic shelf regions, but the Denmark Strait and Iceland–Scotland Overflows also belong to this category. The second process is open–ocean convection occasionally reaching large depths at a few known sites which are the central Greenland and Labrador Seas, the western Mediterranean, and the Weddell gyre.

The open–ocean convection sites are characterized by a cyclonic circulation, tending to preserve the weak stratification in the interior by inclining the isopycnals towards the surface (doming). A schematic representation of the large scale circulation in the Greenland and Labrador Seas is given in Figure 1.1. Also shown is the topography of a near surface isopycnal, expressing the doming. In the Labrador Sea the cyclonic gyre is formed by the northwestward flowing West Greenland Current and the southeastward flowing Labrador Current. The gyre in the Greenland Sea consists of the West Spitsbergen Current to the east, the East Greenland Current to the west, and the Jan Mayen Current to the south. During winter, strong buoyancy loss associated with the prevailing meteorological conditions causes vertical overturning of the water column in the convection regions.

The convection process is often divided into three phases, for which the terms *preconditioning*, *violent mixing*, and *sinking and spreading* were coined (MEDOC Group, 1970). The preconditioning phase refers to the autumn and early winter months during which the shallow summer mixed layer is gradually eroded through cooling and evaporation. Once the near–surface layer has been homogenized, additional forcing can overcome the generally small remaining stratification of the deeper layers, triggering the violent mixing phase. During this period of deep mixing, the water column is overturned through convective cells (plumes), distributing the dense surface water in the vertical. Acting in concert, the plumes generate a mixed patch of dense water. With progressing time the horizontal gradient between the dense water in the interior and the less dense water in the surroundings increases, causing baroclinic instabilities to develop at the edge of the homogenized region. This results in a spreading of the dense water and a gradual restratification of the convection region. The vertical and horizontal mixing phases are not necessarily sequential but may occur concurrently.

Associated with the three phases of deep convection is a hierarchy of scales on which the dominant processes during the individual phases occur. The largest scale is that of the convectively

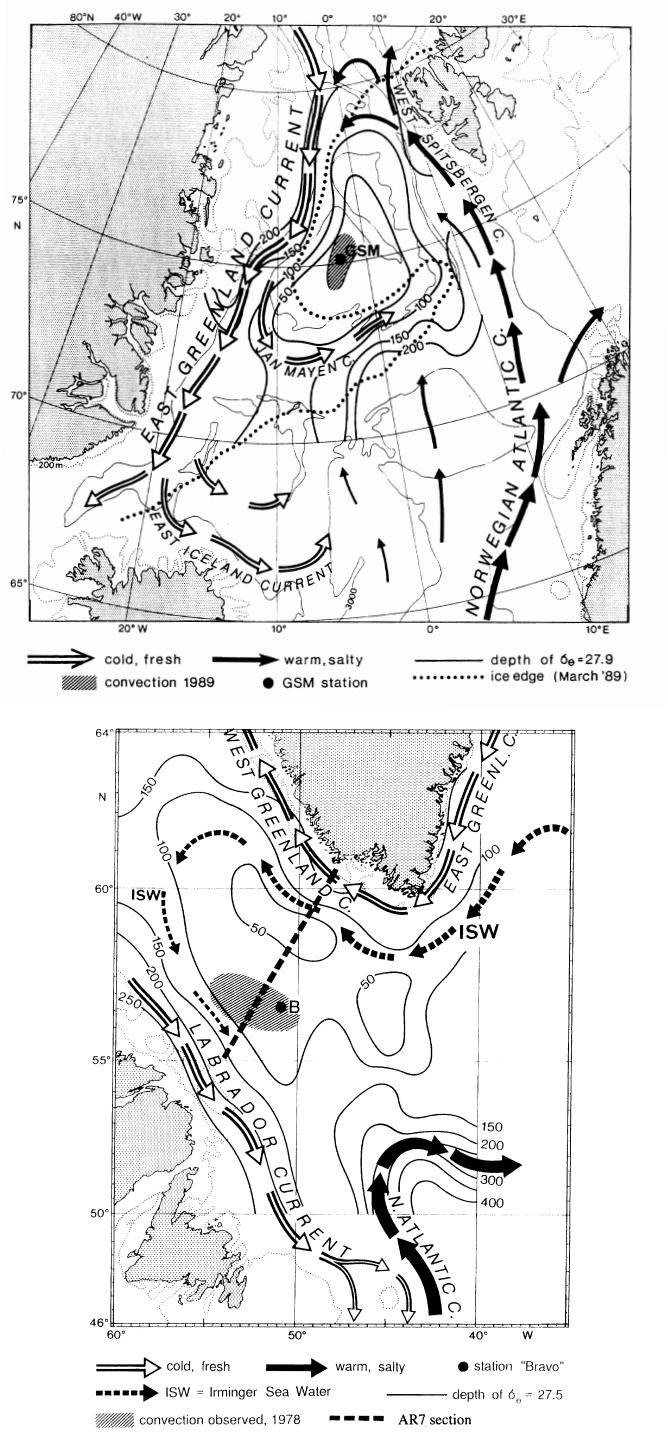


FIG. 1.1: Schematic representation of the large scale circulation in the Greenland Sea (upper panel) and the Labrador Sea (lower panel), depicting the cyclonic circulation of the convection regimes (from Marshall and Schott, 1999). Doming is indicated by the depth of isopycnals $\sigma_\theta = 27.9$ and $\sigma_\theta = 27.5$, respectively. *GSM* is the location of repeated moored stations in the Greenland Sea and *B* is the position of the former Ocean Weather Station *Bravo*.

generated patch of nearly homogeneous water. This scale of 50 – 100 km and larger is set during the preconditioning (Swallow and Caston, 1973). The lateral scale of the individual convective plumes, observed during the violent mixing phase, is less than one kilometer and short bursts of downward motion of 10 cm $s^{-1}$ and more occur (Schott and Leaman, 1991; Schott et al., 1993; Lilly et al., 1999). The third scale is that of the eddies or instabilities associated with the break–up of the mixed patch. Their scale of 5 – 10 km is related to the internal Rossby radius of deformation (Gascard, 1978; Gascard and Clarke, 1983).

The observation of small–scale convective plumes motivated a number of laboratory and numerical experiments regarding their physical properties (e. g. Jones and Marshall, 1993; Maxworthy and Narimousa, 1994; Coates et al., 1995). One of the conclusions from these studies was that the velocity and length scales of plumes could be described through external parameters such as the buoyancy flux at the surface, the mixed layer depth, and the rotation rate. Assuming that the growth of plumes is constrained by the Earth's rotation, two flow regimes were derived which are characterized through different scaling laws. A measure for the importance of rotation is the turbulent Rossby number. For Rossby numbers larger than a critical value the turbulence is three–dimensional, but with decreasing Rossby number the flow field becomes rotationally controlled and quasi–2D vortex structures are formed (Coates and Ivey, 1997). However, it is not clear which of the two regimes is appropriate for oceanic conditions.

The volume of newly formed deep water depends crucially on the physical properties of the convective plumes. The intense downward flow of the plumes is compensated by weak upward motion inbetween, but a net downward volume transport in the interior of the mixed patch may occur. On the large scale, a net downward motion would generate a horizontal circulation around the mixed patch, cyclonic near the surface and anticyclonic at depth, according to vorticity conservation.

Send and Marshall (1995) investigated the integral effect of convective plumes in a non–hydrostatic model and concluded that the mean downward velocity has to be much less than 0.01 cm $s^{-1}$, which would be insignificant for deep water formation rates and not even measurable with present day instrumentation. Klinger et al. (1996) compared plume–resolving model runs with the results of both a slow and an instantaneous convective adjustment scheme. The slow adjustment scheme is equivalent to employing a large vertical diffusion, while instantaneous adjustment corresponds to an infinite diffusivity. They found that a mixing model of convection is adequate to represent gross properties of the plumes seen in the high–resolution model.

In consequence, the role of plumes in the convection process is to efficiently mix the water column instead of funneling water downward. The actual sinking of the newly formed deep water to its neutrally buoyant level has to occur on a longer timescale and is probably associated with geostrophic eddy dynamics (Marshall and Schott, 1999). The implication for the volume of newly formed deep water is that the additional volume transferred to a new density class has to be

considered, instead of the time and area integral of the vertical velocity during the violent mixing phase.

Open–ocean deep convection is not a regular process where every winter a distinct amount of new deep water is formed, but is subject to considerable interannual variability. Such variability has been found at all known convection sites ranging from vigorous convection activity completely overturning the water column to its total absence. Evidence was found that the variability of convection intensity in the Greenland and Labrador Seas is linked to the North Atlantic Oscillation (NAO), a dominant mode of atmospheric variability over the Atlantic sector of the northern hemisphere (Dickson et al., 1996).

Ongoing convection to the ocean bottom has not been observed in the Greenland Sea at present, but is suspected to occur occasionally because of the water mass properties of the Greenland Sea Deep Water (GSDW). The low temperatures and salinities of GSDW compared to the neighbouring deep basins (Aagaard et al., 1985) as well as the high concentrations of anthropogenic tracers (Peterson and Rooth, 1976; Bullister and Weiss, 1983; Smethie, Jr. et al., 1986) suggest an occasional deep mixing of Greenland Sea surface waters. Convection below 2000 m apparently occurred in the central Greenland Sea during the 1960s and early 1970s as temperature measurements show cooling of GSDW during this period and warming during the 1950s and 1980s (Clarke et al., 1990; Meincke et al., 1992). Tracer observations also suggest a reduced GSDW formation during the 1980s (Schlosser et al., 1991).

Interannual variability of deep convection has also been observed in the central Labrador Sea. Between 1964 and 1968 convection to intermediate depths (400 – 1200 m) occurred at ocean weather station (OWS) *Bravo*, while between 1969 and 1971 convection activity ceased and the depth of the winter mixed layer did not exceed 200 m (Lazier, 1980). The shutdown of convection during 1969–71 is often attributed to the freshwater advected through the so called *Great Salinity Anomaly* that passed the Labrador Sea during this time (Dickson et al., 1988), but coincided with mild winters which is probably the primary reason. This is supported by the fact that the freshwater anomaly was still present (and strongest) in the Labrador Sea in late 1971, but exceptionally strong forcing resulted in convection to 1500 m and down–mixing of the freshwater (Lazier, 1980; Dickson et al., 1996).

During the late 1970s Clarke and Gascard (1983) observed convection to depths greater than 2000 m in 1976 and to a depth of 1200 to 1400 m in 1978. Generally, years of intense cooling are accompanied by thickening of the Labrador Sea Water (LSW) layer, which was found in the early 1970s and after 1983 onto the early 1990s (Curry et al., 1998). The deep water formed in the early 1990s was the coldest from all records, and by 1992 an almost homogeneous LSW layer extending below 2300 m was found (Lazier, 1995; Dickson et al., 1996).

The convective history of the Greenland and Labrador Seas led to the conclusion that the winter convection activity at the two sites was in phase but of different sign and in synchrony with the NAO

(Dickson et al., 1996). The cooling of GSDW indicating deep convection activity during the 1960s and the rather weak convection activity in the Labrador Sea corresponded to a period of negative NAO, while the intense convection in the Labrador Sea during the early 1990s was during a phase of positive NAO with no deep convection below 1500 m in the Greenland Sea.

Convection sites are obviously source regions for the water masses found in the deep ocean which form the lower branch of the thermohaline circulation (THC), yet the sensitivity of the THC to the intensity of deep convection is controversially discussed in numerical studies of large–scale circulation variability. A number of coarse resolution, coupled ocean–atmosphere models suggest a relation between the strength of the THC and the variability of the surface conditions in the deep water formation regions.

Delworth et al. (1993) found irregular oscillations of the THC in the North Atlantic with a time scale of about 50 years, driven by density anomalies in the sinking region of their model. Timmermann et al. (1998) discussed a coupled air–sea mode in the northern hemisphere with a period of about 35 years. A strong THC in the North Atlantic resulted in positive sea surface temperature (SST) anomalies, causing a strengthened NAO. The resulting sea surface salinity anomalies in the oceanic sinking regions weaken deep convection and subsequently the THC, leading to a reduced poleward heat transport and the formation of negative SST anomalies.

In contrast, sensitivity studies with a high–resolution, ocean–only model showed very little effect on the meridional overturning rate, even with a complete shutdown of deep convective mixing in the Labrador Sea, but a stronger dependence on changes in the overflow conditions (Böning et al., 1996; Döscher and Redler, 1997). In their study of an idealized three–dimensional model, Marotzke and Scott (1999) even questioned whether deep water formation by convective mixing is a necessary ingredient of a THC.

An extensive simulation with a coupled atmosphere–ocean–ice model (HadCM3) has been carried out by Wood et al. (1999). The improvements include an increased ocean horizontal resolution ($1.25° \times 1.25°$) and inclusion of a convection scheme in regions of dense overflows. They obtained realistic representations of overturning rates, deep water formation and overflows, without the need of unphysical *flux adjustments* (artificial corrections of the air–sea fluxes to keep the model from drifting). In a simulation with increased greenhouse–gas concentrations, the model responded by a collapse of convection and the circulation in the Labrador Sea, while the strength of the overflow appeared insensitive to $CO_2$ changes. Due to the absence of deep water formation in the Labrador Sea, the maximum overturning at 24° N dropped by about 20% in their model.

A large number of studies have been undertaken to improve the understanding of the convective process in the open ocean and its representation in models. These include several field experiments as well as laboratory and numerical modeling efforts (see Marshall and Schott, 1999, for a review). During the past years intense observations of ocean convection were carried out in the Greenland and Labrador Seas, far exceeding previous efforts (GSP Group, 1990; The Lab Sea Group, 1998).

Based on multi–year observations of the mixed layer development and the three–dimensional flow field in the Labrador Sea between 1994 and 1999 and in the Greenland Sea between 1988 and 1995, two major tasks are addressed in this study: First, the interannual variability of convection activity in the respective regions is described and linked to the prevailing boundary conditions. Second, the physics of the convection process itself are analyzed. Theoretical scaling laws derived from numerical and laboratory experiments are tested against the observations.

A description of the measurement setup is given in Chapter 2. Chapter 3 summarizes the general meteorological and ice conditions in the central Greenland and Labrador Seas. Chapter 4 focuses on the seasonal and interannual variability of convection activity. The relative importance of surface forcing, stratification, and sea ice is discussed with regard to the observed depths and water mass properties of the winter mixed layer.

Finally, Chapter 5 gives a closer examination of the violent mixing phase, characterized by enhanced vertical velocity activity. The observed spatial and velocity structure of convective plumes is discussed as well as the vertical heat flux associated with them. The observations are compared to theoretical scaling laws, relating the velocity and length scales of plumes to external parameters. Conclusions are drawn on diffusivities adequate to represent convective plumes as a vertical mixing process.

# 2. OBSERVATIONS

Deep convection in the open ocean takes place during late winter in remote and hostile regions. While shipboard observations during periods of active convection were only sparsely carried out in the past, moored stations with instruments capable to measure the three–dimensional flow field provide an ideal means to aquire detailed information about the physical processes of such events. An overview of the mooring work in the Labrador and Greenland Seas is given in the following sections. For an in–depth compilation of employed instruments, as well as their accuracy and calibration the reader is referred to Appendix A.

## *2.1 Labrador Sea 1994 – 1999*

The formation of LSW through deep convection in the Labrador Sea is one of the key objectives of the research program entitled *Dynamics of Thermohaline Circulation Variability* (SFB 460) initiated at the Institut für Meereskunde Kiel (IfM Kiel) in 1996. The major field activities started in the summer of 1996 concurrently with the *Labrador Sea Deep Convection Experiment* (The Lab Sea Group, 1998). Besides the mooring work, the components of the observational programs were meteorological and air–sea flux measurements, hydrographic surveys, surface drifters, and different types of floats (PALACE floats, profiling RAFOS floats, and 3D Lagrangian floats).

The mooring work focused on three objectives: point measurements of convection, observations in the boundary current region, and monitoring of integral quantities using acoustic tomography. CTD surveys were carried out each summer during the mooring deployment and recovery cruises. The positions of the moored stations are shown in Figure 2.1. Additionally, two winter cruises were carried out with R/V *Knorr*, one in February/March 1997 and one in January/February 1998. The *Labrador Sea Deep Convection Experiment* lasted for a period of two years, ending in the summer of 1998, while the convection observations in the framework of SFB 460 were continued. In general, the moorings were replaced every summer in July/August, and by the time of this writing three periods, up to summer 1999, were completed.

The observation of deep convection in the Labrador Sea at moored stations already started in the summer of 1994 with a single US/Canadian/German (University of Washington/Bedford Institute of Oceanography/IfM Kiel) mooring. The position of this mooring was chosen close to the WOCE AR7W repeat hydrography section (B1226 in Figure 2.1). It is often called *Bravo* mooring, due

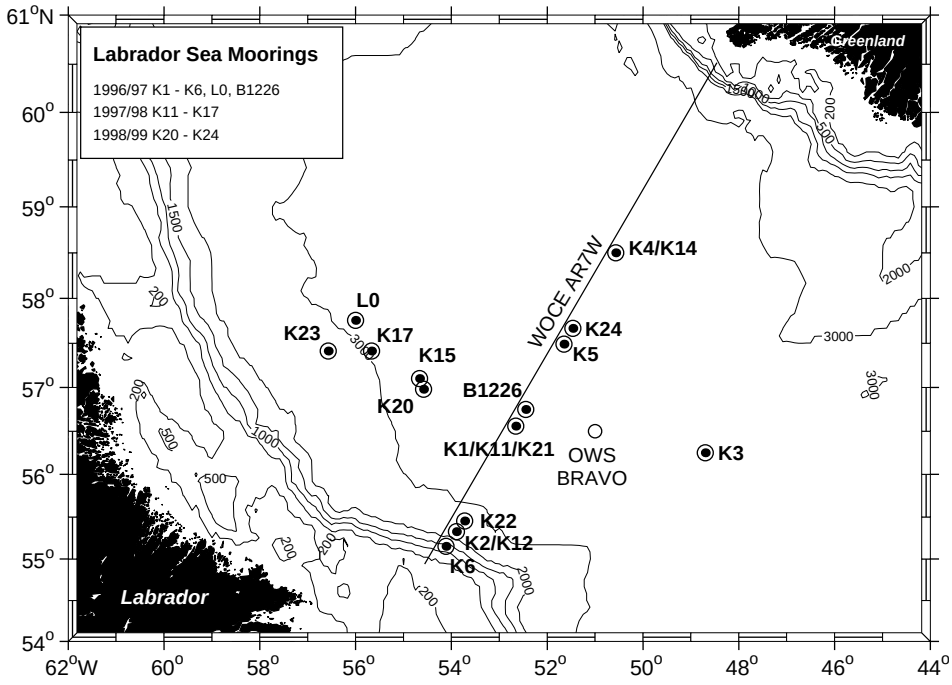


FIG. 2.1: Positions of IfM Kiel moorings in the Labrador Sea during the three observational periods between summer 1996 and summer 1999. Also shown is the position of the former ocean weather station (OWS) *Bravo*. The mooring B1226 (University of Washington/Bedford Institude of Oceanography) is occupied since summer 1994 and serves as a continuation of the *Bravo* time series.

to the proximity of its position to the operation area of the former ocean weather station (OWS) *Bravo*.

OWS *Bravo* was located at 56°30'N, 51°00'W, near the center of the Labrador Sea. Surface meteorological measurements were carried out there from 1946 to 1974, and deep hydrographic profiles from 1964 to 1974 (Lazier, 1980). Mooring B1226 is intended to serve as a continuation of the *Bravo* time series. After the successfull observation of deep convection during the winter of 1995 (Lilly et al., 1999), the following deployment period 1995/96 suffered a major loss of instruments. Only three deep current meters of this mooring were recovered.

The main site of convection observations was at mooring K1 (Figure 2.1), deployed in August 1996 and replaced by the moorings K11 and K21 for the following winter seasons. These convection moorings carried acoustic Doppler current profilers (ADCPs) recording all three velocity components, single point current meters to measure horizontal currents, and temperature/conductivity recorders (SeaCATs and MicroCATs) to follow the development of the stratification (Figure 2.2).

In addition to the convection moorings, a new observational technique was introduced with the moored profiler, designed to climb up and down the mooring wire while aquiring CTD data (Doherty et al., 1999). Newer versions of this instrument include current measurements. For the

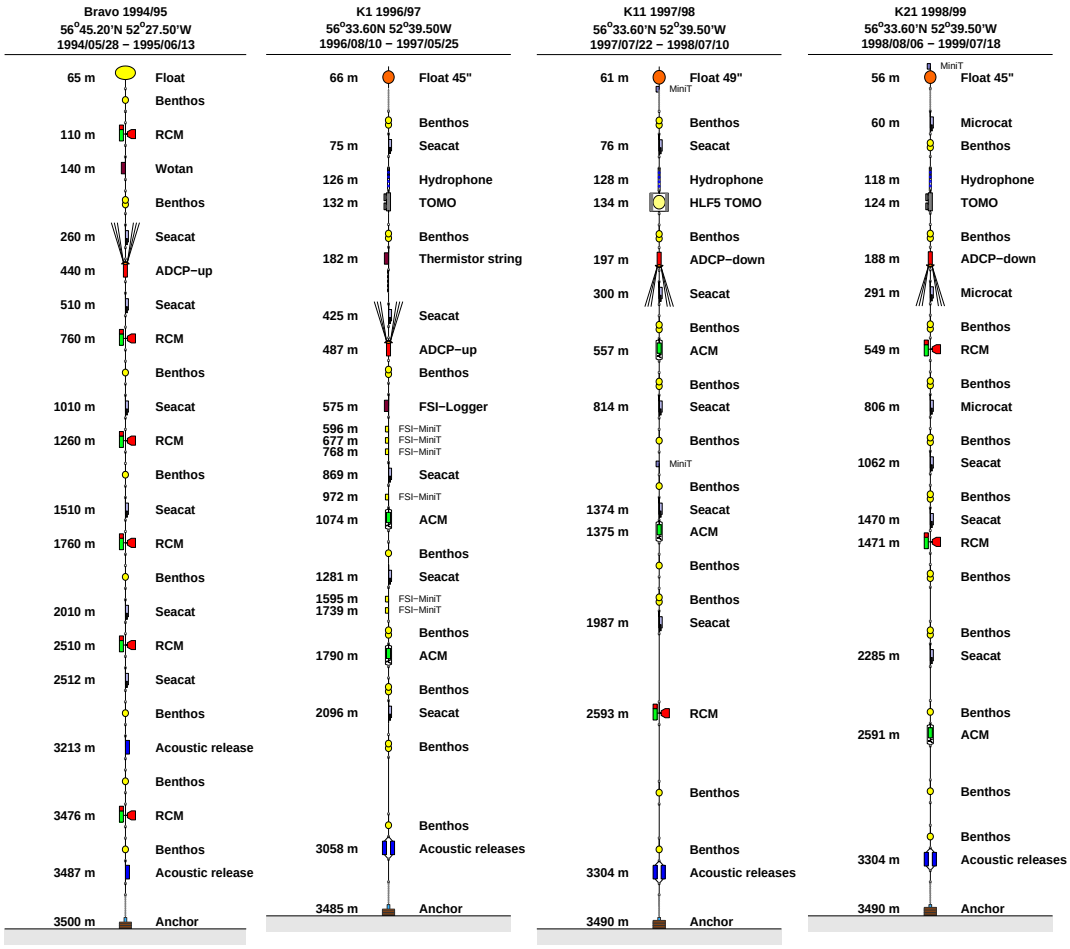


FIG. 2.2: Schematic diagram of the convection moorings in the central Labrador Sea as deployed in the winters of 1994/95 (participation on Univ. Washington/BIO *Bravo* mooring), 1996/97 (K1), 1997/98 (K11), and 1998/99 (K21).

first year (1996/97), the CTD profiler was part of mooring K5, located northeastward of K1. The profiler was intended to cover the upper 2500 m, profiling every other day. Unfortunately, during the deployment the induced electromagnetic force from the instrument sliding on the wire overloaded the instrument's driving motor; it never profiled. This misfunction in the initial design of the instrument was removed by the manufacturer before the next deployments.

For the following years the position of the profiler mooring was shifted northwestward of K1, where the deepest mixed layer was observed during the R/V *Knorr* cruise in March 1997 (moorings K15, and K20). For those two deployments the instrument operated over the whole period, but in both cases only the lower half of the profiling range was covered towards the end of the time series, missing the part of the water column where convection took place. The profiler moorings were additionally equipped with a downward looking ADCP on top.

Observations in the boundary current region were initiated in summer 1996 with mooring K2, located at the 2400 m isobath, and mooring K6, located at the 1200 m isobath. Both moorings were equipped with upward looking ADCPs. Mooring K6 had two additonal current meters of which one returned data, while mooring K2 was fully equipped as a convection mooring to record eventually happening convection in the boundary current region as suggested by Pickart et al. (1997). Mooring K2 was replaced by K12, with similar instrumentation, in summer 1997, while K6 was not continued. For the third deployment period (K22, 1998/99) the position was shifted to the 2800 m isobath, which is at the core of the deep Labrador Current.

The main purpose of the remaining moorings (K3, K4/K14/K24, and L0/K17/K23) was to carry the acoustic tomography instruments. Two of them (K17, K23) had additional ADCPs and a minor number of current meters and SeaCATs. The analysis of the tomography data is ongoing work at the moment and not further considered here.

## *2.2 Greenland Sea 1988 – 1995*

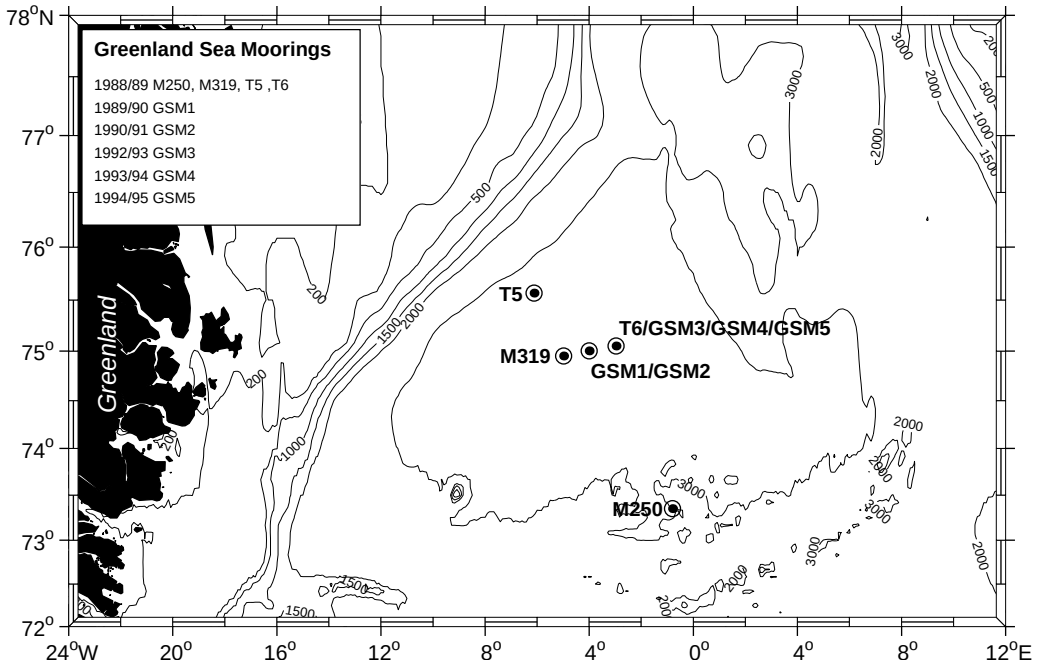


FIG. 2.3: Positions of convection moorings in the Greenland Sea between 1988 and 1995.

The positions of the moorings operated in the Greenland Sea between 1988 and 1995 are shown in Figure 2.3. The observations started within the framework of the Greenland Sea project (GSP), a major investigation of the circulation, general hydrography, and deep water formation, carried out between 1987 and 1993. An intense field operation took place between summer 1988 and

summer 1989 (GSP Group, 1990). The mooring work in the central Greenland Sea consisted of convection moorings (Schott et al., 1993) and an acoustic tomography array (Worcester et al., 1993; Pawlowicz et al., 1995; Morawitz et al., 1996). Two of the convection moorings were part of the tomography array (T5, T6). In summer 1989 the mooring array was replaced by a single station that was subsequently replaced every summer (with gaps) until 1995. A large number of CTD surveys were carried out over this period (e. g. Budéus et al., 1993, 1998; Lherminier et al., 1999).

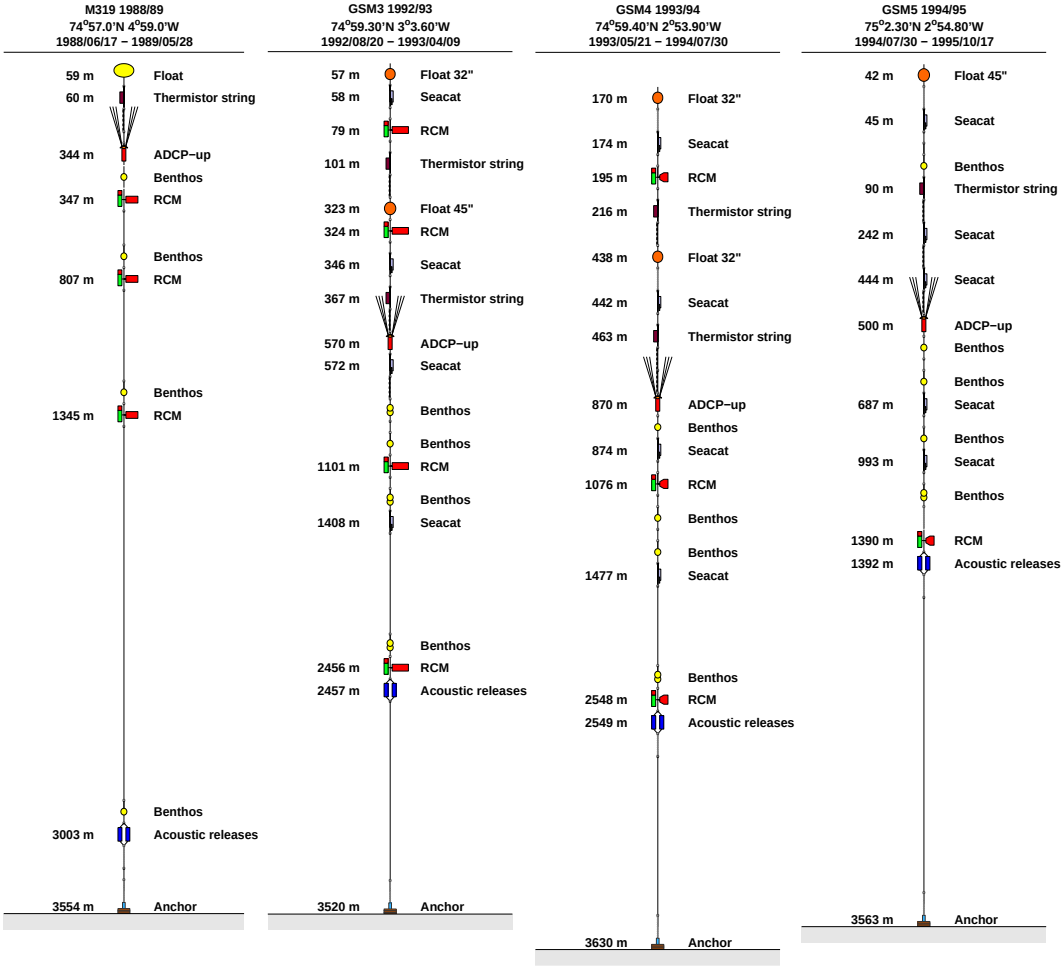


FIG. 2.4: Schematic diagram of the convection moorings in the central Greenland Sea as deployed in the winters of 1988/89 (M319), 1992/93 (GSM3), 1993/94 (GSM4), and 1994/95 (GSM5).

The distribution of instruments in mooring M319 is shown in Figure 2.4. The instrumentation of the southeastward mooring M250 was very similar to that of M319. Mooring T6 had two ADCPs, one looking downward at 200 m and one looking upward at 1400 m. Additionally T6 was equipped with SeaCATs, recording both temperature and conductivity (Roach et al., 1993).

During the first period of continued observations, the winter of 1989/90, a single mooring was deployed at a position inbetween the former M319 and T6 positions (GSM1, not shown in

Figure 2.4). The instrumentation was similar to mooring M319 with one upward looking ADCP at 321 m, a thermistor string, and four current meters. After its recovery it turned out that the ADCP already had stopped working during the deployment. Thus no ADCP data were obtained during the winter of 1989/90.

Mooring GSM1 was replaced by GSM2 in July 1990. It was equipped with two ADCPs at 300 m depth (one upward and one downward looking), two thermistor strings, four current meters, and two SeaCATs. Unfortunately this mooring could never be recovered. All instruments were lost, except for the upward looking ADCP, which was found by the Norwegian Navy in summer 1995. The instrument still contained data from the winter of 1990/91. The loss of the mooring made it impossible to continue the observations into the next winter of 1991/92, due to the lack of instruments.

The observations were resumed in summer 1992 with mooring GSM3, continued over the winter of 1993/94 (GSM4), and were terminated in October 1995 with the recovery of mooring GSM5. All three moorings were located at about 75° N 4° W, and had very similar instrumentations (Figure 2.4). Instrument failures were the thermistor strings in mooring GSM3 and the ADCP in mooring GSM4, which returned no data.

Overall, the nearly continuous time series aquired in the central Greenland Sea between 1988 and 1995 and in the central Labrador Sea between 1994 and 1999, represent one of the most extensive data sets ever gained at convection sites.

# 3. SURFACE BOUNDARY CONDITIONS

The deepening of the oceanic mixed layer, reaching large depths in convection regions, is driven by air–sea fluxes of momentum and mass associated with the prevailing meteorological and sea surface conditions. As density fluctuations appear in the governing equations always multiplied by the gravitational acceleration $g$, it is convenient to introduce an expression for the buoyancy (e. g. Niiler and Kraus, 1977):

$$b = -g\frac{\rho - \rho_0}{\rho_0}. \tag{3.1}$$

Using a linearized equation of state

$$\rho = \rho_0[1 - \alpha(\theta - \theta_0) + \beta(S - S_0)] \tag{3.2}$$

results in

$$b = g[\alpha(\theta - \theta_0) - \beta(S - S_0)], \tag{3.3}$$

where $\alpha$ and $\beta$ are the thermal expansion and haline contraction coefficients, respectively. $\theta$ is the potential temperature, $S$ is the salinity, and $\rho$ is the density. The subscript zero denotes reference values. Values of $\alpha$ and $\beta$ suitable for wintertime conditions in the Greenland and Labrador Seas are given in Table 3.1.

Note that in the Greenland Sea the thermal expansion coefficient is only one third of that in the Labrador Sea. Thus the same heat flux causes a three times higher temperature change (and corresponding buoyancy flux) in the Labrador Sea compared to the Greenland Sea. The haline contraction coefficient is about the same in both regions.

With the temperature and salinity changes caused by air–sea fluxes, the buoyancy flux at the sea surface can be expressed in terms of heat and freshwater fluxes using Equation 3.3:

$$B = g\left[\alpha\frac{Q}{\rho_0 c_p} - \beta S_0(E - P)\right]. \tag{3.4}$$

Here $Q$ is the surface heat flux (negative values mean flux of heat from the ocean to the atmosphere), $E - P$ represents the net freshwater flux (evaporation minus precipitation), and $c_p$ is the specific heat capacity. The surface buoyancy flux $B$ is the fundamental quantity driving convection in the ocean. It is typically of the order of $10^{-7}$ m$^2$ s$^{-3}$ during periods of strong wintertime surface

TABLE 3.1: Values of thermal expansion $\alpha$ and haline contraction $\beta$ coefficients as a function of typical wintertime surface temperature and salinity in the Greenland and Labrador Seas.

| | $\theta_0$ °C | $S_0$ | $\rho_0$ kg m$^{-3}$ | $\alpha$ $\times 10^{-4}$ K$^{-1}$ | $\beta$ $\times 10^{-4}$ |
|---|---|---|---|---|---|
| Greenland Sea | -1.3 | 34.7 | 1027.9 | 0.3 | 7.9 |
| Labrador Sea | 3.2 | 34.7 | 1027.6 | 0.9 | 7.8 |

forcing at the convection sites. Negative values denote a loss of buoyancy of the ocean, causing a density increase in the oceanic mixed layer.

## *3.1 Atmospheric Forcing*

Measurements of meteorological parameters, and in particular air–sea fluxes, are not routinely available for the remote convection regions. A notable exception is the Labrador Sea Deep Convection Experiment where direct measurements of heat fluxes have been obtained during a winter cruise of R/V *Knorr* in February/March 1997 (The Lab Sea Group, 1998). The availability of atmospheric fields such as from the National Centers for Environmental Prediction/National Center for Atmospheric Research (NCEP/NCAR) reanalysis project is therefore of great benefit.

The NCEP/NCAR reanalysis project uses a frozen global data assimilation system to produce a global record of analysed atmospheric fields. The data assimilation system is kept unchanged over the reanalysis period. This eliminates climate jumps that may otherwise be associated with changes in the data assimilation system (Kalnay et al., 1996).

### *3.1.1 Shipboard Observations*

Although it is beyond the scope of this work to validate the NCEP/NCAR reanalysis data, some remarks should be made regarding their reliability compared to other sources. Direct measurements of the turbulent flux of sensible heat were carried out during the R/V *Knorr* cruise 147. Additionally a regional atmospheric circulation model (REMO) was set up for comparison. Measurements of evaporation could not be performed due to the predominant air temperatures being below the freezing point. The surface meteorological data from the *Knorr* cruise were not entered onto the GTS (Global Telecommunication System), and therefore not used in the NCEP/NCAR model analysis.

Comparing the direct estimates of the sensible heat flux to fluxes obtained with bulk parameterizations, the best agreement was found using exchange coefficients as given by Isemer and Hasse (1987), this holds for both the *Knorr* and the REMO data (K. Bumke, personal communication). Figure 3.1 shows a comparison of basic meteorological quantities and flux estimates between the different sources. Two versions of the NCEP/NCAR flux data are shown: One as provided in the

original fields and one computed from basic atmospheric data using the parameterization of Isemer and Hasse (1987). Mean values of the flux estimates are listed in Table 3.2.

Regarding the sensible heat flux the bulk estimates from the *Knorr*, REMO, and NCEP/NCAR meteorological data compare rather well, while the original NCEP/NCAR flux is about 80 W $m^{-2}$ higher in the mean. This would suggest to favor fluxes computed from the basic atmospheric data. On the other hand, the original NCEP/NCAR latent heat flux is in good agreement with the REMO data, while the bulk estimates appear to be too low.

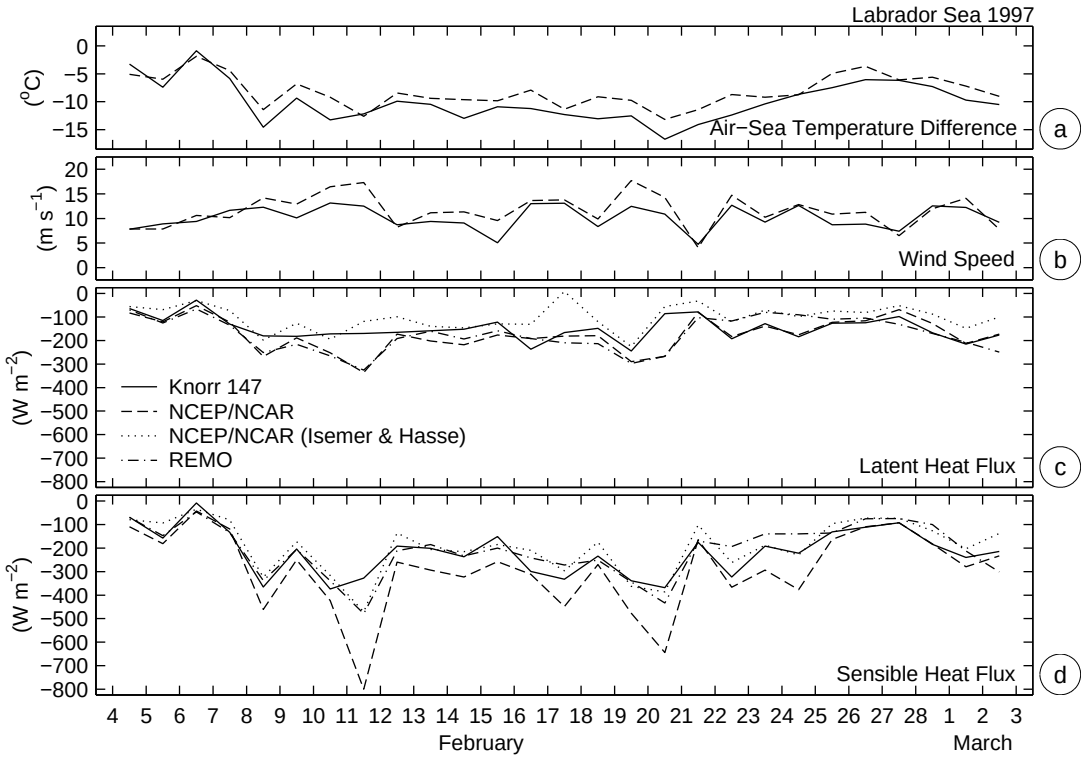


FIG. 3.1: Comparison of daily mean (a) air–sea temperature difference, (b) wind speed, (c) latent heat flux, and (d) sensible heat flux between February 4 and March 3 1997 in the Labrador Sea from R/V *Knorr* cruise 147 shipboard observations (solid), NCEP/NCAR reanalysis data (dashed), and results of the regional model REMO (dashdot). NCEP/NCAR and REMO data were extracted from grid points corresponding to the cruise track of the *Knorr*. Also shown are fluxes recomputed from NCEP/NCAR basic atmospheric data (dotted) using the parameterization of Isemer and Hasse (1987) (REMO and R/V *Knorr* data by courtesy of K. Bumke).

As the bulk parameterization of Isemer and Hasse (1987) results in rather high fluxes compared to exchange coefficients proposed by other authors (e. g. Large and Pond, 1982; Smith, 1989), the even higher values from the original NCEP/NCAR data might be considered unreliable. Renfew et al. (1999) compared the meteorological data obtained during the *Knorr* cruise with model analysis data from the European Centre for Medium Range Weather Forecasting (ECMWF) and reanalysis data from NCEP/NCAR, using a bulk algorithm following Smith (1988) and DeCosmo

TABLE 3.2: Mean values for the period between February 4 and March 3 1997 of latent and sensible heat flux in the Labrador Sea shown in Figure 3.1.

| | Latent Heat Flux ($W\,m^{-2}$) | Sensible Heat Flux ($W\,m^{-2}$) |
|---|---|---|
| Knorr 147 | -148 | -218 |
| NCEP/NCAR | -174 | -294 |
| NCEP/NCAR (Isemer & Hasse) | -102 | -194 |
| REMO | -174 | -210 |

et al. (1996). They found that the overestimation in the NCEP/NCAR flux data is mainly related to discrepancies in the sea surface temperature or the relative humidity data. They concluded that the roughness length formula used in the NCEP/NCAR reanalysis is inappropriate for situations of large air–sea temperature differences and high wind speeds.

On the other hand it is not clear whether the results of the direct measurements could be generalized to other seasons and areas (as the Greenland Sea). It remains an ongoing research which bulk parameterization gives the best estimates of surface heat fluxes under a wide range of atmospheric conditions. Therefore the NCEP/NCAR reanalysis flux data, with the advantage of being a consistent data set over several decades, will be used unmodified in the following. Nevertheless, the absolute flux values have to be used with caution.

### *3.1.2 Climatological Wintertime Conditions*

The availability of the four decades spanning NCEP/NCAR reanalysis data set allows to discuss some climatological aspects of the surface forcing relevant for deep convection, as its temporal and spatial distribution. Figure 3.2 shows the mean total heat flux and 10 m wind for the winter months (December through March) for the period from 1958 to 1999, covered by the NCEP/NCAR reanalysis data.

The mean winter situation is characterized by high pressure over Greenland and low pressure southwest of Iceland and along the Norwegian coast. This situation causes strong northerly winds over the Greenland Sea and northwesterly winds over the Labrador Sea, both bringing cold and dry air of arctic origin over the convection regions. The high wind speeds as well as the large air–sea temperature contrasts associated with these outbreaks result in the large fluxes of sensible and latent heat necessary for deep convection to occur.

In the Labrador Sea the maximum average heat loss, exceeding 350 $W\,m^{-2}$, is located in the northwestern part along the Labrador coast just off the ice edge. The climatological ice edge appears as a sharp gradient in the heat flux distribution. Further downstream into the region of weekest stratification, where deep convection is observed, the heat loss drops to about 250 $W\,m^{-2}$.

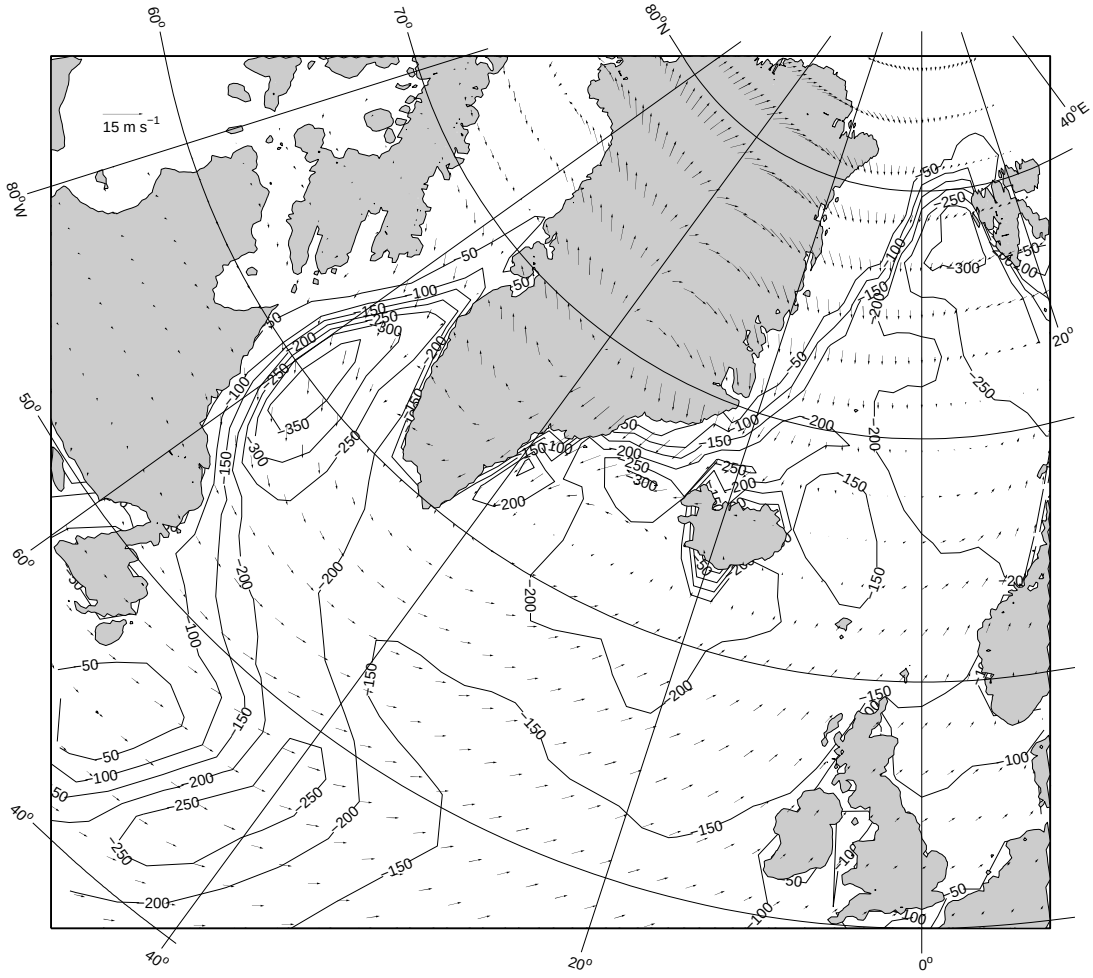


FIG. 3.2: Spatial distribution of mean total surface heat flux and 10–m wind (vectors) from NCEP/NCAR reanalysis over the winter months (December through March) for the period 1958–1999.

In the Greenland Sea, the maximum heat loss of about 300 W m$^{-2}$ is found west of Spitsbergen in the region where the relatively warm water of Atlantic origin carried by the West Spitsbergen Current encounters the cold arctic air. To the center of the Greenland Sea gyre the average heat loss drops to about 230 W m$^{-2}$. As in the Labrador Sea, the climatological ice edge appears in the heat flux distribution as a sharp gradient, originating in the center of the Fram Strait and reaching the Greenland coast south of the Denmark Strait.

The mean seasonal cycle of surface heat fluxes, air temperature, and wind speed from the NCEP/NCAR reanalysis data is shown in Figure 3.3 for a grid point in the convection region of the central Greenland Sea. The cooling season, when the total surface heat flux drops below zero, starts by mid–September and ends by the end of April. The incoming shortwave radiation vanishes during the polar night (October to February). Peak values of heat flux exceeding 300 W m$^{-2}$

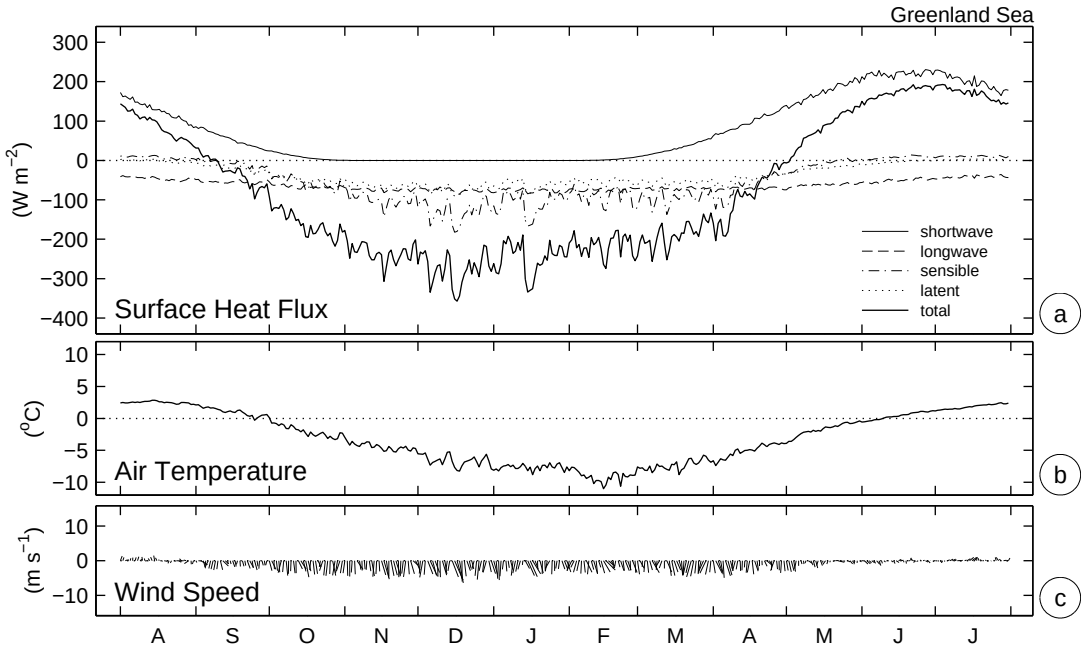


FIG. 3.3: 42–year (1956–1999) mean daily surface heat fluxes (a), air temperature (b), and 10–m wind vectors (c) from NCEP/NCAR reanalysis at 75° 14.1'N, 1° 52.5'W in the convection region of the central Greenland Sea.

even in the long term mean are found during the months of December and January with more than half of it contributed by sensible heat fluxes. In February and March the typical heat loss is of about 200 W $m^{-2}$. The air temperature reaches the freezing point by the end of September, afterwards it drops nearly linearly to its minimum of about -10 °C in mid–February. From then on the temperature rises, again nearly linearly, and reaches the freezing point by the end of May. Northerly winds dominate over the whole cooling season with speeds of about 5 m $s^{-1}$ in the climatological mean. Off the cooling season the mean wind speeds are rather small.

The mean seasonal cycle of surface forcing in the central Labrador Sea (Figure 3.4) is very similar to the Greenland Sea. The cooling season, starting by mid–September and ending by mid–April, is only about two weeks shorter. The typical wintertime heat loss values of 200 – 300 W $m^{-2}$ are the same as in the Greenland Sea, but maximum values occur about one month later, during the months of January and February. The contribution of the latent heat flux to the total heat flux is larger compared to the Greenland Sea, but the sensible component is still dominant. The cycle of the air temperature is of similar shape, but about 7 °C warmer, with minimal temperatures at the beginning of February. Westerly winds dominate over the first winter months, until January where they shift somewhat to more northwesterly directions. Wind speeds of 5 m $s^{-1}$ and more are found during the whole cooling period in the climatological mean values.

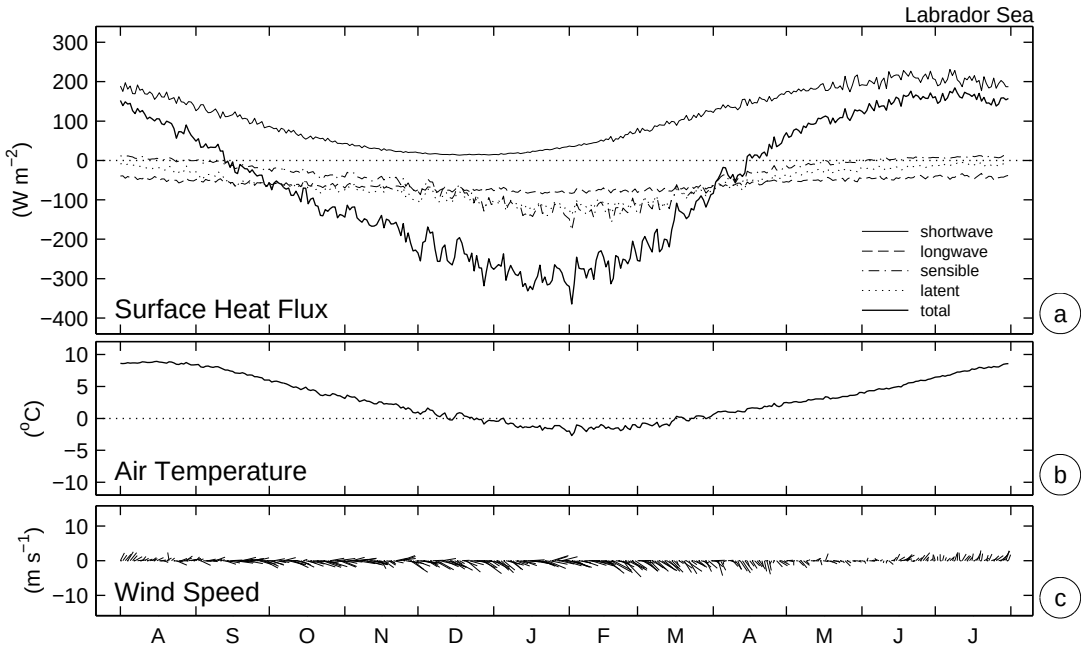


FIG. 3.4: Same as Figure 3.3 at 56° 11.4'N, 50° 37.5'W in the central Labrador Sea.

### *3.1.3 Interannual Variability*

The intensity of deep convection in the Greenland and Labrador Seas shows great interannual and interdecadal variability, and evidence was found that this variability is linked to the North Atlantic Oscillation (NAO) (Dickson et al., 1996). The NAO is the dominant mode of atmospheric variability over the Atlantic sector of the northern hemisphere (e. g. van Loon and Rogers, 1978; Wallace and Gutzler, 1981). The oscillation is present throughout the year but most pronounced during winter (Barnston and Livezey, 1987), where the NAO accounts for more than 36% of the variance of the mean sea level pressure field (Hurrell, 1995). Basically the NAO is a measure of the strength of the westerlies over the North Atlantic between the Icelandic Low and the Azores High.

Rogers (1984) defined an index of the NAO as the difference between normalized mean winter (December through February) pressure anomalies at Akureyri, Iceland, and Ponta Delgada, Azores. The normalization is done by dividing the winter pressure anomalies by the long–term standard deviation of the mean pressure. Hurrell (1995) selected Stykkisholmur, Iceland, and Lisbon, Portugal, in order to extend the record an additional 30 years, and used the months of December through March for the winter means. Jones et al. (1997) extended the further index back to 1823 using early pressure records from Gibraltar and south–west Iceland. Their normalization was performed on a monthly basis, with means and standard deviations produced from the period 1951 to 1980 (Figure 3.5).

During periods of high NAO index the westerly winds over the North Atlantic are stronger

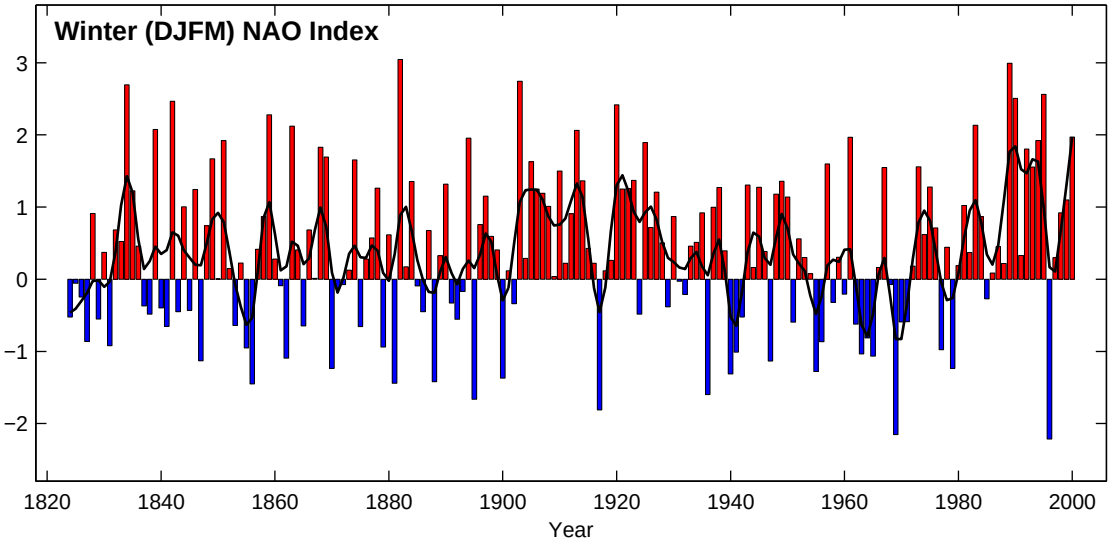


FIG. 3.5: Time series of the winter mean (December through March) of the Jones et al. (1997) NAO index. Beginning in 1823 and updated to the winter of 1999/2000. Normalization was performed on a monthly basis, with means and standard deviations produced from the period 1951 to 1980. The heavy solid line is the 5–year lowpassed time series.

than normal, leading to warmer and wetter than normal conditions over northern Europe and colder than normal conditions over eastern Canada (Hurrell, 1995; Hurrell and van Loon, 1997). Cayan (1992) analyzed the temporal and spatial variability of monthly mean latent and sensible heat fluxes derived from the Comprehensive Ocean–Atmosphere Data Set (COADS) and found large covarying patterns in association with the NAO in the North Atlantic. In the subpolar North Atlantic, the heat fluxes show a positive correlation with the NAO during the winter months. However, the Greenland Sea area was not included in that analysis.

The NAO index shows both high frequency variability from year to year and low frequency variability where anomalous circulation patterns persisted over several winters. The later part of the record shows a trend from low values during the 1960s to high values in the 1990s. The relation between the NAO index and the total winter surface buoyancy loss, derived from the NCEP/NCAR reanalysis data, in the convection regions of the Labrador and Greenland Seas is shown in Figure 3.6.

As to be expected from the analysis of Cayan (1992), there exists a close relation between the NAO and the wintertime surface forcing in the Labrador Sea. The NAO index accounts for about 33% of the variability of the NCEP/NCAR mean winter buoyancy flux. The periods of weak surface forcing during the 1960s and the period of strong surface forcing during the 1970s in general have their counterparts in the NAO index. An exception is the winter of 1971/72, where the highest buoyancy loss is found in the NCEP/NCAR data, but only a moderate NAO situation prevailed.

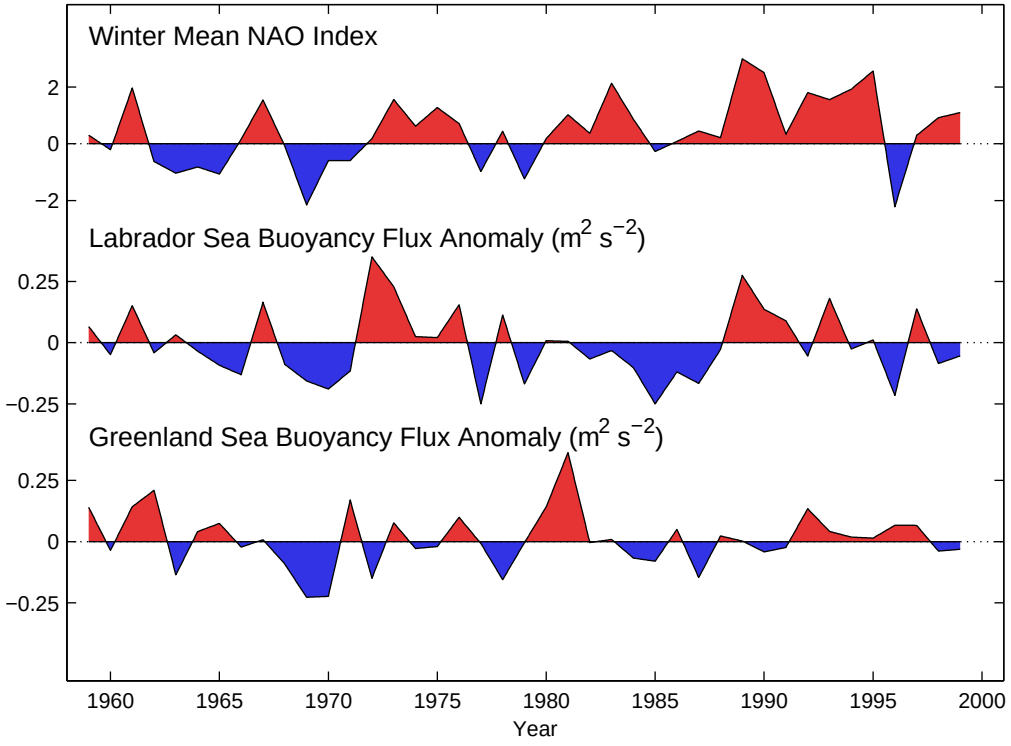


FIG. 3.6: Time series of the winter mean (December – March) NAO index (Jones et al., 1997) and anomalies of the total wintertime buoyancy loss (December – March) derived from NCEP/NCAR reanalysis data in the central Labrador and Greenland Seas from 1959 – 1999.

The period of weak surface forcing during the 1980s does not show a corresponding low NAO, but during the late 1980s and early 1990s strong surface forcing coincides with high values of the NAO index. In the Greenland Sea, however, such a relation between the NAO and the NCEP/NCAR surface flux data during wintertime does not exist.

Considering the winters where the observations at the moored stations were carried out in the convection regions of the Greenland Sea (1989 – 1995) and the Labrador Sea (1995 – 1999), the NAO index was high during the period of observations in the Greenland Sea, except for the winter of 1990/91. The winter of 1994/95, where the observations started in the Labrador Sea, was the last of a sequence of high NAO index winters. In the following winter the index dropped to an unprecedented minimum. During the winter of 1996/97 the index was positive again, and subsequently it increased from winter to winter.

The mean wintertime surface forcing conditions, as they result from the NCEP/NCAR reanalysis data, for the observational winters are summerized in Table 3.3, and time series of the integrated surface buoyancy flux are shown in Figure 3.7 together with the 41–year means and standard deviations. The mean heat fluxes and their variability are very similar in both areas, as well as the freshwater flux and the corresponding haline component of the buoyancy flux. The thermal compo-

nent of the buoyancy flux in the Labrador Sea is more than twice as much as that of the Greenland Sea due to the larger thermal expansion coefficient as discussed above. The interannual variability of the buoyancy flux again is nearly the same in both regions. In the Greenland Sea additional freshwater flux may occur through ice formation or melting. The ice conditions will be discussed in the following section.

TABLE 3.3: Mean surface fluxes as derived from the NCEP/NCAR reanalysis data at single grid points in the central Greenland and Labrador Seas for the winters between 1988/89 and 1998/99. Means are taken for the months of December through March. Also shown are the 41–year winter means and standard deviations.

| | Heat Flux ($W\ m^{-2}$) | Freshwater Flux (mm) | Buoyancy Flux Thermal ($m^2\ s^{-2}$) | Haline ($m^2\ s^{-2}$) | Total ($m^2\ s^{-2}$) |
|---|---|---|---|---|---|
| *Greenland Sea, 75° 14.1' N, 1° 52.5' W* | | | | | |
| 1988/89 | -261 | -124 | -0.17 | -0.03 | -0.20 |
| 1989/90 | -190 | -66 | -0.14 | -0.02 | -0.16 |
| 1990/91 | -219 | -85 | -0.15 | -0.02 | -0.17 |
| 1991/92 | -300 | -162 | -0.29 | -0.04 | -0.34 |
| 1992/93 | -269 | -109 | -0.21 | -0.03 | -0.24 |
| 1993/94 | -218 | -89 | -0.20 | -0.02 | -0.22 |
| 1994/95 | -247 | -60 | -0.20 | -0.02 | -0.21 |
| 41–yr Mean | -231 | -77 | -0.20 | -0.02 | -0.22 |
| 41–yr Std | ± 90 | ± 91 | ±0.11 | ±0.02 | ±0.13 |
| *Labrador Sea, 56° 11.4' N, 50° 37.5' W* | | | | | |
| 1994/95 | -256 | -186 | -0.51 | -0.05 | -0.56 |
| 1995/96 | -173 | 10 | -0.34 | 0.00 | -0.34 |
| 1996/97 | -299 | -92 | -0.66 | -0.02 | -0.69 |
| 1997/98 | -203 | -101 | -0.44 | -0.03 | -0.47 |
| 1998/99 | -212 | -64 | -0.48 | -0.02 | -0.50 |
| 41–yr Mean | -242 | -94 | -0.52 | -0.02 | -0.54 |
| 41–yr Std | ± 60 | ± 85 | ±0.13 | ±0.02 | ±0.14 |

Although the temporal evolution of surface forcing differs from year to year in the central Greenland Sea (Figure 3.7), the total buoyancy loss by the end of winter is always rather similar. During most of the winters of the observational period the surface forcing was slightly below average. The weakest forcing occurred during the winter of 1989/90, and the strongest forcing was during the winter of 1992/93. The winter of 1991/92 shows even higher buoyancy loss (only listed in Table 3.3), but no mooring data are available for this winter. The variability of surface forcing was much larger during the observations in the Labrador Sea than in the Greenland Sea. During the first winter (1994/95) the buoyancy flux followed closely the mean curve between November and

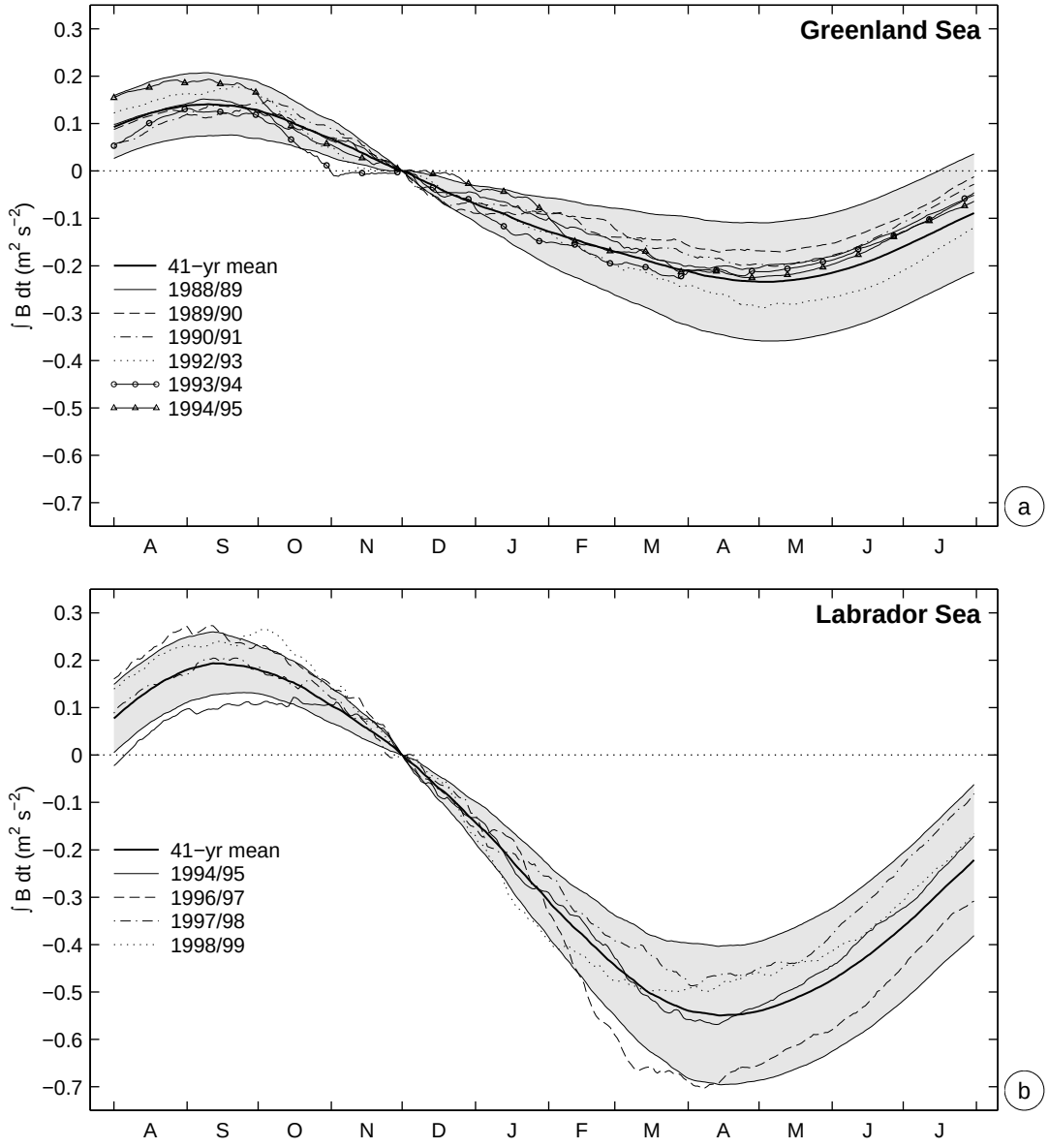


FIG. 3.7: Integrated surface buoyancy flux from NCEP/NCAR reanalysis in the central Greenland (a) and Labrador (b) Seas for the winters between 1988/89 and 1998/99 where observations at moored stations were carried out. The long term mean (1959–1999) is shown as heavy line. The shading denotes the corresponding standard deviation of the integrated buoyancy fluxes. The fluxes were integrated starting from 1 December.

April. The winter of 1996/97 denotes a rather extreme situation, as severe cooling set in by mid–January, leading to a net buoyancy loss well above average. The following winter was rather mild, and in 1998/99 strong surface forcing occurred during January but ceased subsequently, resulting in a total buoyancy loss below average.

## *3.2 Ice Cover*

Sea ice plays an important role for the freshwater budget of the convection regions in the Greenland and Labrador Seas. It provides a buoyancy loss through brine release when new ice is formed, while freshwater input through ice melting has a stabilizing effect. In the Greenland Sea, ice cover may insulate the convection area from the atmosphere, resulting in reduced thermal buoyancy fluxes.

### *Greenland Sea*

In the Greenland Sea a special feature interacts directly with the convection process. A large tongue of sea ice begins to develop in early winter which was known to whalers and sealers as Is Odden or simply Odden; the bight of open water between the marginal ice zone (MIZ) and the Is Odden is being known as Nordbukta (Wadhams, 1986). The Odden grows eastward from the East Greenland ice edge and curves northeastward into the central Greenland Sea. Generally the Is Odden continues to be present until April.

Ice conditions are observed through satellite passive microwave measurements since October 1978. First with the scanning multichannel microwave radiometer (SMMR) on board of the NIMBUS–7 satellite that operated successfully until the summer of 1987. From then on with the special sensor microwave/imager (SSM/I) carried by satellites of the US Defence Meteorological Satellite Program (DMSP). Ice concentrations for the antenna footprint are derived from the satellite measured brightness temperature data (Toudal, 1999).

Figure 3.8 shows snapshots of ice concentration for the years of convection observations at moored stations in the central Greenland Sea. A time series of ice concentration along 75 °N is shown in Figure 3.9. The satellite observations show that the Is Odden–Nordbukta system is subject to large intra- and interannual variability. The edge of the Odden can rapidly expand or contract over hundreds of kilometers within several days. Shuchman et al. (1998) related the Is Odden variability to meteorological data. They found that at air temperatures below -8.7 °C and moderate winds from the northwest significant growth occurs, while the Odden decays during warmer conditions with strong northerly winds.

During November 1988 the MIZ propagated rapidly eastward, and reached the position of the convection mooring M319 by the end of the month. The convection region remained ice covered until mid–January, when the Nordbukta opened. The ice formation in the convection region was a substantial mechanism to remove buoyancy from the water column through brine release during

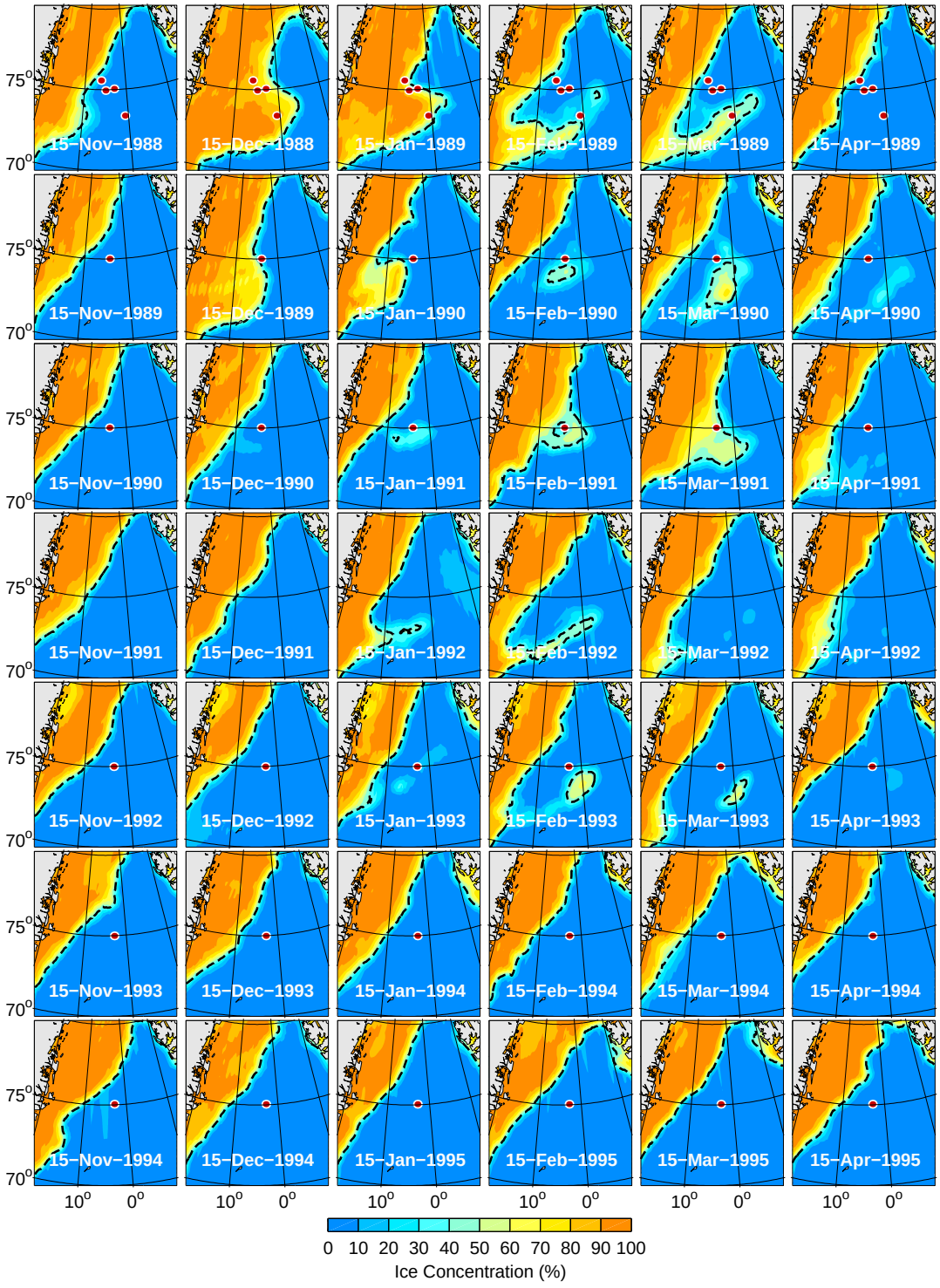


FIG. 3.8: Ice concentration derived from SSM/I data in the Greenland Sea between the winters of 1988/89 and 1994/95. The 40% contour line is marked (dashed) and the mooring positions are shown as dots (data courtesy of L. Toudal).

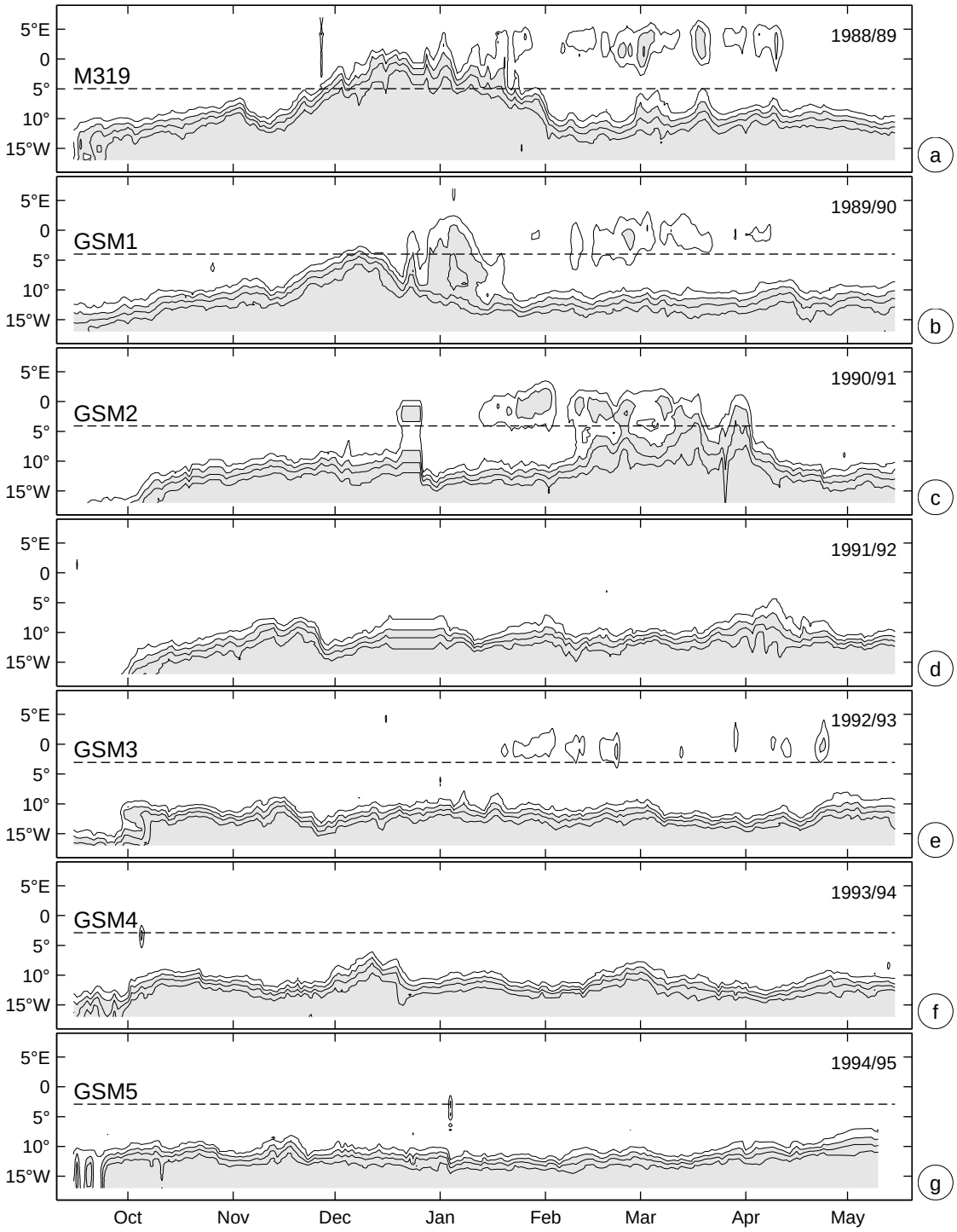


FIG. 3.9: Daily SSM/I ice concentration in the Greenland Sea along 75° N. Positions of moorings are shown as dashed lines. The contour interval is 20% and shading indicates ice concentrations exceeding 40% (data courtesy of L. Toudal).

the preconditioning period of this winter (Roach et al., 1993; Visbeck et al., 1995; Pawlowicz et al., 1995). The following winter (1989/90) began similarly with ice at the mooring (GSM1) location in early December, but a quick retreat of the MIZ occurred afterwards and ice was found only occasionally over the convection mooring for the remaining winter. During the winter of 1990/91 considerable ice cover did not appear at the mooring (GSM2) location before mid–February, and remained there until the end of April.

The winters from 1991/92 to 1994/95 showed substantially less ice compared to the previous twelve years of satellite observations (Toudal, 1999). The mooring locations were almost permanently ice free, except for a short period in February 1993. The development of the 1993 Odden ice tongue was observed through a combination of remote sensing and direct field measurements (Wadhams et al., 1996; Toudal et al., 1999). A comparison of SSM/I retrievals and ERS 1 synthetic aperture radar (SAR) imagery showed good agreement for the position of the 1993 ice edge. The shipboard observations in the area showed that the Odden consisted almost entirely of frazil and pancake ice, rather than older ice types advected eastward from the pack ice. During the winters 1993/94 and 1994/95 no ice was formed in the Greenland Sea. These observations were verified by two airborne campaings, one on 5–6 March 1994 and one on 24 March 1995 (Toudal et al., 1999).

### *Labrador Sea*

The Labrador Sea convection site is generally ice free during the whole winter (Figure 3.10). One exception during the period of convection observations at the moored stations (1994–1999) was the winter of 1995/96 where the satellite observations show ice appearing sporadically in the interior of the Labrador Sea, but no mooring observations are available for this winter. The freezing starts usually in October and, advancing from north to south, a stretch of sea ice is formed along the Labrador and Newfoundland shelf (e. g. Wang et al., 1994). The moorings deployed in the Labrador Sea boundary current region were generally ice covered during the months of February and March. Typical ice concentrations were 40 – 60%. Less ice occurs along the west coast of Greenland due to the presence of the relatively warm West Greenland Current.

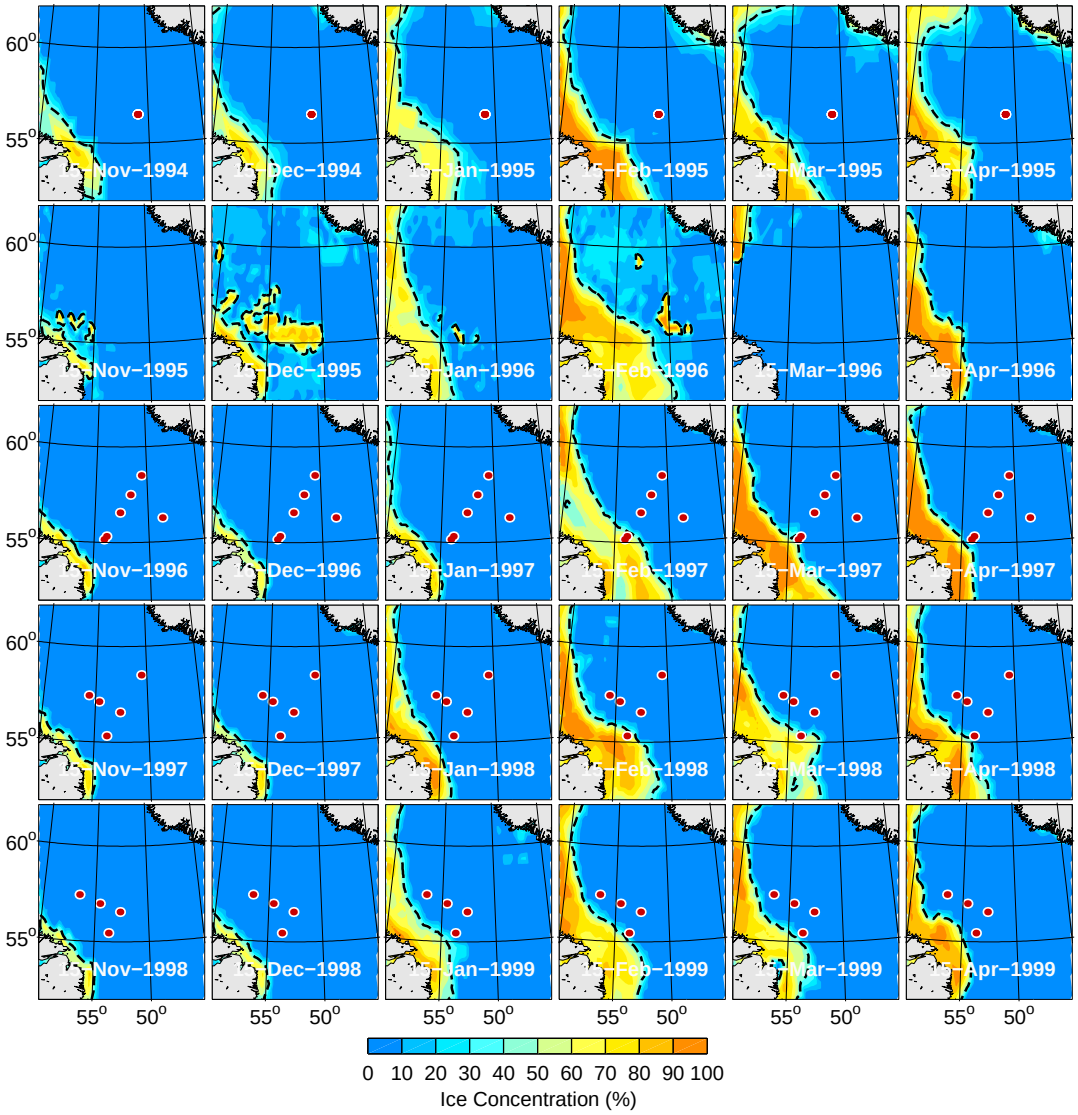


FIG. 3.10: NCEP OMB ice concentration derived from SSM/I data in the Labrador Sea between the winters of 1994/95 and 1998/99. The 40% contour line is marked (dashed) and the mooring positions are shown as dots.

# 4. INTERANNUAL VARIABILITY OF DEEP CONVECTION

Convection activity in the Labrador and Greenland Seas is known to be subject to considerable interannual variability, ranging from deep overturning of the water column to winter mixed layers of only a few hundred meters thickness. In this chapter the observations of the seasonal cycle and the convection variability at the moored stations are discussed, and related to the prevailing hydrographic, meteorological, and sea ice conditions.

## *4.1 Development of Stratification*

### *4.1.1 Labrador Sea*

#### *General Wintertime Evolution*

The temperature evolution observed during the winter of 1994/95 and the three consecutive winters between 1996 and 1999 at the central Labrador Sea moorings is shown in Figure 4.1. Between 1996 and 1999 complementary measurements were obtained at additional moorings, using both traditional point measurements and a moored CTD profiler (Figure 4.2). Although the profiler data are incomplete, especially during the convection periods, they are shown here for the sake of completeness. Further, the profiles obtained at K20 by the end of March indicate that the convection was somewhat deeper than observed at mooring K21. The most prominent features of the temperature time series are the continuously decreasing convection and the general warming of the water column.

First signs of cooling generally appear at the near–surface sensors during January. Subsequently, it takes several weeks of cooling to overcome the density contrast between the surface layer and the warmer but saltier Irminger Sea Water (ISW) below, due to the extremely low salinity of the surface layer. The mixed layer depth does not increase significantly during this period. Convection to large or intermediate depths takes place towards the end of the cooling season during February and March. After the convection, temperature fluctuations increase and the homogeneity quickly disappears, denoting lateral mixing of the convective patch.

The maximum depth of convection reduced considerable over the years of observations. While in 1995 the maximum depth of convection was of about 1800 m, only 1300 m were reached at the mooring location in 1997. The mixed patch of the winter 1997 was mapped during the winter cruise of the *Knorr* in February/March, showing that the mooring was located towards its south-

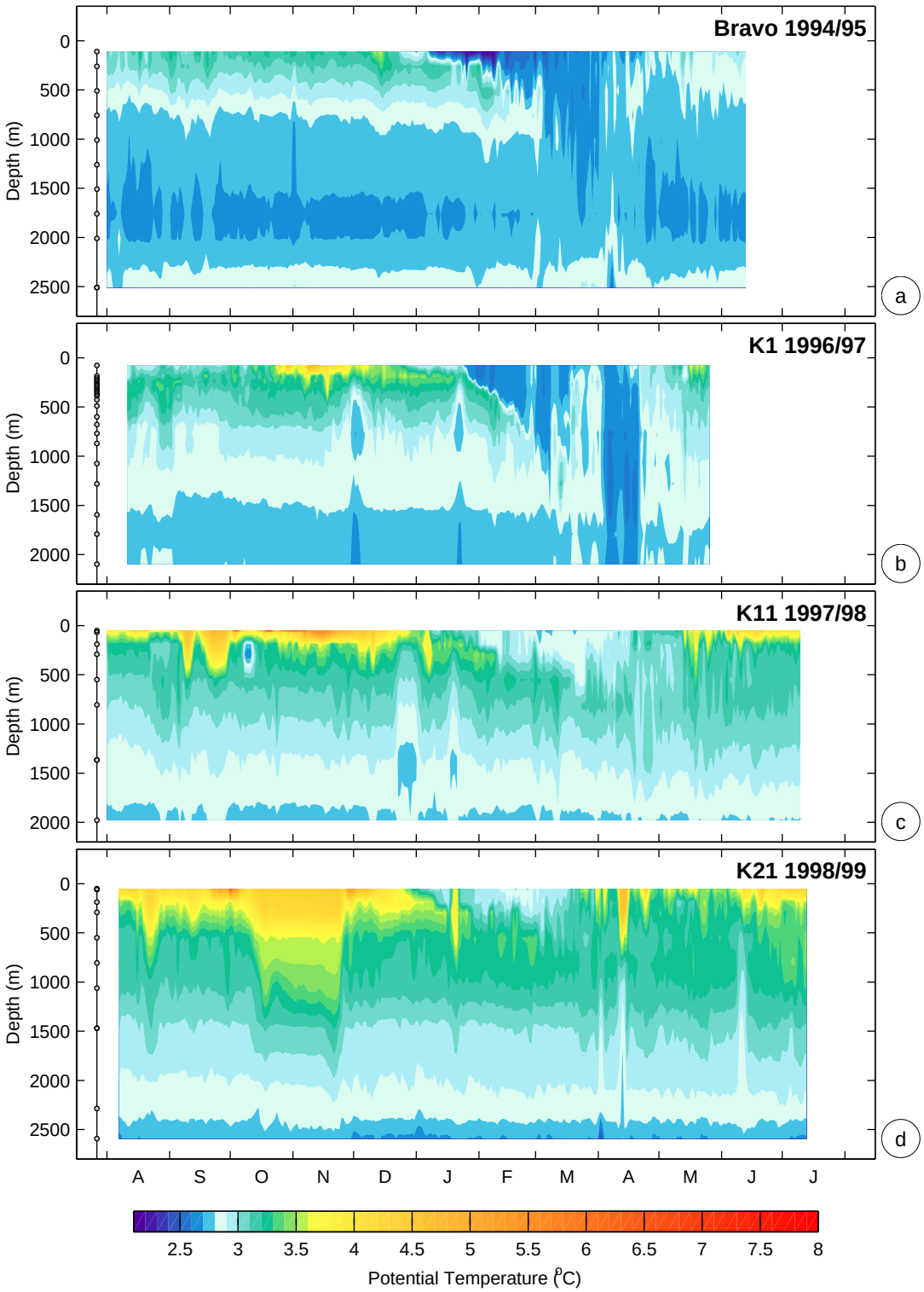


FIG. 4.1: Mean daily potential temperature at the convection moorings in the central Labrador Sea. (a) *Bravo* 1994/95 (courtesy of J. Lazier and P. Rhines.), (b) K1 1996/97, (c) K11 1997/98, and (d) K21 1998/99. Instrument depths are marked as dots on the lefthand side. The contour interval is 0.1 °C.

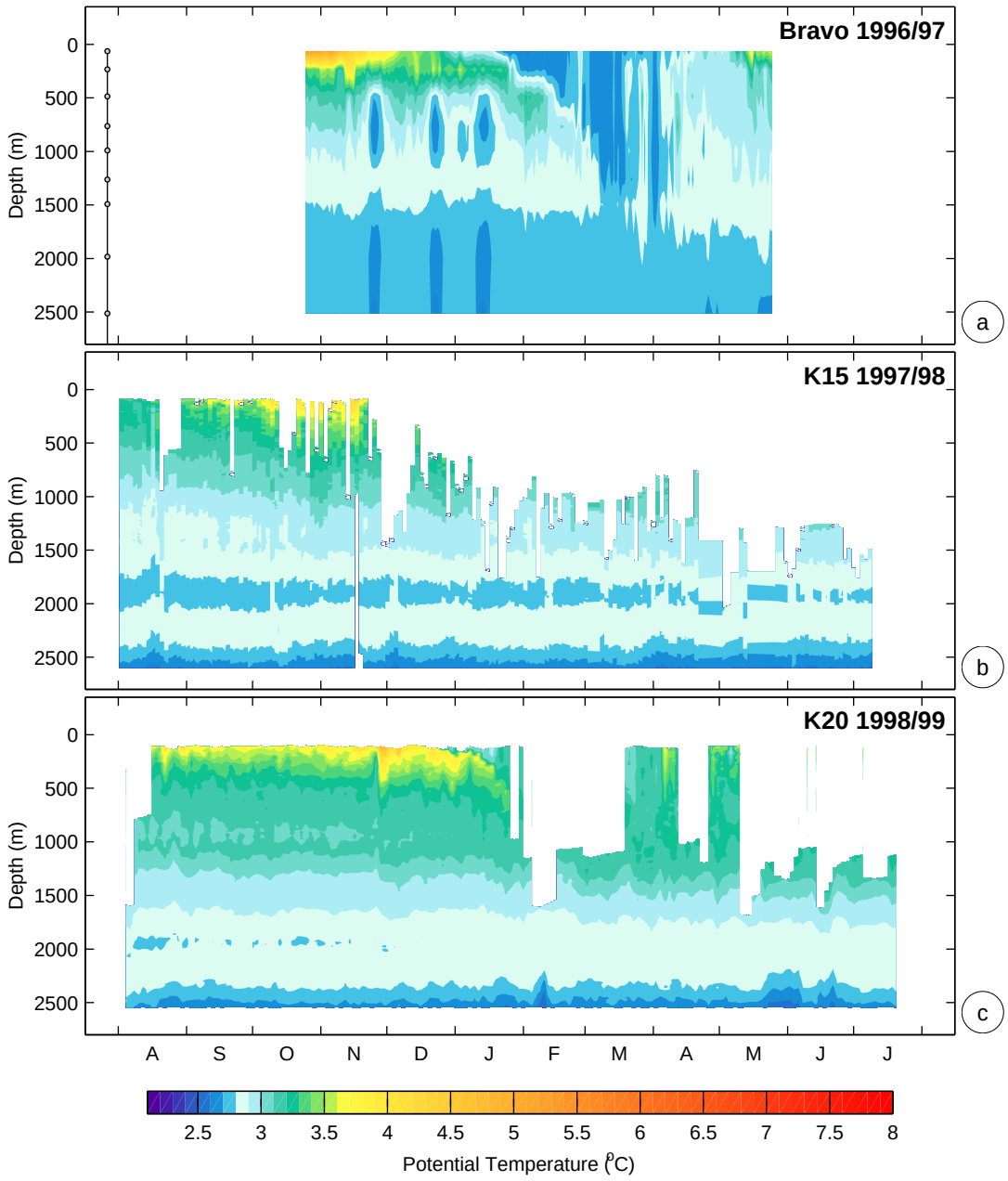


FIG. 4.2: Same as Figure 4.1 at mooring *Bravo* 1996/97 (courtesy of J. Lazier and P. Rhines) (a), and from data of the moored CTD profiler at K15 1997/98 (b) and K20 1998/99 (c).

eastern edge (The Lab Sea Group, 1998). Thus, somewhat deeper mixing might have occurred northwestward of mooring K1. The convection activity decreased further during the winter of 1997/98, where the maximum mixed layer depth was only about 600 m. The shallowest winter mixed layer was found during the winter of 1998/99 at mooring K21. Here, only mixing to about

500 m was observed for a few days. However, some CTD profiles obtained with the moored profiler at mooring K20 by the end of March indicate deeper mixing down to 800 – 900 m depth northwest of K21.

### *Preconvection Cold Events*

During the winter of 1996/97 cold water appeared between 500 and 1000 m at mooring K1 long before deep convection set in. One event occurred at the beginning of December and one during the second half of January. Both events lasted for about 5 days. The minimum temperatures were below 2.7 °C. Since temperatures that low in the LSW layer could only be generated by convective activity, it is feasible that this water was formed in a preceding winter and subsequently trapped in a mesoscale eddy for at least one year. Three similar events occurred at the nearby *Bravo* mooring (distance 25 km), two of them shortly before they appeared at K1. However, a correlation between the events at *Bravo* and K1 was not found, and it is not clear whether the temperature anomalies belong to a single eddy or different ones subsequently passing the moorings.

During the following winter of 1997/98 two cold events were observed at mooring K11, with minimum temperatures below 2.8 °C at about 1500 m depth. One at the end of December and one during mid–January. No similar events were found at the northwestward mooring K15. A strong warming event occurred during October/November 1998 in the upper 1000 m at mooring K21, but again no corresponding signal appeared at the profiler mooring K20. Generally these advective events appear to have minor impacts on the stratification at the mooring sites, instead they are of a more transient nature and the stratification returns mostly to its previous condition after they passed by.

In April 1997, cold water appeared over the whole instrument range at mooring K1. This event was most likely not related to active convection at the mooring location (discussed in more detail in Section 5.1.2). Instead, it possibly belonged to a mesoscale eddy that trapped convectively generated water in its center. No corresponding feature was observed at the nearby *Bravo* mooring.

### *General Hydrography*

During the mooring deployment and recovery cruises, CTD stations were occupied along the western part of the WOCE AR7W line each summer between 1996 and 1999 (Figure 4.3). Due to the mooring work, the sections are composite and not necessarily synoptic. The density surfaces shown in Figure 4.3 separate the water masses of the Labrador Sea.

The deepest water mass is the Denmark Strait Overflow Water (DSOW) below a density of $\sigma_\theta = 27.88$, characterized by the lowest temperatures in the deep water. The salinity maximum between $\sigma_\theta = 27.80 - 27.88$ belongs to Iceland–Scotland Overflow Water (ISOW) that entered the western North Atlantic through the Charlie Gibbs Fracture Zone. Labrador Sea Water (LSW)

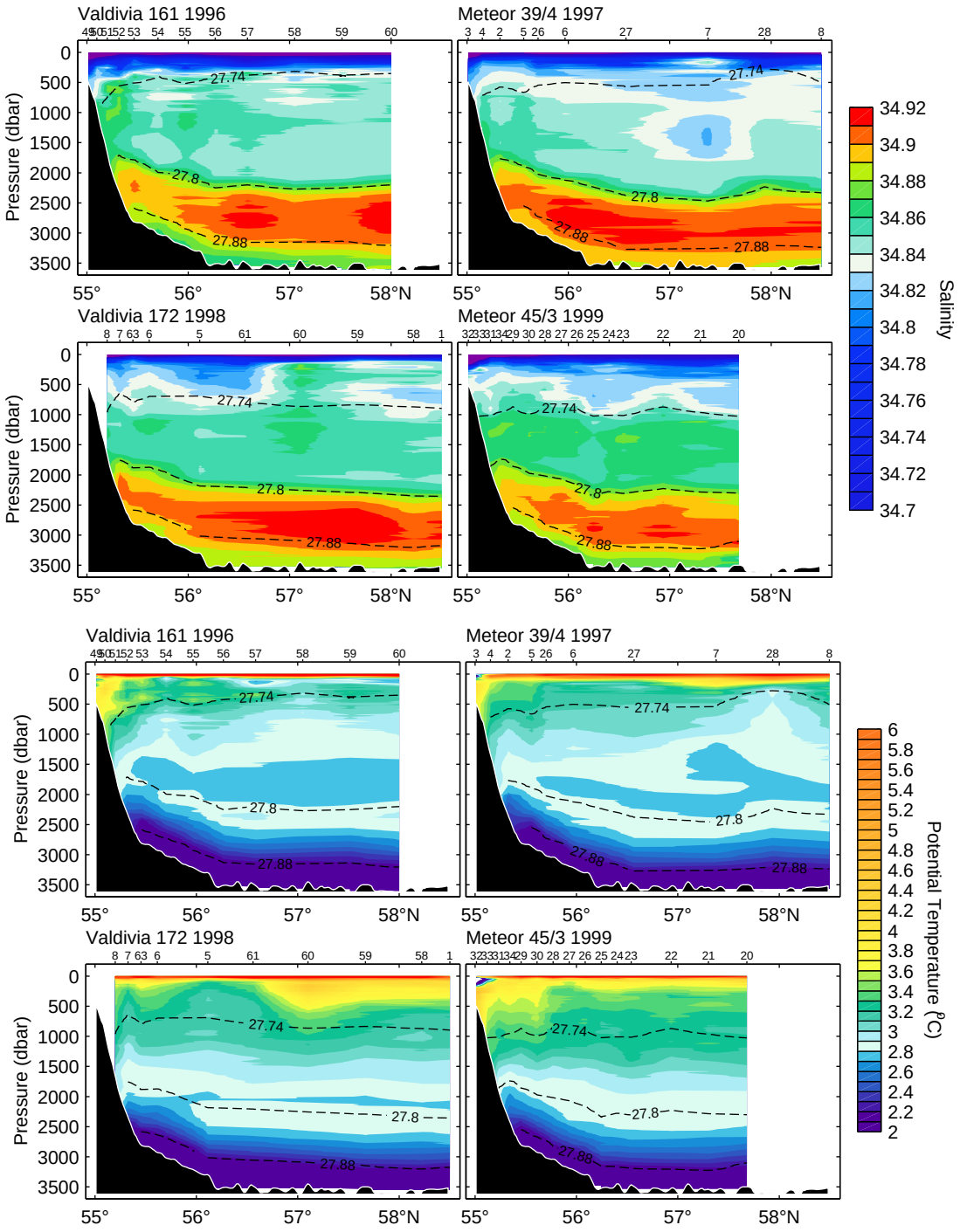


FIG. 4.3: Salinity and temperature sections along the western part of the WOCE AR7W line obtained during consecutive summers cruises between 1996 and 1999. The salinity contour interval is 0.01 and the temperature contour interval is 0.1 °C. Isopycnals denoting water mass boundaries are shown as dashed lines.

occupied the density range $\sigma_\theta = 27.74 - 27.80$ in summer 1996. Over the observational period the $\sigma_\theta = 27.74$ surface deepened from about 500 m in 1996 to about 1000 m in 1999, due to the decreasing convection activity. The characteristics of the water masses below the LSW and the depth of their bounding density surfaces stayed nearly unaffected between the repeated surveys, while the warming of LSW found in the mooring time series occupies the whole section and is accompanied by increasing salinity.

During the summer months the surface layer of the Labrador Sea is characterized by relatively high temperature and low salinity. The warming arises from insolation, while the freshening results from ice melting in the boundary current region and probably precipitation and river runoff. The thickness of this low density layer was typically of about 25 m by the time of the summer surveys, too shallow to be sensed by the moorings. Due to its low density the surface layer contains much of the buoyancy that has to be removed during the preconditioning to expose the weaker stratified waters below to the surface forcing and allow for deep convection.

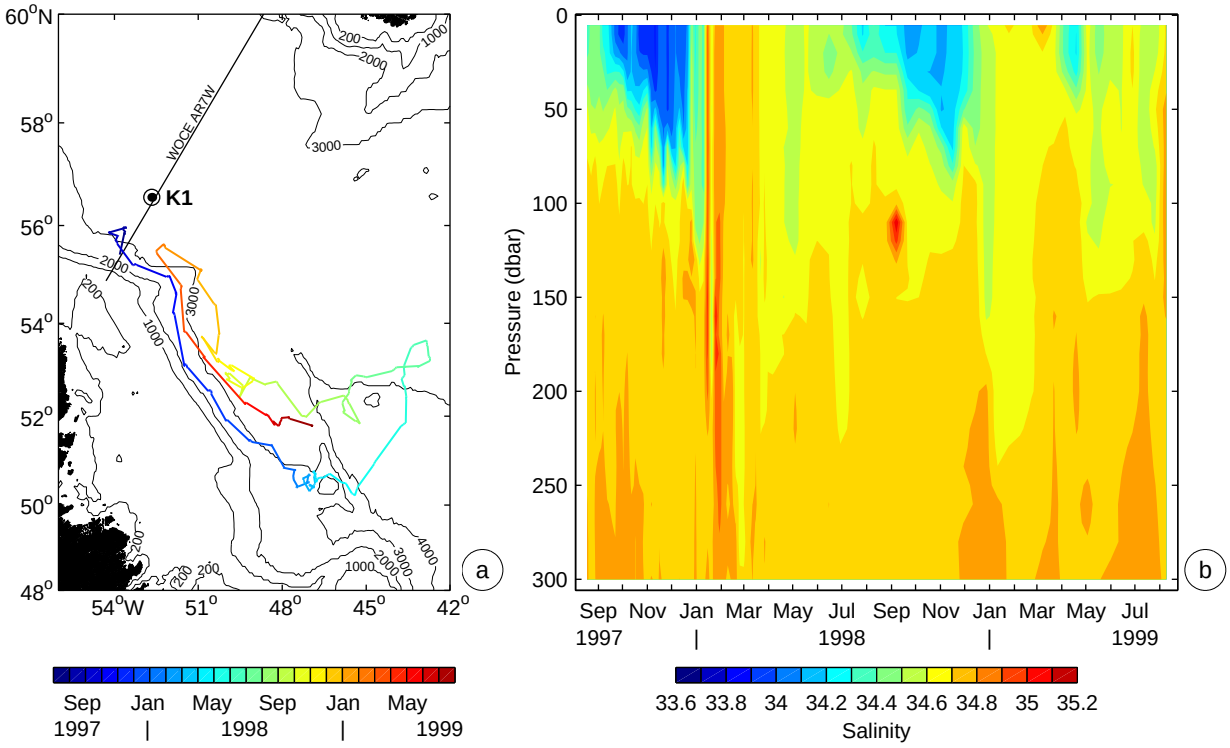


FIG. 4.4: (a) Trajectory with color coded time information and (b) salinity in the upper 300 m versus time since deployment from PALACE float 8637 in the Labrador Sea between July 1997 and August 1999. The trajectory includes surface and deep drifts at 1500 m.

Figure 4.4 shows the trajectory of a profiling float (PALACE) in the Labrador Sea and the corresponding time series of salinity in the upper 300 m. This float was one of 15 deployed in the

boundary current region during spring and summer 1997 (Fischer and Schott, 2000). These floats were ballasted to drift at a depth of 1500 m in the deep Labrador Current. The float shown here followed the boundary current until May 1998 and recirculated offshore from the boundary current into the Labrador Sea. In January 1999 it had nearly returned to its deployment position close to the WOCE AR7W line, where it reentered the boundary current and again drifted southeastward until summer 1999.

Although PALACE float profiles are a mixture in space and time, they illustrate the seasonal cycle of the water column, especially near the surface where mooring time series are difficult to obtain. The salinity time series in Figure 4.4b shows that the surface freshwater layer generally starts to form in April. During most of the summer its depth is limited to the upper 50 m, while its salinity decreases continuously. Deepening of this surface layer starts in September due to increased wind mixing. By the end of December the maximum depth of 80 – 100 m is reached. Afterwards the low salinities disappear, as the surface layer is mixed with the more saline ISW below. In autumn 1997, the salinities were much lower compared to autumn 1998. This is probably due to the fact that the float was closer to the shelf in 1997 than in 1998.

### *Initial Conditions for Convection*

When comparing the maximum depths of convection observed during the individual winters to the corresponding surface forcing (Figure 3.7, Table 3.3), it can easily be seen that no straightforward relation between these quantities exists. During the winter of 1996/97 the surface forcing was strongest, while the convection was deeper during the winter of 1994/95 with less intense forcing. Further, larger buoyancy loss occurred during the winter 1998/99 compared to 1997/98, but the convection activity was less intense. Although the NCEP/NCAR reanalysis fluxes are possibly biased (Section 3.1.1), the relative changes of the fluxes appear to be reliable. A more likely candidate to resolve the discrepancy between surface fluxes and mixing depth are changes of the stratification of the water column.

The relation between the properties of the convectively modified water column and the summer stratification can be explored by one–dimensional budgets of temperature and salinity. The temperature and salinity changes leading to the wintertime mixed layer properties are given by the difference between summer and winter conditions:

$$\Delta\theta = \frac{1}{h}\int_h^0 (\theta(z) - \theta_{ml})dz = \frac{1}{h}\int_h^0 \theta(z)dz - \theta_{ml}, \tag{4.1}$$

$$\Delta S = \frac{1}{h}\int_h^0 (S(z) - S_{ml})dz = \frac{1}{h}\int_h^0 S(z)dz - S_{ml}. \tag{4.2}$$

Here $h$ is the maximum mixed layer depth in winter, $\theta_{ml}$ and $S_{ml}$ are the corresponding mixed layer temperature and salinity, and $\theta(z)$ and $S(z)$ are the summer temperature and salinity profiles.

Neglecting lateral advection and assuming a linear equation of state (Equation 3.2), the observed temperature and salinity changes can be related to the surface heat and freshwater fluxes, or the corresponding buoyancy flux (see also Chapter 3):

$$\int_0^t B dt = g \int_0^t \alpha \frac{Q}{\rho_0 c_p} dt - g \int_0^t \beta S_0 (E - P) dt = g\alpha h \Delta\theta - g\beta h \Delta S. \tag{4.3}$$

With Equations 4.1 and 4.2 this results in

$$\int_0^t B dt = g \int_h^0 (\alpha\theta(z) - \beta S(z)) dz - gh(\alpha\theta_{ml} - \beta S_{ml}) = \int_h^0 (b(z) - b_{ml}) dz \tag{4.4}$$

For a nonpenetrative convection process this relation can also be used to estimate the mixing depth from the time integral of the surface buoyancy flux and a given CTD profile (e. g. Send and Käse, 1998). At the base of the winter mixed layer, steps are generally found in the temperature and salinity profiles which are compensated in density, indicating that deep mixing is, to zero order, nonpenetrative (Marshall and Schott, 1999).

The shallow, warm, and fresh surface layer during summer is of major importance for the total buoyancy budget of the water column, but poorly sampled by the moorings. Figure 4.5 shows mean CTD profiles obtained during the summer months in the interior Labrador Sea, as well as the corresponding buoyancy frequency and the vertically integrated buoyancy according to Equation 4.4. The upper 200 m are shown on an expanded scale, and the integrated buoyancy is shown relative to the surface and relative to 100 m to separate the contributions of the surface and the deeper layers.

In summer 1996, the surface layer showed an exceptional low salinity and high temperature. While the high temperatures are limited to the upper 30 – 60 m, low salinities are found down to about 300 m. The corresponding low density of the surface layer results in the highest stability in the pycnocline of the years of observations. The additional buoyancy flux necessary to erode this low density layer during the preconditioning is of about 0.15 – 0.25 $m^2\ s^{-2}$ compared to the other summers, which is 20 – 50% of typical total wintertime buoyancy fluxes.

The low surface temperature and density of the 1994 profiles partially results from the fact that they were obtained earlier in the year. Between 1997 and 1999, the summer conditions at the surface were rather similar, but in summer 1997 the water column between 50 and 75 m was warmer and less saline, resulting in an additional buoyancy flux of about 0.1 $m^2\ s^{-2}$ to erode this layer compared to summer 1998.

The summer 1996 profiles not only show the highest buoyancy content in the near–surface layer, but also over a large part of the LSW layer. This high buoyancy content of the water column is an additional reason for the less deep convection compared to the winter of 1994/95. The weak stratification of summer 1994 in the deeper layers was probably a result of intense convection taking place during the previous winter.

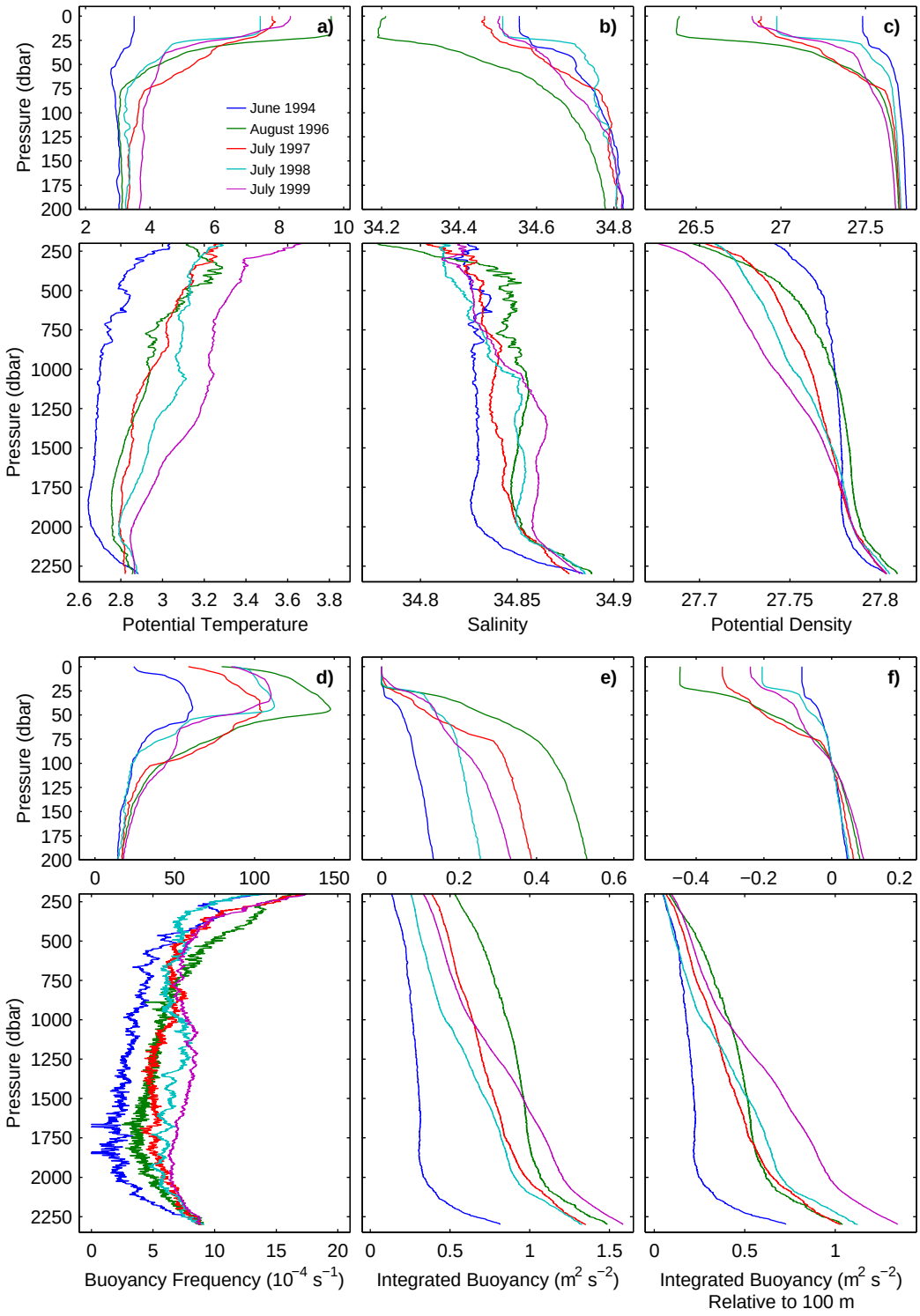


FIG. 4.5: Mean profiles of potential temperature (a), salinity (b), potential density (c), buoyancy frequency (d), integrated buoyancy (e), and integrated buoyancy relative to 100 m (f) from summer CTD casts near the Labrador Sea convection moorings; upper panels 0 – 200 m (enlarged vertical scale) and lower panels 200 – 2300 m (June 1994 data courtesy of J. Lazier). For the time of observations see legend in (a).

The strong stratification of summer 1996 was completely removed in the upper 1000 m through the convection in winter 1996/97. Below 1500 m the stratification increased continuously over the years, due to the absence of convection below this level after 1995. After 1997, the stratification increased also between 1000 and 1500 m, because of the reduced convection intensity. Generally, the summer CTD profiles show warming and increasing salinity between 1000 and 2000 m, except for summer 1997 where cold and less saline water was mixed down by convection. Between 300 and 1000 m the density decreased continuously, partly due to warming but also due to decreasing salinity because of convection.

Regarding the restratification of the water column, Lilly et al. (1999) already found a continuous supply of heat below the mixed layer in the one–year *Bravo* data of 1994/95. Figure 4.6 shows the temperature anomalies (relative to 3 °C) at the convection moorings between summer 1996 and summer 1999, averaged over 500 m layers.

Computing the averaged temperatures from the time series of the moored instruments requires to assume that each sensor represents a layer of the thickness given by the instrumental spacing. This implies that the topmost sensor is always representative for the surface layer, which does not hold during the summer months when the mixed layer is shallower.

The temperature time series show a general warming of the upper 2000 m of the water column over the three years of observations. The largest warming occurred in the upper 500 m with the annual cycle superimposed. A linear trend fitted to the temperature time series shows that the warming decreases towards the lower layers. The annual warming rate resulting from the linear fits ranges from 0.16 °C/yr in the upper 500 m to 0.09 °C/yr for the 1500 – 2000 m layer. The heat fluxes equivalent to the increasing temperature range from 10.3 W $m^{-2}$ in the upper layer to 5.8 W $m^{-2}$ in the lowest layer. The mean annual warming rate over the 2000 m water column results to 0.13 °C/yr with a corresponding net heat flux of 34.1 W $m^{-2}$.

As the annual mean of the air–sea heat flux in the central Labrador Sea is generally negative (-61 W $m^{-2}$ for 1996 to 1999 in the NCEP/NCAR reanalysis data), both the net surface heat loss as well as the observed warming have to be supplied by lateral advection. This results in a total advection of heat of 95 W $m^{-2}$, which is most likely an upper limit due to the possible overestimation of heat loss in the NCEP/NCAR data.

### *One–Dimensional Budgets*

An interesting question is to what extent convection can be described by one–dimensional vertical mixing driven by surface heat and freshwater fluxes. In fact, the Equations 4.1 – 4.4 represent the simplest possible mixed layer model, where the water column is convectively overturned by prescribed surface fluxes. Instead of running it forward to predict the mixed layer development from the surface fluxes, this model can be used to directly estimate the fluxes necessary to reach the mixed layer conditions observed in winter. A comparison of the summer CTD profiles with

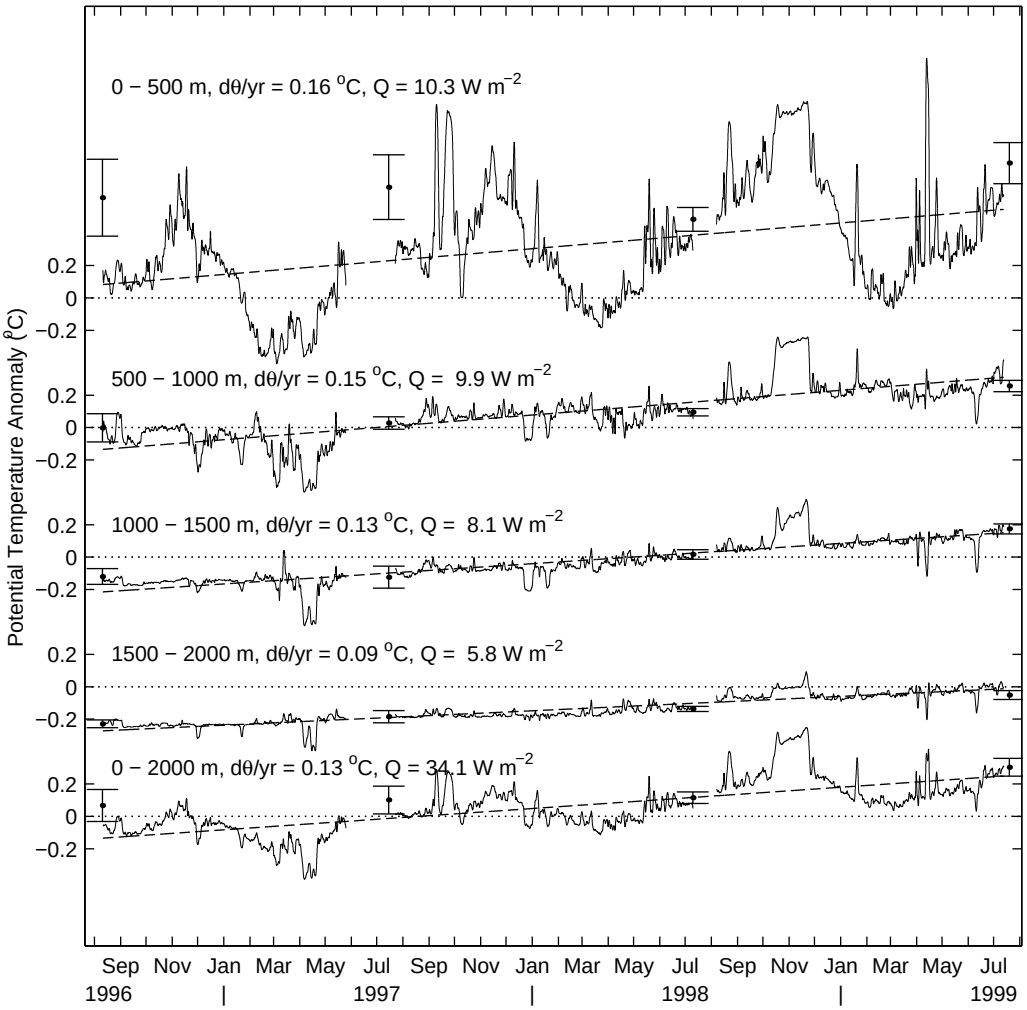


FIG. 4.6: Potential temperature anomaly (3 °C subtracted) averaged over 500 m layers at the Labrador Sea convection moorings K1 (1996/97), K11 (1997/98), and K21 (1998/99). A linear trend fitted to the temperature time series is shown as a dashed line. Each curve is labeled with the warming rate and the equivalent heat flux (for that particular layer) resulting from the fit. Mean and standard deviations from CTD profiles are shown as dots and errorbars.

the mixed layer conditions by the time of deepest convection is shown in Figure 4.7. The fluxes result from the temperature and salinity differences between the winter mixed layer and the mean temperature and salinity of summer profiles over the winter mixed layer depth. An evaluation of the terms in Equations 4.1 – 4.4 is given in Table 4.1, compared to the corresponding NCEP/NCAR reanalysis fluxes. Figure 4.8 shows the total fluxes of heat, freshwater, and buoyancy estimated from the hydrographic conditions, compared to the respective NCEP/NCAR fluxes.

Together with the decreasing depth of convection over the years, the water mass properties of the winter mixed layer show increasing temperature and decreasing salinity. Consequently the

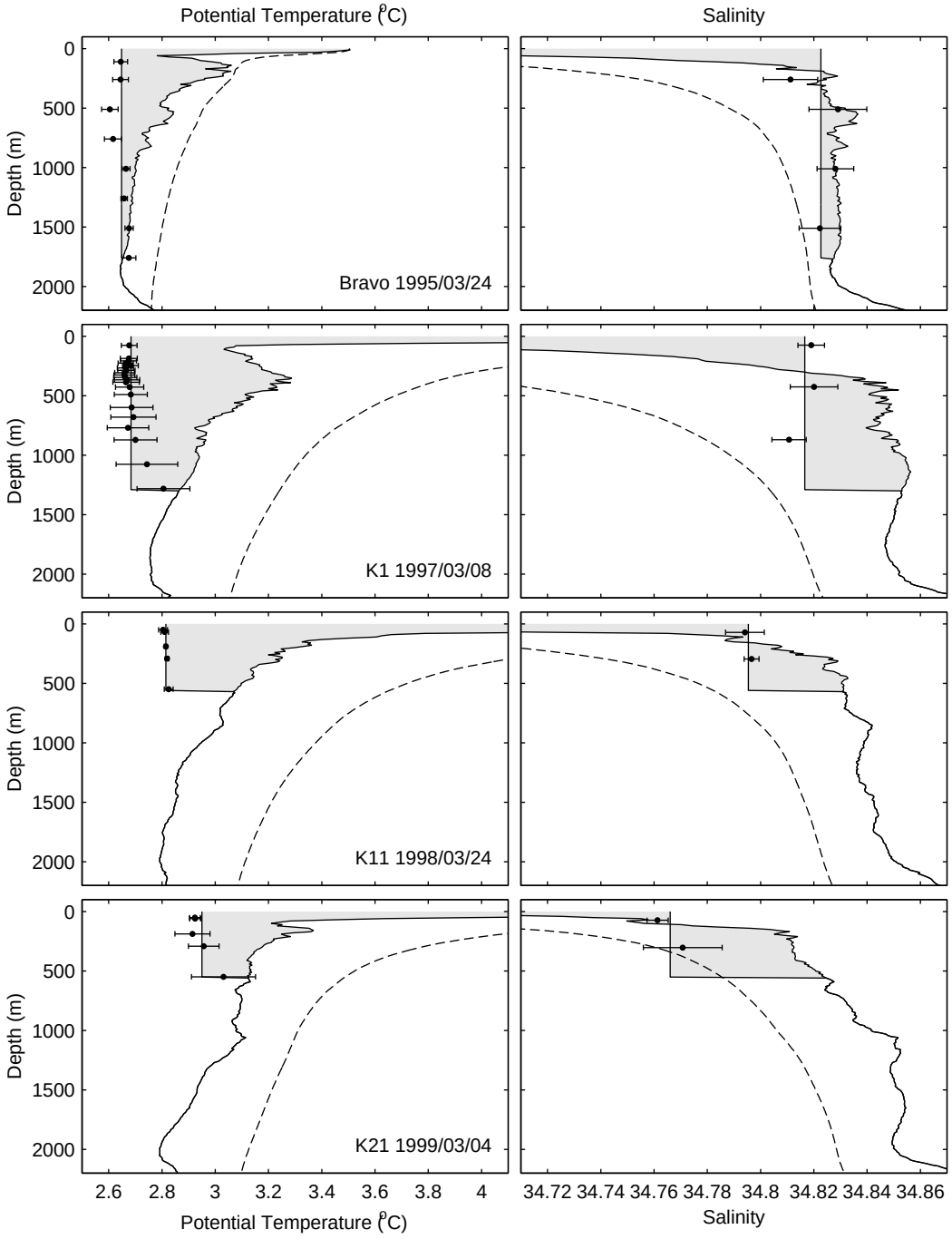


FIG. 4.7: Comparison between summer temperature and salinity profiles (same as in Figure 4.5) and winter mixed layer conditions at the Labrador Sea moorings by the time of deepest convection (dots). The errorbars denote standard deviations over two days (plus/minus one day of the dates given in the temperature panel). The cumulative means of the summer profiles $\frac{1}{h}\int_h^0 \theta(z)dz$ and $\frac{1}{h}\int_h^0 S(z)dz$ are shown as dashed lines. The difference between the observed mixed layer properties and the cumulative means at mixed layer depth is a measure of the heat and freshwater fluxes needed to produce them.

TABLE 4.1: Properties of the winter mixed layer observed at the moorings in the central Labrador Sea compared with conditions found during summer CTD surveys and the resulting net fluxes as well as the corresponding NCEP/NCAR reanalysis fluxes.

| | | Bravo 24 Mar 1995 | K1 8 Mar 1997 | K11 24 Mar 1998 | K21 4 Mar 1999 |
|---|---|---|---|---|---|
| | *Observations* | | | | |
| Mixed layer depth (m) | $h$ | 1760 | 1290 | 560 | 550 |
| Mixed layer temperature (°C) | $\theta_{ml}$ | 2.65 | 2.68 | 2.81 | 2.95 |
| Mixed layer salinity | $S_{ml}$ | 34.82 | 34.82 | 34.80 | 34.77 |
| Mixed layer density | $\sigma_{\theta ml}$ | 27.78 | 27.77 | 27.74 | 27.70 |
| Time difference (days) | $\Delta t$ | 295 | 209 | 252 | 237 |
| Temperature integral (°C) | $\frac{1}{h}\int_h^0 \theta(z)dz$ | 2.78 | 3.24 | 3.65 | 3.49 |
| Temperature change (°C) | $\Delta\theta$ | -0.13 | -0.56 | -0.84 | -0.54 |
| Heat flux (W m$^{-2}$) | $\frac{1}{\Delta t}\rho_0 c_p h\Delta\theta$ | -38 | -164 | -88 | -59 |
| Salinity integral | $\frac{1}{h}\int_h^0 S(z)dz$ | 34.82 | 34.80 | 34.78 | 34.79 |
| Salinity change | $\Delta S$ | 0.01 | 0.01 | 0.01 | -0.02 |
| Freshwater flux (mm) | $-h\Delta S/S_0$ | -260 | -491 | -211 | 307 |
| Thermal buoyancy flux (m$^2$ s$^{-2}$) | $B_T = g\alpha h\Delta\theta$ | -0.24 | -0.82 | -0.55 | -0.36 |
| Haline buoyancy flux (m$^2$ s$^{-2}$) | $B_S = -g\beta h\Delta S$ | -0.07 | -0.13 | -0.06 | 0.08 |
| Total buoyancy flux (m$^2$ s$^{-2}$) | $B = B_T + B_S$ | -0.31 | -0.95 | -0.61 | -0.27 |
| | *NCEP/NCAR Reanalysis* | | | | |
| Heat flux (W m$^{-2}$) | $Q$ | -70 | -200 | -105 | -118 |
| Temperature change (°C) | $\Delta\theta = Q\Delta t/(\rho_0 c_p h)$ | -0.25 | -0.68 | -1.00 | -1.07 |
| Evaporation (mm) | $E$ | 600 | 701 | 589 | 602 |
| Precipitation (mm) | $P$ | 590 | 570 | 616 | 691 |
| Freshwater flux (mm) | $F = -(E-P)$ | -10 | -131 | 27 | 90 |
| Salinity change | $\Delta S = -S_0 F/h$ | 0.00 | 0.00 | 0.00 | -0.01 |
| Thermal buoyancy flux (m$^2$ s$^{-2}$) | $B_T = g\alpha\Delta\theta$ | -0.26 | -0.82 | -0.48 | -0.52 |
| Haline buoyancy flux (m$^2$ s$^{-2}$) | $B_S = -g\beta\Delta S$ | 0.00 | -0.03 | 0.01 | 0.02 |
| Total buoyancy flux (m$^2$ s$^{-2}$) | $B = B_T + B_S$ | -0.27 | -0.85 | -0.47 | -0.50 |

maximum density reached by the convection decreased from year to year. While it is self–evident that cooling is necessary to arrive at the observed mixed layer temperature, all winters except 1998/99 need a rather large supply of salt to explain the observed mixed layer salinity. The mixed layer of the winter 1998/99 was less saline than the mean summer salinity, indicating a necessary freshwater input to explain the mixed layer salinity. The NCEP/NCAR data do indeed show a net freshwater gain over the winter, but of much smaller magnitude.

The magnitude of the NCEP/NCAR freshwater fluxes is generally too small. The evaporation was larger than the observed increase of the mixed layer salinity, but compensated by the precipi-

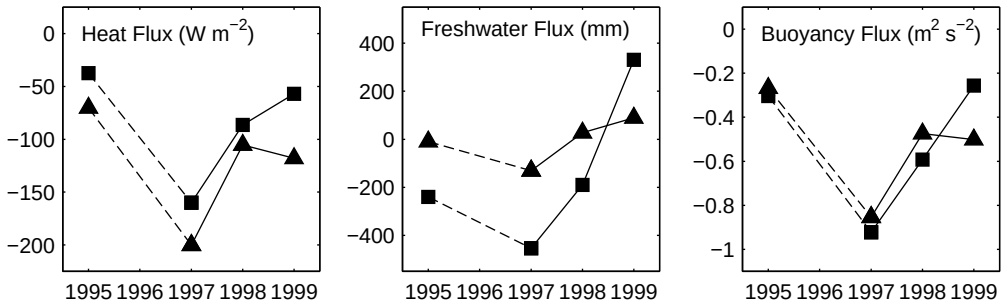


FIG. 4.8: Net fluxes of heat, freshwater, and buoyancy, estimated from difference between the conditions found during summer CTD surveys and the water mass properties of the deepest mixed layer at the Labrador Sea convection moorings (squares). The corresponding NCEP/NCAR reanalysis fluxes are shown as triangles.

tation. Thus, either the precipitation is too large (respectively evaporation too small) or salt has to be supplied advectively. However, an advective trend in the salinity time series, comparable to the advection of heat in the temperature evolution (Figure 4.6), cannot be identified. The heat fluxes of the NCEP/NCAR data are typically 20 – 50% larger than the observed heat loss between summer and winter, but it cannot be separated to what degree this imbalance is due to overestimations of the heat fluxes or the lateral advection of heat.

### *Relation to NAO*

The observations of convection at the moorings in the central Labrador Sea show a decreasing intensity of convection. The water mass properties of the winter mixed layer show increasing temperature and density and decreasing salinity. Regarding the relation between the convection intensity and the NAO, as suggested by Dickson et al. (1996), there is clearly no direct link between the convection intensity during a particular winter and the winter mean NAO index, making it impossible to deduce the convection intensity from the knowledge of the index alone. While the convection intensity decreased over the observation period, the winter mean NAO index increased continuously between 1996 and 1999 (Figure 3.6).

In 1994/95 the index was high and the maximum depth of convection was largest, but the corresponding surface forcing was weaker than in 1996/97. The deep convection in 1994/95 was more a result of the prevailing weak stratification, which was most likely a result of intense convection during the previous winters. The winter of 1996/97 was one of rather strong surface forcing, but moderate NAO index. The buoyancy content of the water column observed during summer 1996 was the highest from all years. This was partly due to the warm and low salinity surface layer, but also the deeper layer showed relatively high stability.

The relation between the NAO and the convection intensity in the Labrador Sea should be

considered on a longer time scale than year to year changes. Regarding the observations between 1996 and 1999, the mean NAO index was moderate and convection was more or less to intermediate depths. Further, a relation between the NAO index and the wintertime surface forcing does exist, as about 30% of the variability of the buoyancy flux are explained by the index. Thus, several years of high NAO index, as during the late 1980s and early 1990s, increase the likelyhood that a winter of strong surface forcing occured with substantial weakening of the stratification by deep convection. During subsequent winters, convection could more easily reach to large depths. On the other hand, during a several–year period of low or moderate NAO index, strong convection may occur only sporadically, as in the winter of 1996/97, and has to counteract the restratification.

### 4.1.2 Greenland Sea

During summer, the stratification of the upper water column in the central Greenland Sea is characterized by a shallow surface mixed layer with low salinity due to ice melting and relatively high temperatures. The highest temperatures and lowest salinities of the surface layer are generally found during August/September, by the time of least sea ice coverage (Pawlowicz, 1995). The more saline water at intermediate depths is usually classified as Arctic Intermediate Water (AIW).

The freshwater content of the near–surface layer can make it far too light to reach the density of the deeper water even when cooled to the freezing point. Several mechanisms were proposed in the past to overcome this problem. Motivated by the lack of observational evidence for a deep homogeneous water column, both double–diffusive convection and cabbeling were suggested as responsible for the formation of Greenland Sea Deep Water (GSDW) (Carmack and Aagaard, 1973; McDougall, 1983). Häkkinen (1987) put forward the possibility that upwelling at the ice edge might be important to trigger deep mixing. However, the ADCP measurements from the winter of 1988/89 showed no indications of vertical velocity events associated with the passage of the ice edge (Schott et al., 1993).

The first direct observation of a 1200 m deep mixed layer in the central Greenland Sea in February 1988 (Rudels et al., 1989) led to the idea of haline convection, driven by freezing at the sea surface (Rudels, 1990). Finally, the extensively observed convection to about 1500 m in March 1989 was found to be thermally driven as the convection site was ice free during this period (Schott et al., 1993; Pawlowicz et al., 1995). The temperature development at one of the convection moorings in the central Greenland Sea from the winter of 1988/89 is shown in Figure 4.9, in comparison to temperature time series obtained during later winters. Figure 4.10 shows contour plots of the temperature evolution observed during the winters of 1993/94 (GSM4) and 1994/95 (GSM5).

Although the central Greenland Sea was ice free during the convection in March 1989, ice formation played an important role in preconditioning the water column. From the observations of the winter of 1988/89 and a mixed layer model simulation Visbeck et al. (1995) developed the following preconditioning scenario: the mixed layer temperature is reduced to the freezing point by cooling in early winter. Subsequent brine release through ice formation and entrainment increase the mixed layer salinity/density. The major finding was that at this time wind–driven southwestward ice export is important, because it reduces the insulation of the surface waters from the atmosphere and removes freshwater (i. e. buoyancy) out of the system. Once a critical salinity/density is reached, entrainment of AIW keeps the mixed layer above the freezing point and prevents further ice formation. From then on, surface cooling can initiate deeper mixing.

The temperature development at mooring M319 (Figure 4.9a) resembles this scenario. Rapid cooling of the surface layer to temperatures near the freezing point occurred by the end of November 1988. The cooling coincided with ice appearing at the mooring location (Figure 3.9). During the period of ice coverage, the near surface temperature remained close to the freezing point and

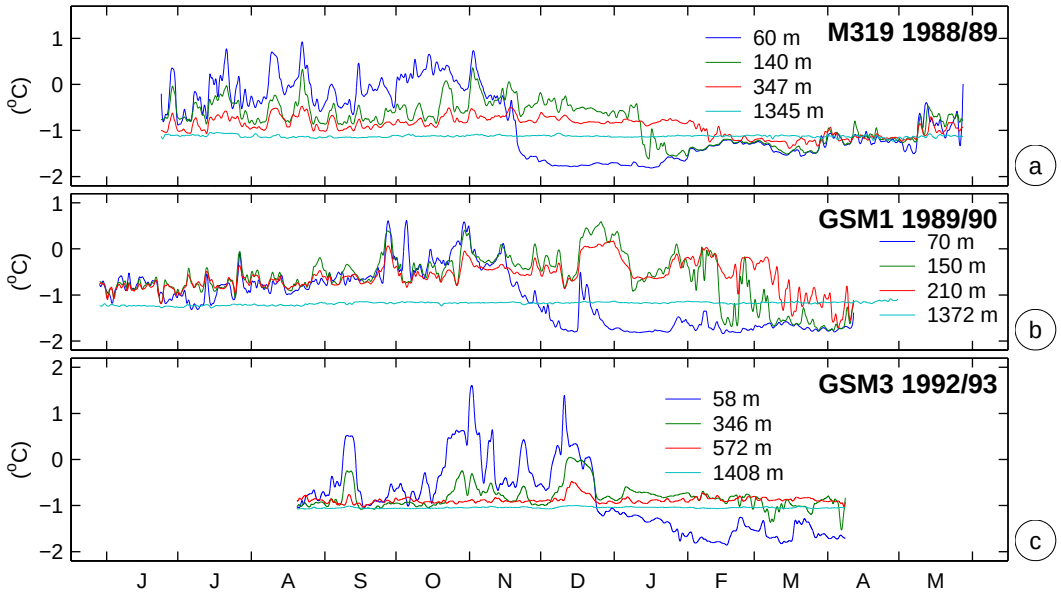


FIG. 4.9: 40–h lowpassed potential temperature time series for selected depths at the convection moorings (a) M319 1988/89, (b) GSM1 1989/90, and (c) GSM3 1992/93 in the central Greenland Sea.

the mixed layer deepened gradually with a rate of about 1 m $d^{-1}$ (Visbeck et al., 1995). The ice coverage ended by mid–January and entrainment of AIW resulted in a warming of the mixed layer. The mixed layer deepened more rapidly in the following and vertical mixing to about 1500 m was observed in March (Schott et al., 1993).

The temperature time series obtained during the following deployment period (1989/90) at mooring GSM1 showed rather homogeneous conditions throughout most of the summer and autumn as a result of the convection during the previous winter. Cooling of the near surface layer began in November, but was slower than in 1988 and the freezing point was reached several weeks later in early December. Sea ice was observed for a short period at the mooring location (Figure 3.9). In contrast to the previous winter, warm water appeared in the upper part of the water column by mid–December, slowing down the preconditioning. The surface layer had to be cooled to the freezing point for a second time and new ice appeared at the mooring location by the beginning of January.

For the remaining winter the mixed layer temperature stayed near the freezing point, indicating that no considerable entrainment of AIW took place. The deeper levels were subsequently incorporated into the mixed layer, but about one month later than during the preceding winter. Overall, it appears that the maximum winter mixed layer depth did not far exceed 200 m, which is supported by CTD measurements from summer 1990 (Budéus et al., 1993). They showed no indication of mixing deeper than 250 m in the Greenland Sea gyre.

The weak convection activity during the winter of 1989/90 has probably three reasons: First,

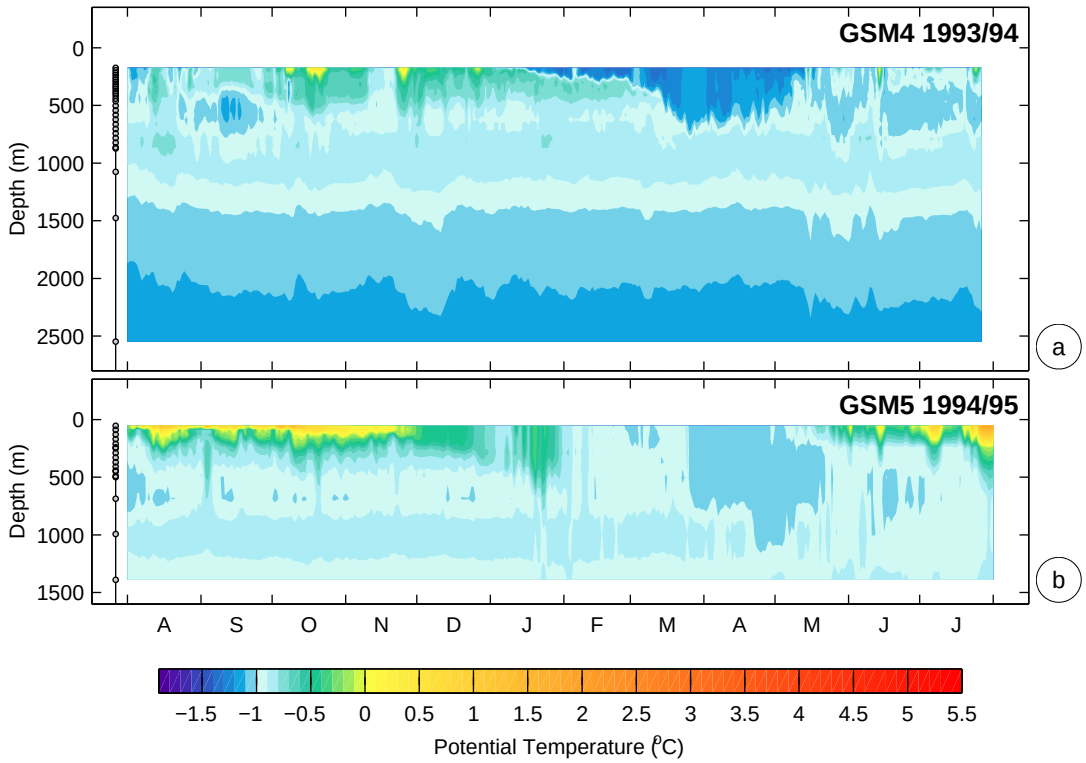


FIG. 4.10: Daily mean potential temperature at the convection moorings (a) GSM4 1993/94 and (b) GSM5 1994/95 in the central Greenland Sea. Instrument depths are marked as dots at the lefthand side. The contour interval is 0.1 °C.

this winter had the weakest surface forcing of all from the observational period (Figure 3.7). Second, only little ice was formed in the central Greenland Sea, resulting in a slower preconditioning, and third, a reset of the preconditioning occurred in December by the advection of warmer water.

The winter of 1992/93 (GSM3) showed the largest buoyancy loss of the observational period, but also events of rather warm water in the surface layer during autumn and early winter as well as little sea ice formation at the mooring location. The cooling of the mixed layer to temperatures near the freezing point took until February, much later than during the previous winters. The remaining winter month showed only little evidence of mixing activity, although CTD measurements revealed convection to 600 – 1000 m depth in the vicinity of the mooring (Lherminier et al., 1999). The cold temperatures at intermediate depths found at mooring GSM4 during September 1993 are probably remnants from the convection of the preceding winter.

Compared to the earlier observations, the situation was rather different during the winters of 1993/94 and 1994/95. The central Greenland Sea remained ice free during both winters (Figure 3.9) and the near surface temperature stayed well above the freezing point (Figure 4.11). Nevertheless, convection to intermediate depths occurred. In 1994 the deepest mixing observed was to a depth

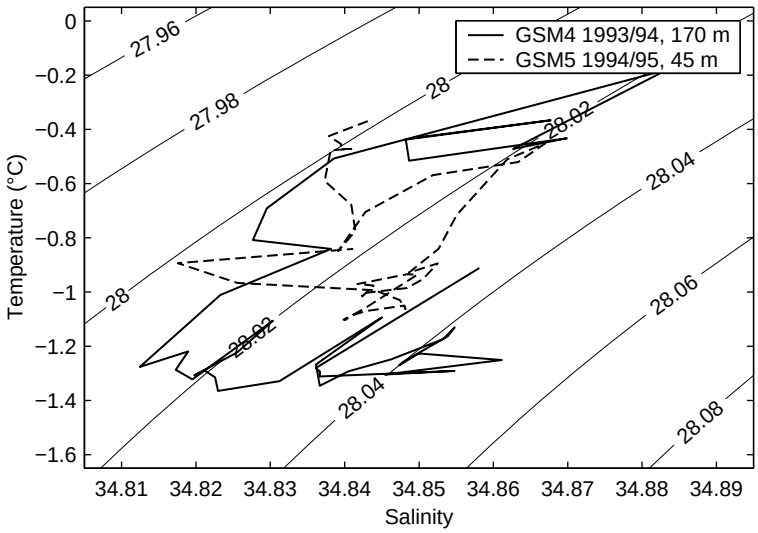


FIG. 4.11: 4–day mean near surface temperature and salinity at the Greenland Sea moorings GSM4 (1993/94) and GSM5 (1994/95) between 1 December and 15 May of the respective winters.

of about 800 m, while in 1995 about 1000 m were reached. In contrast to the scenario developed from the observations of the winter 1988/89 by Visbeck et al. (1995), the convection in 1994 and 1995 was purely driven by air–sea fluxes without sea ice interaction.

During the winter of 1993/94 the cooling started at the 170 m level by the end of December and lasted until mid–January, where the lowest temperature of about -1.3 °C was reached (Figure 4.11). The cooling was accompanied by decreasing salinity due to the downward mixing of low–salinity surface water. For the remaining winter, entrainment of warmer and saltier AIW caused the temperature to stay nearly constant, while the salinity of the mixed layer increased.

In 1994/95 the topmost instrument was closer to the surface and showed relatively high temperatures throughout most of the summer and early autumn. Cooling of the surface layer started in November and already in early January the temperature sensors showed homogeneous conditions in the upper 400 m (Figure 4.10). Serious warming occurred during the second half of January, reestablishing the stratification. Continuing surface forcing eroded the stratification for a second time (discussed in more detail in Section 5.1.1).

## 4.2 Vertical Velocities

The first observations of vertical currents in a convection regime were obtained with rotating deep floats during the classical MEDOC experiments in the western Mediterranean (e. g. MEDOC Group, 1970), showing motions of several centimeters per second at 800 m depth (Voorhis and Webb, 1970). In the Labrador Sea, early rotating float measurements showed downward velocities of up to 9 cm $s^{-1}$ (Gascard and Clarke, 1983). The utilization of moored ADCPs allowed more detailed studies of small–scale processes during deep convection, revealing short downward pulses exceeding 10 cm $s^{-1}$ on horizontal scales of less than 1 km, and slow upward motion inbetween the convective plumes (Schott and Leaman, 1991).

ADCPs were constituents in all Greenland and Labrador Sea convection moorings deployed between 1988 and 1999 with the purpose of observing the three–dimensional velocity structure during convective events and especially the vertical velocity associated with them. Results of the first deployment period in the Greenland Sea (1988/89) are discussed in Schott et al. (1993), and Lilly et al. (1999) analyzed the measurements obtained during the winter of 1994/95 at the *Bravo* mooring in the central Labrador Sea. No ADCP measurements were obtained for the winters of 1989/90 (GSM1) and 1993/94 (GSM4) in the Greenland Sea, due to instrument failures. A summary of the instrument setup and the implied accuracy for all ADCP measurements is given in Appendix A.2. Monthly time series of unfiltered vertical velocity data at 300 m depth, a level that all instruments have in common, from all experiments are shown in Figure 4.12 for the Greenland Sea and Figure 4.13 for the Labrador Sea.

During winters where deep mixing has been observed, the vertical velocity time series show distinct bursts of downward motion, but these are not the most obvious signals in the velocity time series. The Greenland Sea vertical velocity records also show several periods of fairly symmetrical up and downward motions with amplitudes up to $\pm 5$ cm $s^{-1}$, generally during November and December, i. e. long before convection reached the 300 m level. Examples are the second half of November 1988, the first half of December 1990, or the period of mid–December 1992. Consistency test applied to the spectra and cross spectra of the vertical and horizontal current fluctuations suggest, that they most probably are caused by internal waves (Visbeck, 1993). A possible generation mechanism would be turbulence in the upper layer, where enhanced wind mixing in autumn causes pressure fluctuations in the stratified water underneath. Such internal wave variance in stratified layers has also been found in the convection region of the northwestern Mediterranean (Schott et al., 1996). However, in the vertical velocity time series from the Labrador Sea such symmetrical fluctuations appear to be much less pronounced.

Another noise component for the purpose of observing convective plumes is the conspicuous diurnal cycle of upward and downward motion, showing up preferably during the summer months. This well known signal does not reflect water velocity but the vertical migration of zooplankton

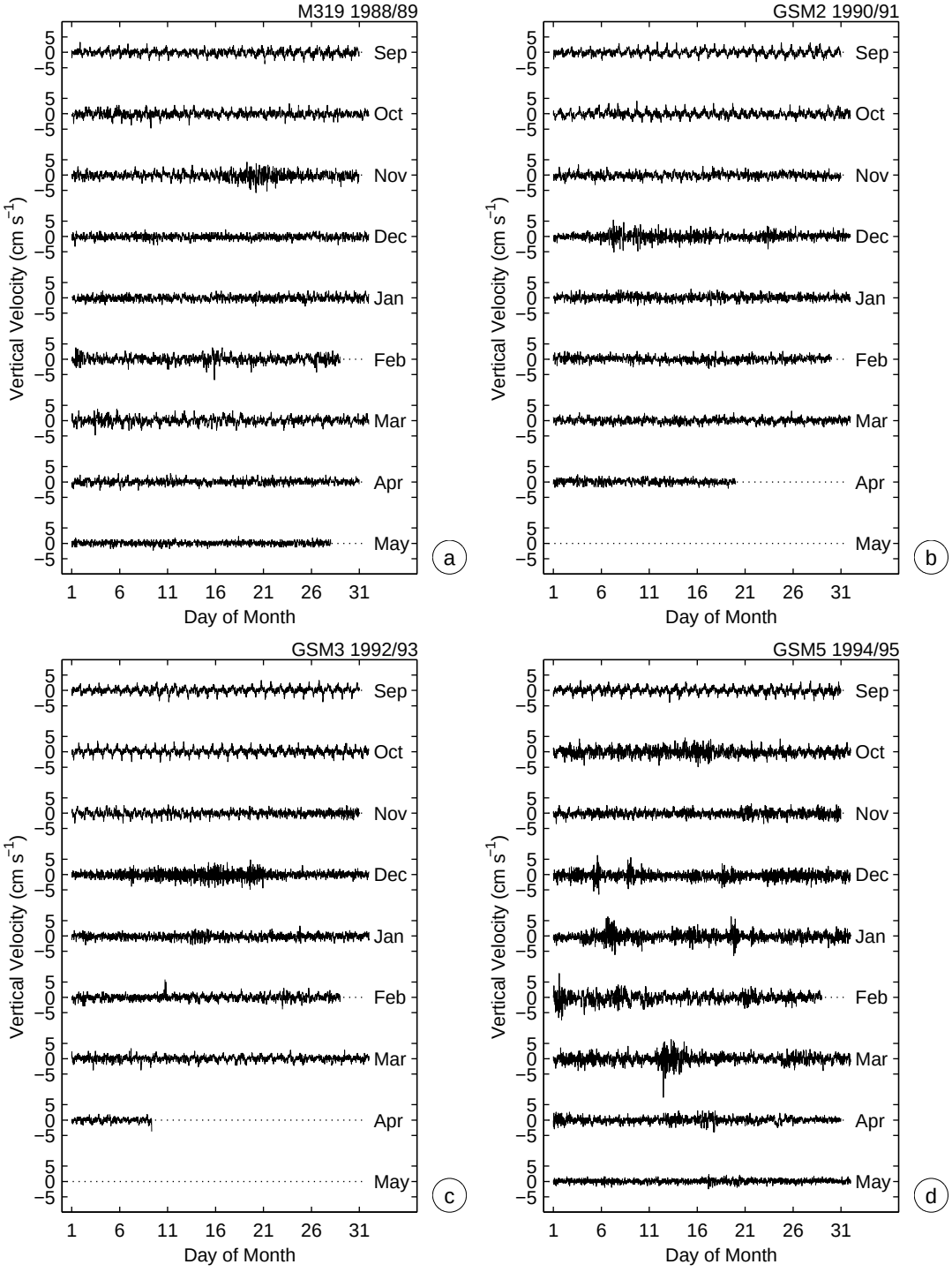


FIG. 4.12: ADCP time series of vertical velocity at 300 m depth in the central Greenland Sea for the winters of (a) 1988/89, (b) 1990/91, (c) 1992/93, and (d) 1994/95.

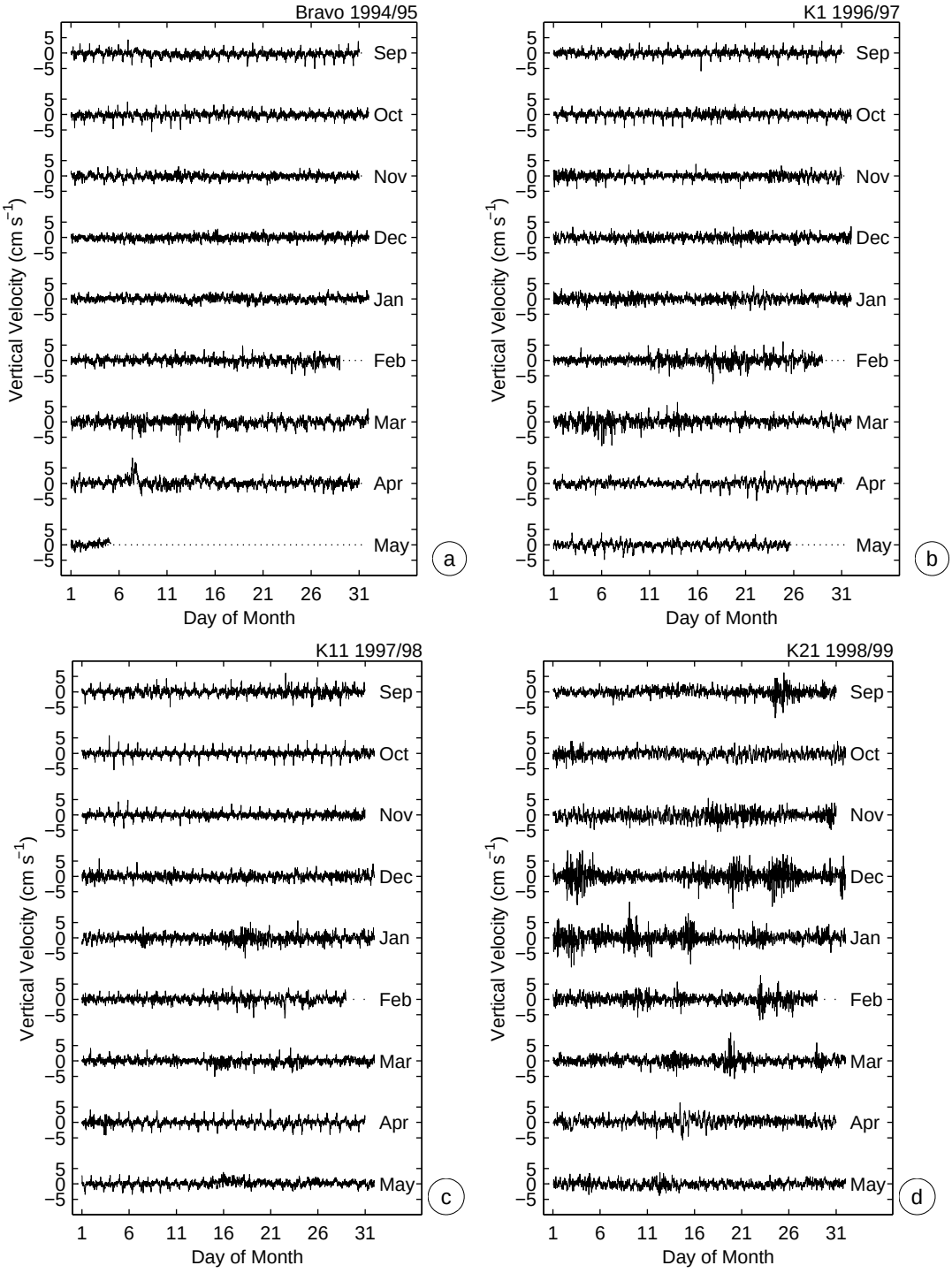


FIG. 4.13: ADCP time series of vertical velocity at 300 m depth in the central Labrador Sea for the winters of (a) 1994/95, (b) 1996/97, (c) 1997/98, and (d) 1998/99.

(Fischer and Visbeck, 1993). The mean migration velocity is of about $\pm 1.5$ cm s$^{-1}$; peak values exceed $\pm 3$ cm s$^{-1}$. Contouring the vertical velocity versus time of day and season shows that the periods of downward motion correspond to the time of sunrise and upward motion to the time of sunset (Figure 4.14). During the winter months the migration signal vanishes in the Greenland Sea, and is less obvious in the Labrador Sea probably because the plankter change their resting horizon to shallower levels (Fischer and Visbeck, 1993).

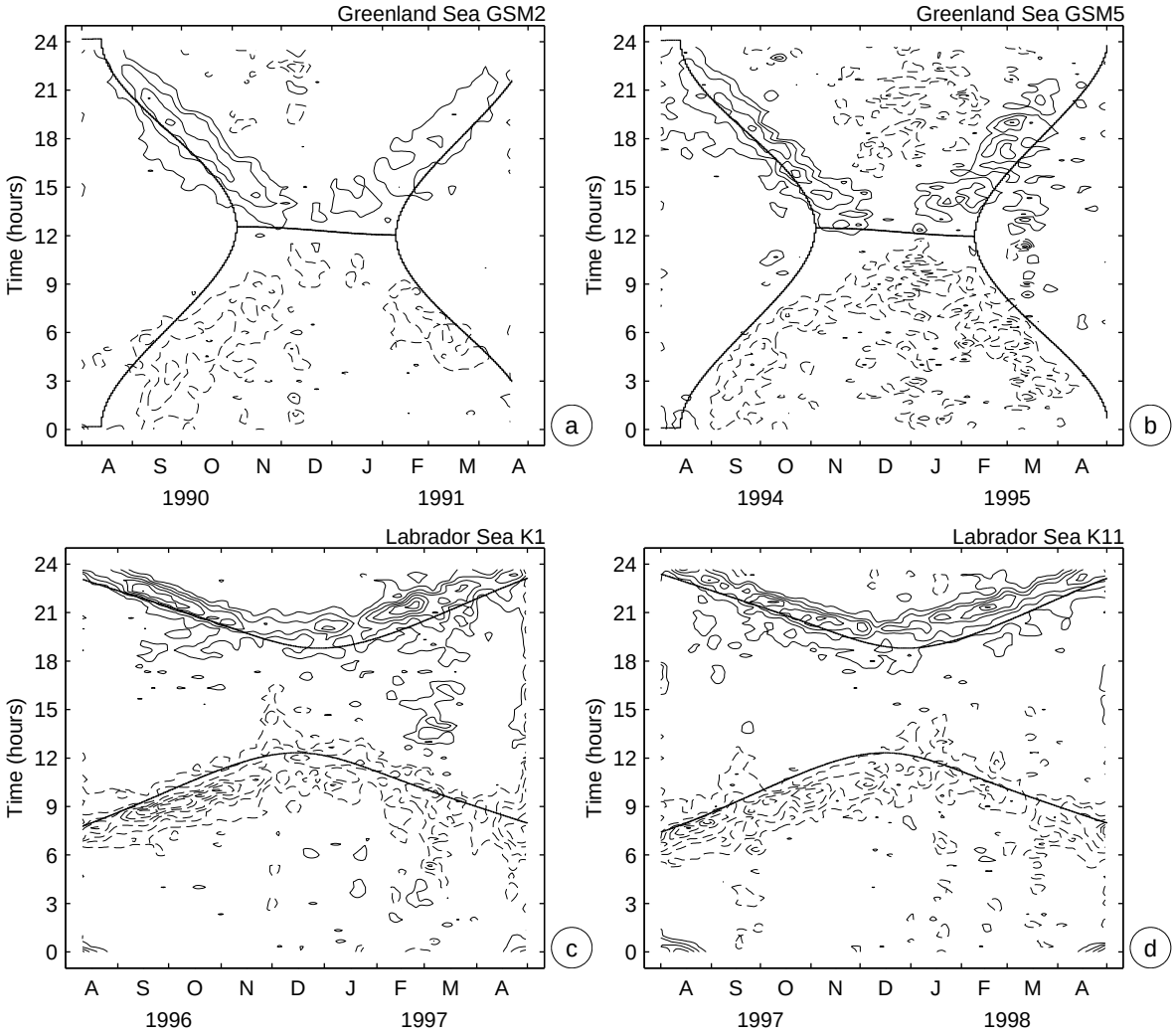


FIG. 4.14: Evolution of the diurnal cycle of vertical zooplankton migration at 300 m depth at two Greenland Sea and two Labrador Sea stations. Upward motion is shown as solid lines, downward motion as dashed lines. The contour interval is 0.5 cm s$^{-1}$; zero contour is not shown. The times of sunrise and sunset are indicated as bold lines.

In the Greenland Sea vertical velocity records, signals of convective plumes are rather sparse, as deep mixing at the mooring location took place only in the winters of 1988/89 and 1994/95.

It has to be remembered that during the winter of 1993/94, where mixing went down to a depth of about 800 m, the ADCP did not return any data. Enhanced vertical velocity fluctuations were observed during this winter with rotating floats between 12 March and 1 April (Lherminier et al., 1999), a period during which mixed layer deepening occurred at the location of mooring GSM4 (Figure 4.10). Events of active vertical mixing in the 1988/89 record appear at the beginning of February, in mid–February, and again at the beginning of March. The observed downward velocities are of about 3 – 5 cm $s^{-1}$. A further event has been found around March 6 at the more eastward mooring T6 (Schott et al., 1993).

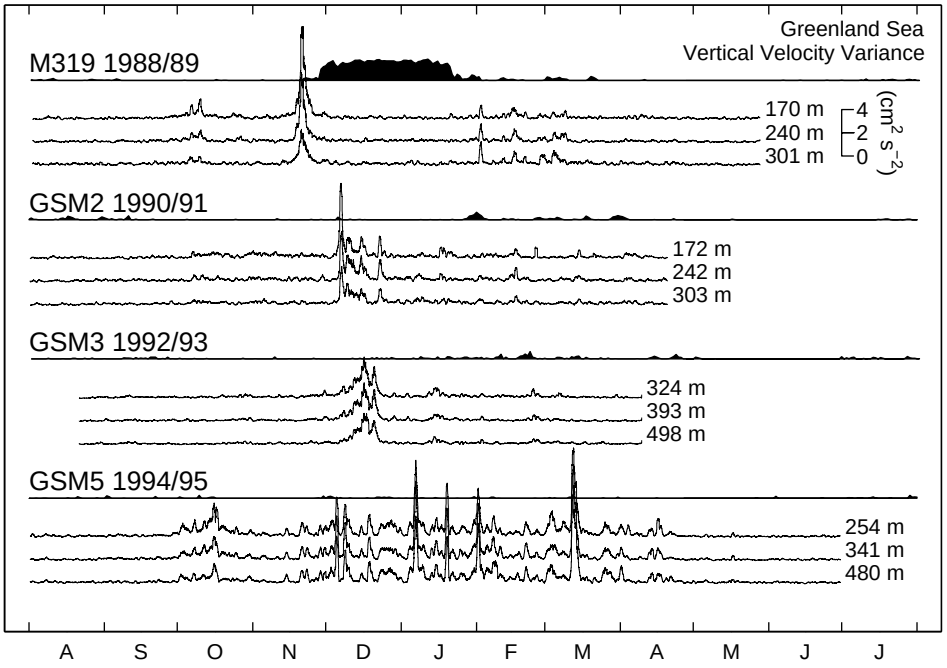


FIG. 4.15: 12-h running mean of variance of high–passed vertical velocity (periods longer than 6 hours eleminated) for selected ADCP bins over the four observational periods in the central Greenland Sea. Ice coverage from SSM/I data is indicated by bar graphs (courtesy L. Toudal).

Convection activity is characterized by enhanced high–frequency variance of the horizontal and vertical velocities. Statistics of ADCP velocity measurements during periods of convection activity are given in Table 4.2 in comparison to the first week of September which was a quiet period in all time series. Figure 4.15 shows the 12–hour running mean of variance of the 6–hour high–passed vertical velocity. Also indicated is the corresponding SSM/I sea ice concentration, revealing the minimal vertical velocity variance during the period of well established ice coverage from late November 1988 until late January 1989. Regarding the occurrence of vertical mixing, ice did not play an important role in the following years. The largest variance in the 1988/89 records is found in November, probably caused by internal waves as discussed above. Similar increased variance

TABLE 4.2: Means and variances of ADCP current measurements (horizontal, vertical, and error velocity) at 300 m during convection periods compared to the first week of September, a quiet period in all time series. Variances are computed from the 6–h high–passed time series (HFKE = horizontal fluctuating kinetic energy).

| | | Mean (cm $s^{-1}$) | | | | Variance ($cm^2$ $s^{-2}$) | | |
|---|---|---|---|---|---|---|---|---|
| Mooring | Time | $\overline{u}$ | $\overline{v}$ | $\overline{w}$ | $\overline{v}_e$ | HFKE | $\overline{w'^2}$ | $\overline{v_e'^2}$ |
| | | *Greenland Sea* | | | | | | |
| M319 | 1988/09/01 – 1988/09/06 | -3.3 | -0.1 | 0.0 | -0.5 | 4.7 | 0.6 | 0.4 |
| M319 | 1989/02/10 – 1989/02/16 | 0.9 | 0.2 | -0.1 | -0.5 | 7.8 | 1.7 | 0.4 |
| M319 | 1989/03/03 – 1989/03/09 | -11.5 | -2.4 | 0.0 | -0.5 | 6.8 | 1.7 | 0.5 |
| GSM2 | 1990/09/01 – 1990/09/06 | -3.3 | -2.7 | -0.5 | -0.5 | 2.9 | 0.6 | 0.3 |
| GSM2 | 1991/02/14 – 1991/02/19 | -0.5 | -2.1 | -0.5 | -0.5 | 4.1 | 0.9 | 0.3 |
| GSM3 | 1992/09/01 – 1993/09/06 | 0.3 | -3.3 | -0.1 | -0.4 | 3.3 | 0.8 | 0.1 |
| GSM3 | 1993/02/21 – 1993/02/26 | 4.2 | -5.3 | -0.1 | -0.4 | 6.3 | 1.1 | 0.1 |
| GSM5 | 1994/09/01 – 1994/09/06 | -1.4 | -1.3 | 0.2 | -0.5 | 3.5 | 0.8 | 0.2 |
| GSM5 | 1995/02/04 – 1995/02/10 | 4.5 | 3.5 | -0.2 | -0.4 | 8.2 | 2.5 | 0.5 |
| | | *Labrador Sea* | | | | | | |
| Bravo | 1994/09/01 – 1994/09/06 | -7.9 | 0.0 | -0.1 | -0.4 | 4.1 | 0.9 | 0.3 |
| Bravo | 1995/02/24 – 1995/03/02 | -4.1 | 5.4 | -0.3 | -0.5 | 7.9 | 1.3 | 0.4 |
| Bravo | 1995/03/04 – 1995/03/10 | -5.9 | 9.6 | -0.1 | -0.4 | 7.1 | 1.5 | 0.3 |
| K1 | 1996/09/01 – 1996/09/06 | -0.8 | -1.6 | -0.1 | -0.4 | 2.5 | 0.6 | 0.1 |
| K1 | 1997/02/18 – 1997/02/24 | -7.3 | -9.5 | 0.0 | -0.4 | 12.1 | 2.1 | 0.7 |
| K1 | 1997/03/03 – 1997/03/09 | -12.7 | -6.6 | 0.0 | -0.4 | 15.0 | 3.5 | 0.8 |
| K11 | 1997/09/01 – 1997/09/06 | -7.0 | 15.7 | 0.0 | -0.4 | 2.4 | 0.8 | 0.1 |
| K11 | 1998/03/15 – 1998/03/21 | -6.2 | 23.4 | -0.2 | -0.5 | 6.1 | 1.0 | 0.3 |
| K21 | 1998/09/01 – 1998/09/06 | -3.5 | 28.1 | -0.1 | -0.4 | 3.7 | 0.6 | 0.3 |
| K21 | 1999/02/22 – 1999/02/28 | -2.4 | 1.2 | 0.0 | -0.4 | 4.0 | 3.6 | 0.3 |

appears in the late autumn periods of the two following winters 1990/91 and 1992/93. After the opening of the Nordbukta at the beginning of February 1989, several periods of increased vertical velocity variance, corresponding to vertical mixing, show up in the time series.

During the following years convection activity was less intense. The 1990/91 records show only slightly increased variance in mid–January and mid–February, and the 1992/93 records show some mixing activity in mid–January and by the end of February. The vertical velocity time series obtained over the last observation period in the Greenland Sea, the winter of 1994/95, is noisier compared to the previous ones, a result of the continuous sampling mode used in the setup of this ADCP (Appendix A.2). Prevailing downward motion occurred at the beginning of February, in mid–March, at the end of March, and for a short period in mid–April.

Convection activity is more pronounced in the vertical velocity time series obtained in the Labrador Sea. The number of individual events observed exceeds by far the number of events observed in the Greenland Sea. During the first deployment period, the winter of 1994/95, the largest downward motions occurred between mid–February and mid–March, with vertical velocities of up to 8 cm $s^{-1}$. The time series of the high–frequency variance of the vertical velocity (Figure 4.16) show increased values over this period.

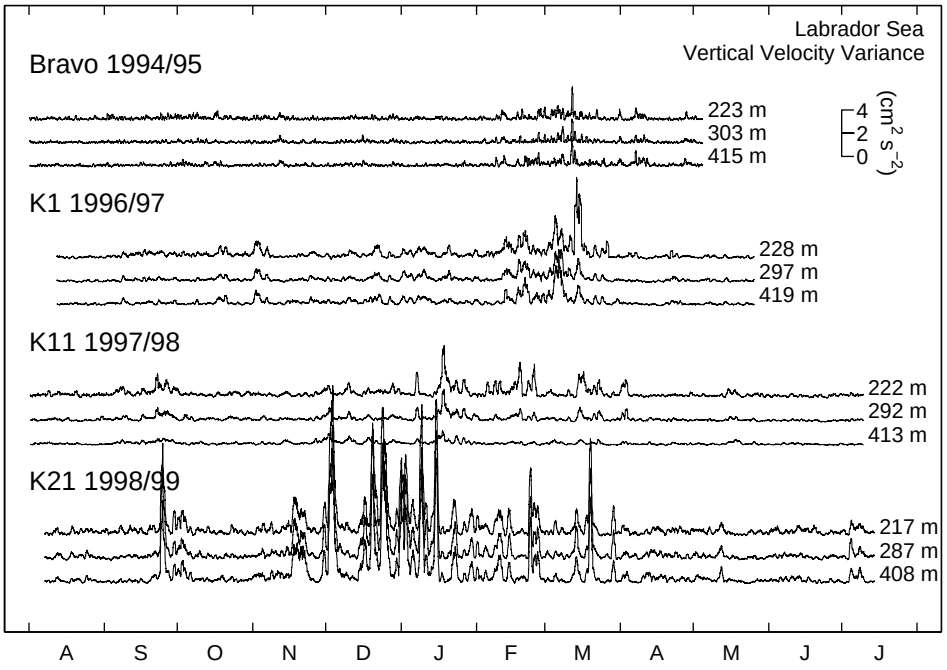


FIG. 4.16: Same as Figure 4.15 for the central Labrador Sea.

The most intense mixing activity of the four years of observations took place in the winter of 1996/97, again between mid–February and mid–March. Here peak values of the vertical velocity exceeded 10 cm $s^{-1}$. In the context of the *Labrador Sea Deep Convection Experiment* vertical velocities were also measured using both profiling vertical current meter floats (VCM) and deep Lagrangian floats. The magnitude of their observed vertical velocity corresponds to the ADCP measurements. During the convection period of 1997 the VCMs recorded several occurrences of vertical flow of 5 cm $s^{-1}$ and peak velocities of 10 cm $s^{-1}$. The water parcel following Lagrangian floats cycled between the surface and 500 – 800 m, with vertical velocities often exceeding 10 cm $s^{-1}$ (The Lab Sea Group, 1998).

## 4.3 Labrador Sea Boundary Current Region

The presence of a core of low salinity and high tracer concentrations in the upper part of the Deep Western Boundary Current (DWBC) south of the Labrador Sea led to a distinction between this water and the underlying LSW (Fine and Molinari, 1988; Pickart, 1992). Fine and Molinari (1988) considered this water to be a warmer type of LSW formed during rather mild winters, while Pickart (1992) argued that the upper waters in the central Labrador Sea are generally too dense and suggested a formation in the southern Labrador Sea.

In late winter 1991, a small lense (20 km radius) of newly ventilated water (termed upper LSW) embedded in the Labrador Current was observed northeastward of Flemish Cap (Pickart et al., 1996). It had the correct density ($\sigma_\theta = 27.68 - 27.72$) to be the source of the high–tracer layer of the upper DWBC observed further south. The core temperature and salinity of the lense were 2.9 °C and 34.87, respectively. From a mixed layer model simulation Pickart et al. (1997) deduced the possibility of this water mass being formed by convection in the main branch of the Labrador Current.

Besides the convection moorings in the central Labrador Sea, the moorings in the boundary current region (Figure 2.1) were also equipped with ADCPs and a number of temperature sensors to register eventually happening convection. Compared to the central Labrador Sea, where a gradual deepening of the surface mixed layer was observed in each winter, the temperature development in the boundary current region was completely different (Figure 4.17). In February 1997, nearly instantaneous cooling of the upper 1000 m was observed at mooring K2. Thereafter, increased fluctuations between cold and warm conditions occurred, again over the upper 1000 m. Such cooling events over a large vertical range cannot be attributed to convection activity at the mooring location. Instead, it appears more likely that the temperature anomalies were laterally advected. A further indication for the absence of local convection is that the temperature fluctuations continued into May/June, while the cooling season ended already by the beginning of April.

Figure 4.18 shows temperature and salinity sections along the western part of the WOCE AR7W line occupied between 4 and 6 March 1997 by the *Knorr*, during a period of intense convection at mooring K1. The pool of convectively generated low temperature and low salinity water is clearly visible in the interior Labrador Sea, while at the location of the boundary current moorings the stratification remained intact. Nevertheless, the front between stratified and unstratified water was located close to mooring K2.

The following two observational periods (1997/98 and 1998/99) show similar enhanced temperature fluctuations occurring simultaneously over the upper part of the water column at the boundary current moorings K12 and K22. Here, the topmost sensors also show some cooling that might be attributed to local mixed layer deepening, but it was limited to the upper few hundred meters. The temperature fluctuations in the deeper layers were less intense than in 1997 and the period of inten-

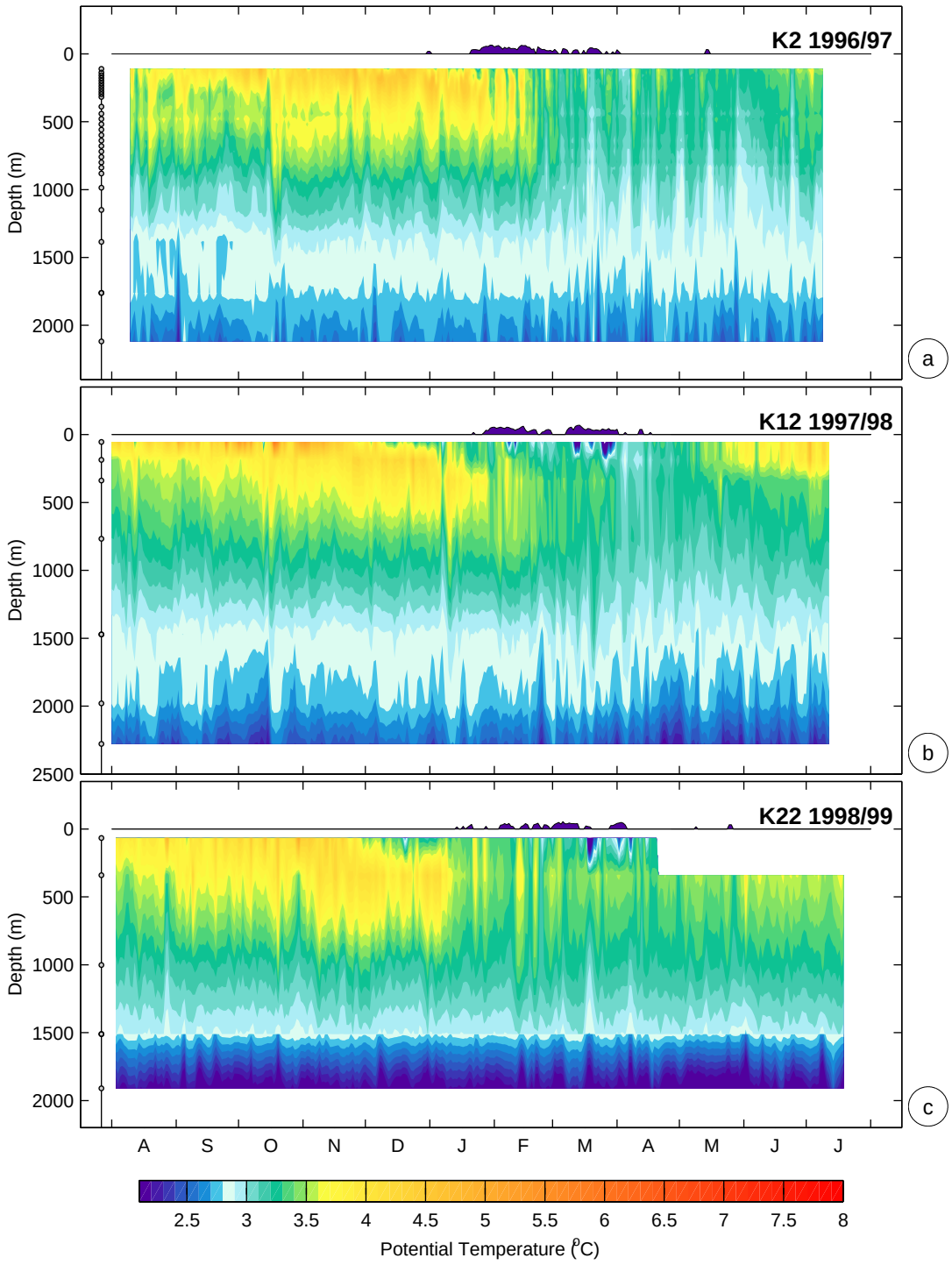


FIG. 4.17: Daily mean potential temperature at the Labrador Sea boundary current moorings. (a) K2 1996/97, (b) K12 1997/98, and (c) K22 1998/99. Instrument depths are marked as dots at the lefthand side. The contour interval is 0.1 °C. Ice concentration from NCEP OMB SSM/I data is indicated on top.

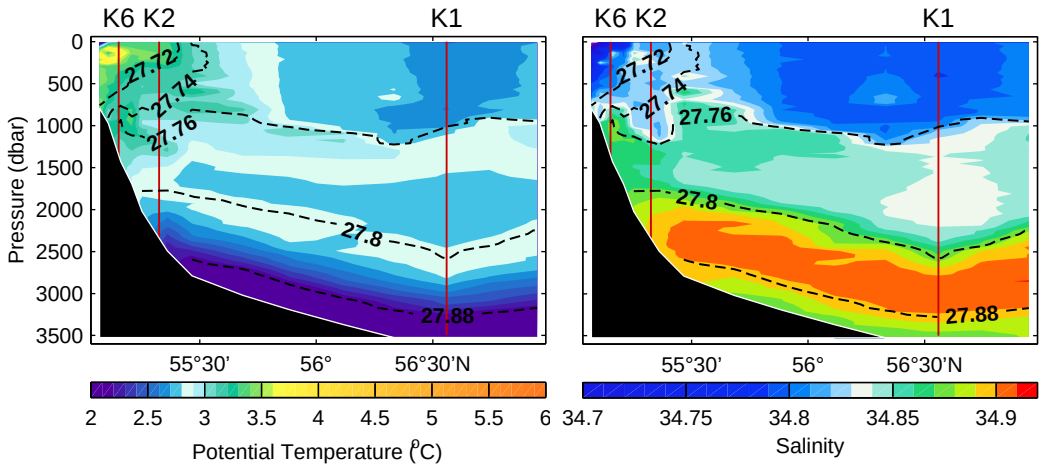


FIG. 4.18: Potential temperature and salinity sections along the western part of the WOCE AR7W line occupied between 4 and 6 March 1997 during R/V *Knorr* cruise 147 (courtesy of R. Pickart). The temperature contour interval is 0.1 °C and the salinity contour interval is 0.01. Isopycnals are shown as dashed lines. The locations of the moorings K1, K2 and K6 are shown as red lines.

sified temperature variability was shorter. Further, the lowest temperatures did not reach the values observed during the first winter.

The vertical velocities measured at 300 m depth at the boundary current moorings K2 and K6 over the winter of 1996/97 and at mooring K12 in 1997/98 are shown in Figure 4.19. At mooring K22 (1998/99) no vertical velocity records were obtained. Figure 4.20 shows the time series of the high–frequency variance of the vertical velocity. The vertical velocity variance at mooring K6 by far exceeds the values observed at the other boundary current moorings (especially during August/September) as well as the vertical velocity variance in the interior Labrador Sea. This is probably because the ADCP was located closer to the surface compared to the other instruments. The record from about 300 m depth is rather comparable to the other observations.

The K2 and K6 vertical velocity measurements both show increased variability over several days by the end of December 1996, but these were symmetrical fluctuations indicating the generation of internal waves in the stratified water column and not associated with local convection. During the remaining winter months of 1997 several periods of enhanced vertical velocity variance occurred at K2 and K6. The amplitudes were comparable to the observations during periods of active convection in the central Labrador Sea, but no period of prevailing downward motion could be identified. Instead, some of the enhanced vertical velocity variance at mooring K2 resulted from spurious upward motion. Moreover, if the peaks in the variance would have been caused in fact by convective plumes, they should be identifiable as distinct downward bursts in the vertical velocity records, because of the characteristic strong downward motion of the plumes and the weaker upward motion inbetween (as seen in typical convection time series, e. g. Figure 4.13).

The vertical velocity records obtained during the winter of 1997/98 at the boundary current

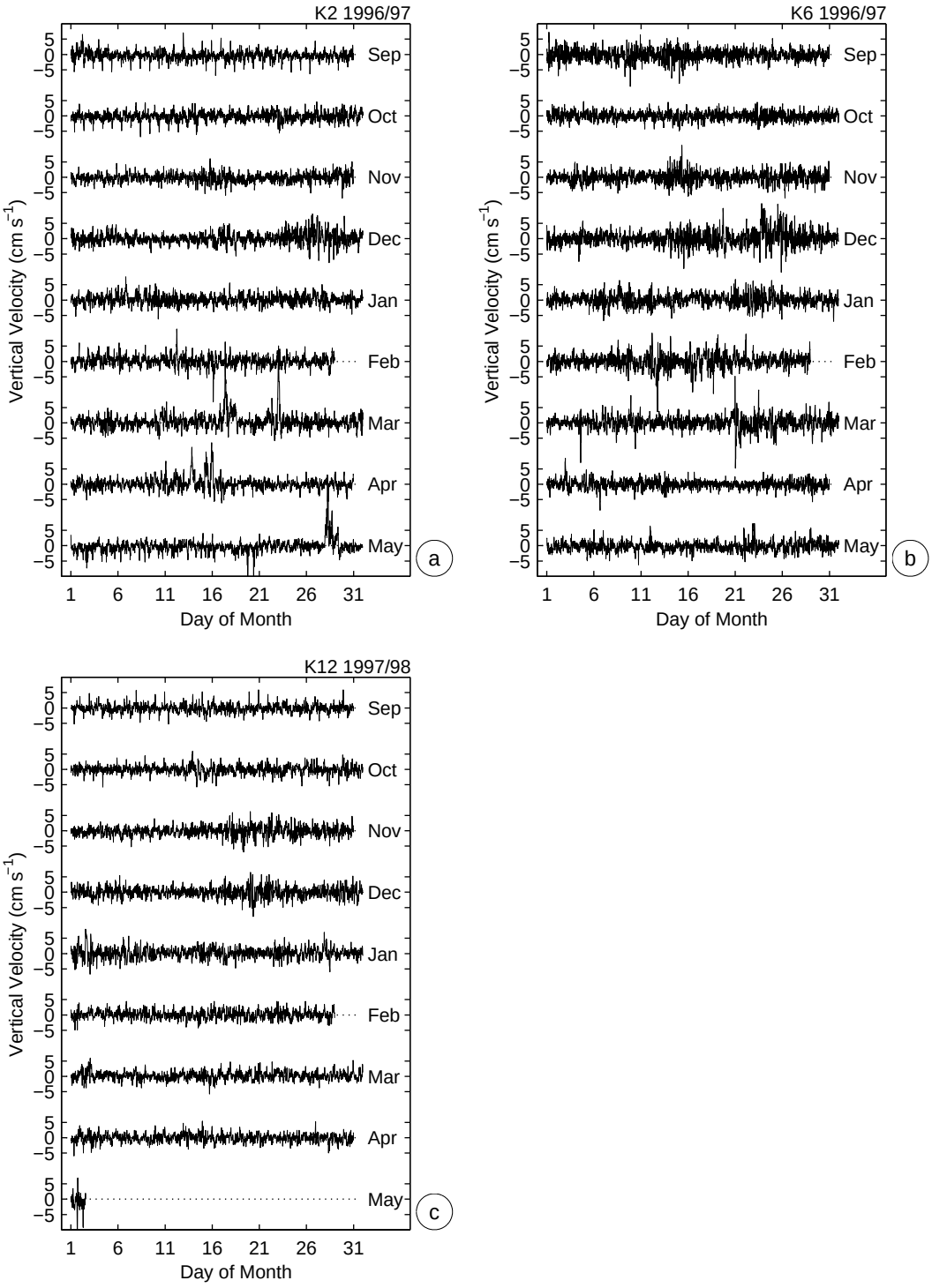


FIG. 4.19: ADCP time series of vertical velocity at 300 m depth in the Labrador Sea boundary current region from the moorings (a) K2 1996/97, (b) K6 1996/97, and (c) K12 1997/98.

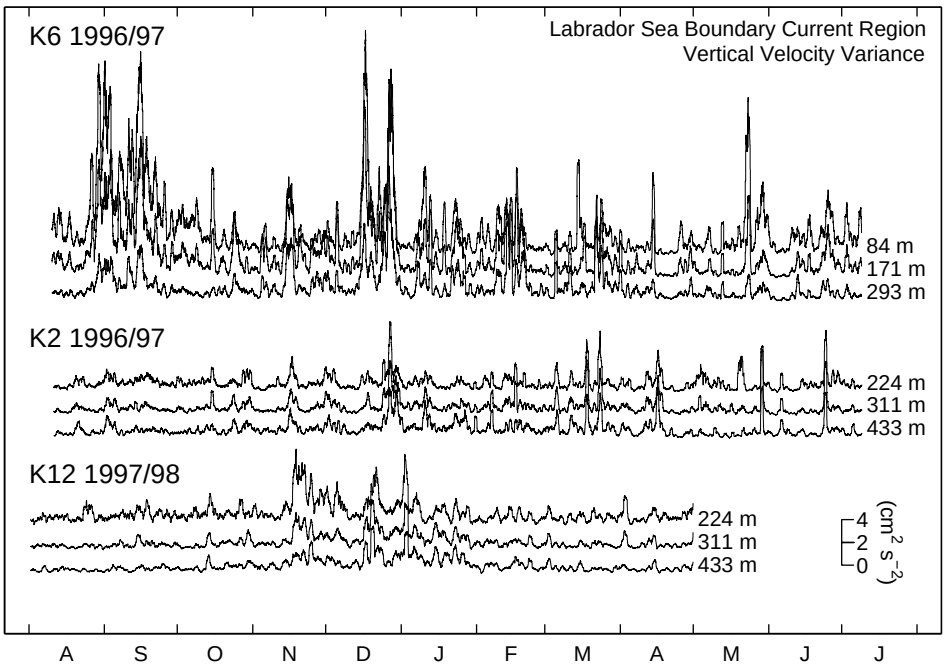


FIG. 4.20: 12-h running mean of variance of high–passed vertical velocity (periods longer than 6 hours eleminated) for selected ADCP bins at the moorings in the Labrador boundary current region.

mooring K12 show similar enhanced high–frequency variance during the early winter months November through January. As in the observations from the previous winter, the fluctuations were symmetrical. They coincided with the development of a shallow mixed layer. During the following winter months the vertical velocity variance decreased and it is clearly visible that no events of downward motion associated with plumes occurred.

A comparison between the water mass properties observed at the central Labrador Sea moorings and at the boundary current moorings is shown in Figure 4.21, for the periods between 1 January and 1 June. Although the scatter is rather large, it is visible that the coldest temperatures in the boundary current are accompanied by lowest salinities. Further, the low temperatures and salinities in the boundary current show a tendency towards the mixed layer properties observed in the interior Labrador Sea during convection. Therefore it appears plausible that the cold anomalies observed at the boundary current moorings during winter are a mixing product between the warmer and more saline water in the boundary current and the colder and fresher water from the interior. This is supported by the close proximity of the mixed patch to the boundary current, as observed during early March 1997 (Figure 4.18).

In summary, it can be said that over the three years of observations in the boundary current region, no evidence for locally occuring convection was found. The vertical velocity measurements revealed only symmetrical fluctuations corresponding to internal waves in conjunction with the

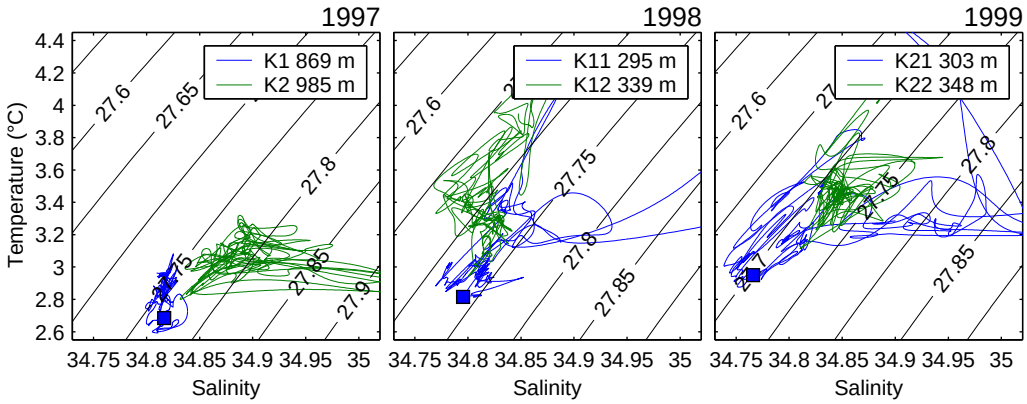


FIG. 4.21: $\theta$/S–scatter from 40–h lowpassed SeaCAT records between 1 January and 1 June from the central Labrador Sea (blue, moorings K1, K11, K21), and from the Labrador Sea boundary current region (green, moorings K2, K12, K22). The water mass properties of the deepest winter mixed layer at the central moorings (Table 4.1) are marked as squares. The unrealistic high salinities that occur sporadically are a result of pressure effects caused by mooring motion, degrading the salinity measurements.

development of a rather shallow mixed layer. Distinct burst of downward motion associated with convective plumes as in the central Labrador Sea were not observed. Instead of a continuous mixed layer deepening, a nearly instantaneous cooling over a large vertical range was observed during all winters and indications were found that this cold and low salinity water can be a result of horizontal mixing with the interior.

Regarding the formation region of the so called upper LSW, it should be noted that the water mass properties of the mixed layer observed in March 1999 at mooring K21 correspond to the properties of the lense of newly ventilated water observed in the Labrador Current by Pickart et al. (1996), indicating the possibility of its formation in the central Labrador Sea during rather mild winters.

# 5. THE VIOLENT MIXING PHASE

The violent mixing phase of deep convection in the open ocean occurs during late winter, usually between February and March. In this chapter the observations of convection, from those winters in the Greenland and Labrador Seas where successfull ADCP measurements were obtained, are analyzed. A particular focus will be on the velocity structures during periods of strong vertical mixing.

## *5.1 Observed Convection Periods*

### *5.1.1 Greenland Sea*

#### *Winter 1988/89*

The observations of deep convection at the moored stations in the central Greenland Sea during the winter of 1988/89 were discussed in detail by Schott et al. (1993). They are summarized here for the sake of completeness and comparison with the observations obtained in the following winters.

Figure 5.1 shows time series of potential temperature and vertical velocity from January to April 1989 and the corresponding total surface buoyancy flux (NCEP/NCAR reanalysis). The firm ice coverage in the central Greenland Sea ended on about 23 – 25 January with the opening of the ice free bay, Nordbukta, and the mixed layer was subject to uninsulated atmospheric forcing for the remaining winter. By then, the mixed layer depth was of about 120 m thickness and its temperature was close to the freezing point. After February 1 the near surface temperature rose to about -1.4 °C and at the 347 m level the temperature variability increased. Some enhanced variance of the vertical velocity appeared during this period, but without dominant downward motion.

The next phase of intensified mixing occurred between 10 and 16 February. It was associated with slight warming at the 60 m level and increased temperature fluctuations at 347 m. The most intense downward motion of this record took place, with vertical velocities of up to 8 cm $s^{-1}$. During the following period of intensified surface forcing and vertical velocity fluctuations, between 2 and 9 March, the temperature recorded at 1345 m decreased significantly for two short periods on 6 and 8 – 9 March, but no total homogenization could be observed. The near surface temperature stayed colder during and after these events. On 16 March a further event of downward motion exceeding 3 cm $s^{-1}$ took place, associated with a temperature drop at the 347 m sensor.

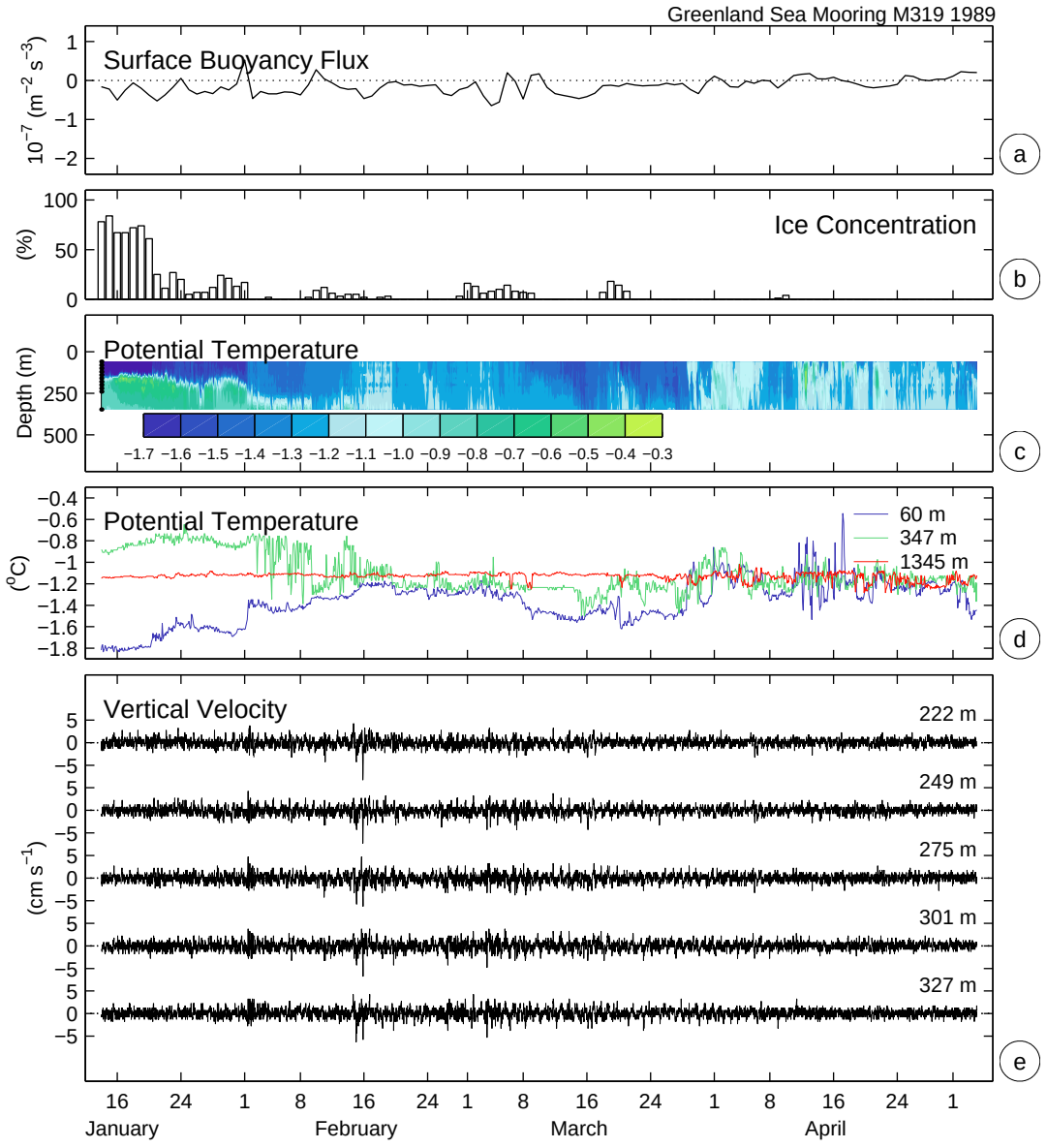


FIG. 5.1: Time series of (a) daily total surface buoyancy flux as derived from NCEP/NCAR reanalysis data, (b) SSM/I ice concentration (courtesy L. Toudal), (c) potential temperature contours with the depths of the sensors indicated as dots on the left hand side, (d) potential temperature at selected depths, and (e) vertical velocity at selected depths at Greenland Sea mooring M319 from mid–January to the beginning of May 1989.

*Winter 1990/91*

During the winter of 1990/91 an Is Odden developed in the second half of January (Figure 3.9), but the location of mooring GSM2 stayed nearly ice free until the beginning of February. The only instrument recovered from this mooring was the ADCP at 320 m, thus only little temperature observations are available from this winter (Figure 5.2).

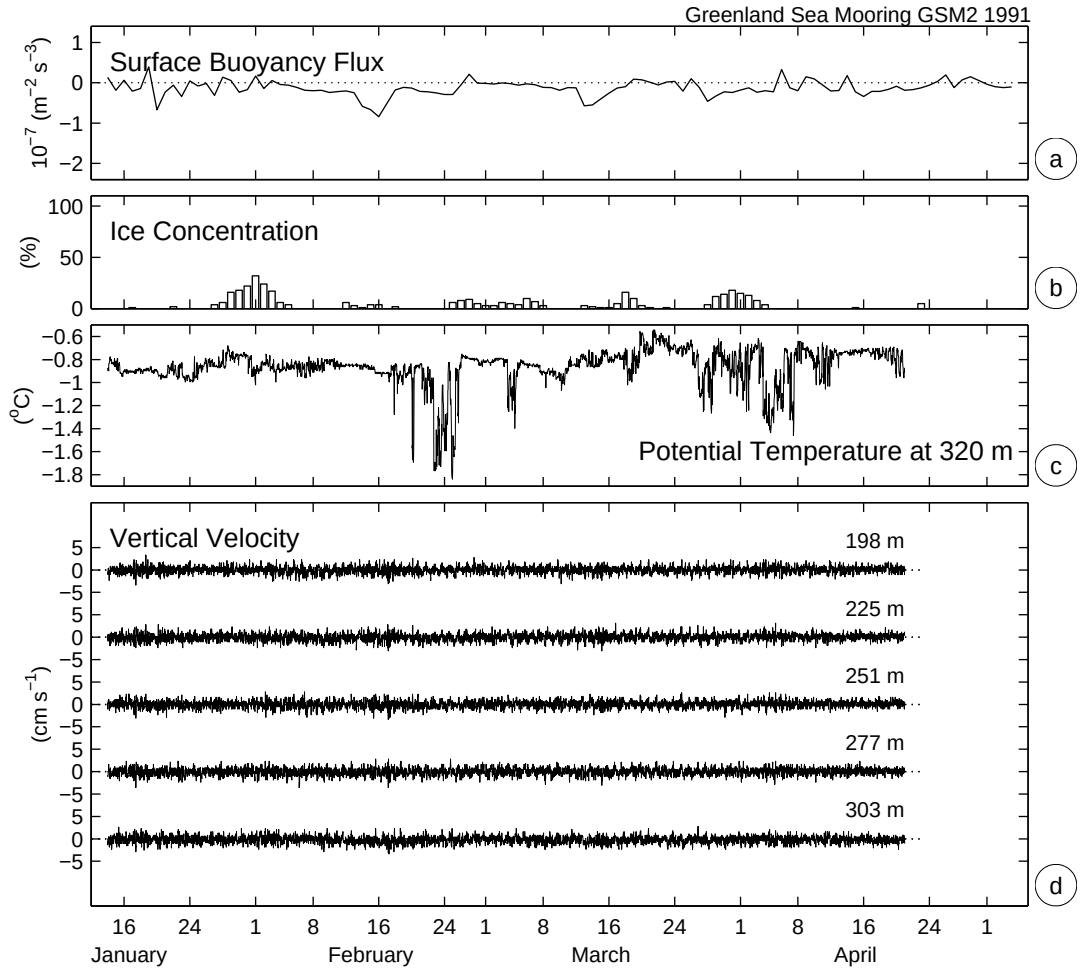


FIG. 5.2: (a) NCEP/NCAR reanalysis daily total surface buoyancy flux, (b) SSM/I ice concentration (courtesy L. Toudal), (c) potential temperature at 320 m, and (d) vertical velocity at selected depths at Greenland Sea mooring GSM2 from mid–January to mid–May 1991.

Until mid–February the temperature at 320 m stayed relatively constant at about -0.9 °C, indicating a shallow mixed layer. An event of strong surface forcing occurred between 14 and 17 February. It was accompanied by slightly enhanced vertical velocity fluctuations, the downward motions reached 3 – 4 cm s$^{-1}$. The ice concentration was rather low during this period, but not zero, thus local ice formation has probably occurred.

A couple of days later, around 22 February, the temperature decreased rapidly by about 0.7 °C to near freezing point values and its variability increased over a few days. The ice concentration increased slightly. As neither enhanced variability appeared in the vertical velocity records nor strong surface forcing took place, the increased temperature variability reflects lateral inhomogeneities.

The remaining winter showed two further cycles of ice formation, corresponding with increased surface forcing, and subsequent melting, as well as periods of increased temperature fluctuations. Further periods of enhanced vertical velocity fluctuations are not identifiable.

*Winter 1992/93*

The measurements obtained during the winter of 1992/93 at mooring GSM3 (Figure 5.3), show similar sparse mixing activity as those from the previous winter. By mid–January the temperature at 58 m was at about -1.3 °, well above the freezing point. The satellite observations show low ice concentrations in the area. Thus the base of the mixed layer must have been well above the topmost sensor, if ice was formed locally.

Towards the end of January the near–surface temperature dropped below -1.8 °C and its variability increased, indicating the incorporation of the 58 m level into the mixed layer. An Is Odden developed during this period, but the Nordbukta remained open with low ice concentrations. The lowest mixed layer temperature was found on 18 February at the beginning of a period of slightly enhanced ice concentration. Considerable vertical velocity fluctuation corresponding to vertical mixing was found only between 22 and 26 February during this winter. The downward motion was of 3 – 4 cm $s^{-1}$ in the upper ADCP records. During this period the mixed layer temperature increased from near freezing point values to about -1.2 °C and the temperature at 346 m dropped to slightly higher values. The ice in the area of the mooring location nearly vanished. A possible reason for the weak vertical velocity activity is that the ADCP was located at a depth of 570 m, while the mixing events occurred only in the upper 350 m, thus barely in the instrument range.

After this short event of vertical mixing, the temperature decreased again until 17 March where it returned to values of about -1.8 °C. This cooling period was only interrupted by a short warming and nearly homogeneous conditions in the upper 350 m around 5 March. The temperature fluctuations at 346 m were high during this period, showing the incomplete mixing as lateral inhomogeneities pass the mooring.

From 17 March onwards, the near–surface temperature increased again to about -1.2 °C on 22 March. Afterwards it returned to low values of about -1.7 °C by 28 March. At the end of the time series the lowest temperature of the record was observed at the 346 m level, collapsing with the 58 m record for a short period. At the same time weak indications of vertical mixing appeared at the 572 m level. A CTD survey along 75 °N showed deep mixing to 600 and 1000 m at two stations, one east and one west of the mooring, in early April (Lherminier et al., 1999).

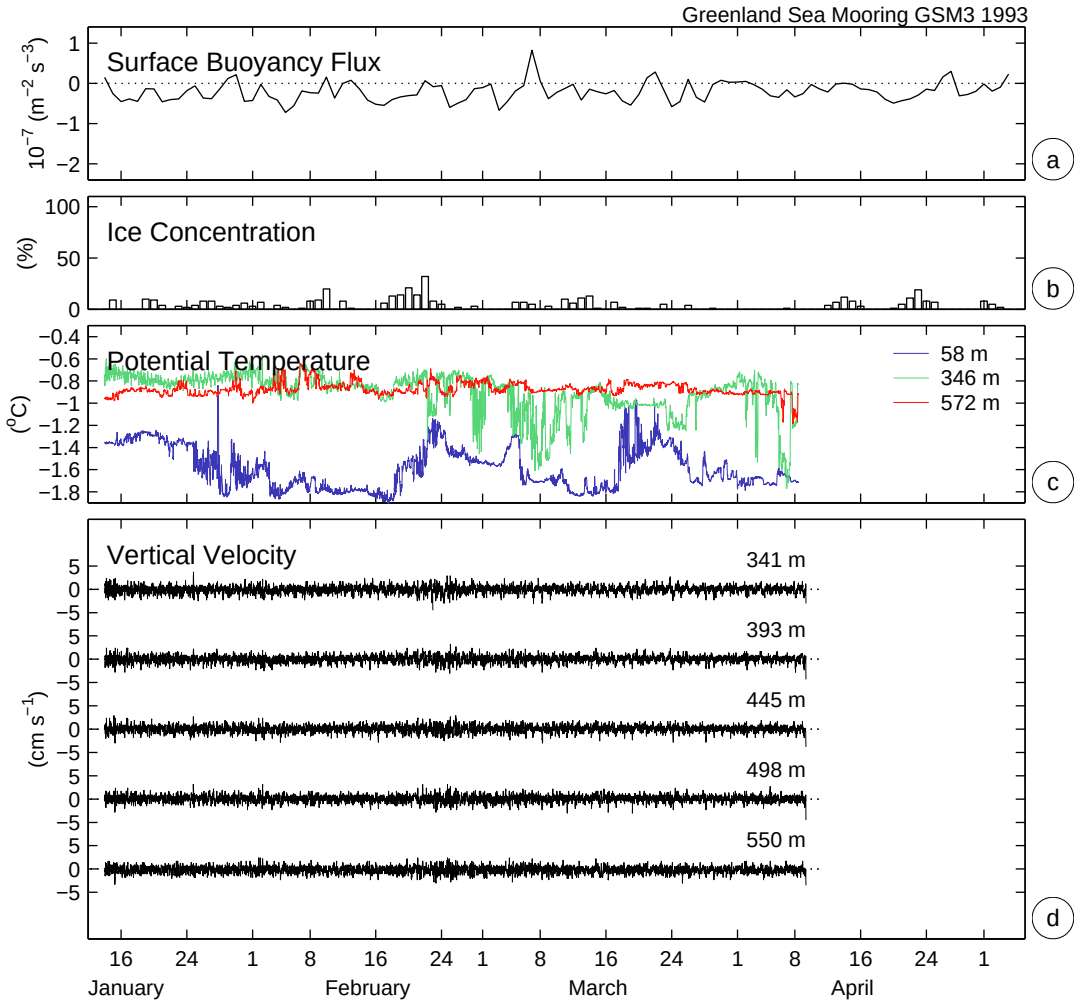


FIG. 5.3: (a) NCEP/NCAR reanalysis daily total surface buoyancy flux, (b) SSM/I ice concentration (courtesy L. Toudal), (c) potential temperature at selected depths, and (d) vertical velocity at selected depths at Greenland Sea mooring GSM3 from mid–January to the beginning of April 1993.

### *Winter 1994/95*

A striking characteristic of the winter of 1994/95 was the complete absence of sea ice in the central part of the Greenland Sea. Further, the surface buoyancy loss showed exceptional high values of nearly $1 \times 10^{-7}$ m$^2$ s$^{-3}$, compared to the typical $0.5 \times 10^{-7}$ m$^2$ s$^{-3}$ of the previous winters (Figure 5.4). Enhanced downward motion and a deepening of the mixed layer to below 600 m occurred already in early February.

An expanded view of the vertical velocity and temperature observations between 4 and 9 February is shown for selected depths in Figure 5.5, together with the corresponding means and standard deviations. The upper temperature records show that convection reached the 687 m level, while the

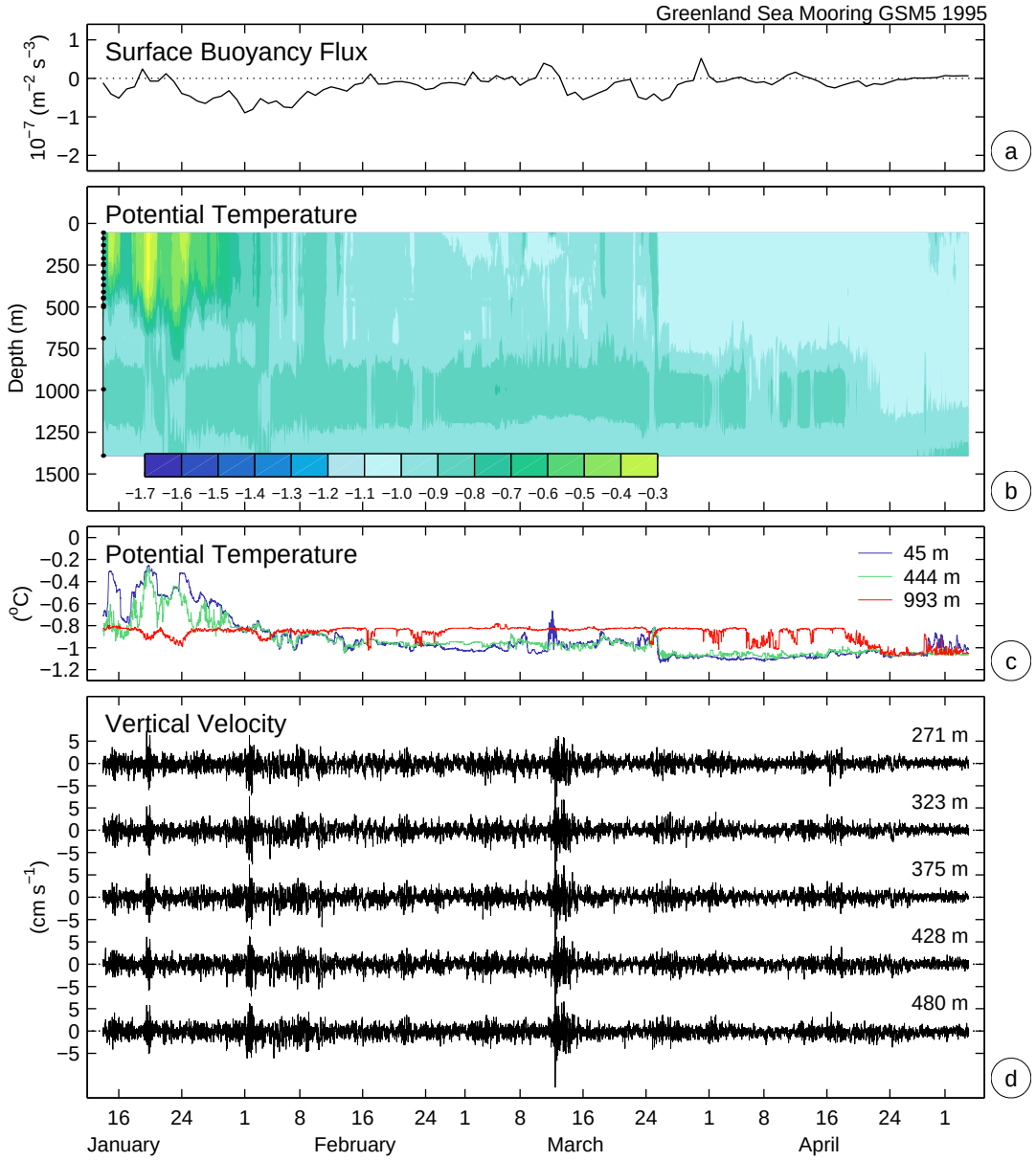


FIG. 5.4: (a) NCEP/NCAR reanalysis daily total surface buoyancy flux, (b) potential temperature contours with depths of the instruments indicated as dots on the left hand side (the contour interval is 0.1 °C), (c) potential temperature at selected depths, and (d) vertical velocity at selected depths at Greenland Sea mooring GSM5 from mid–January to the beginning of May 1995. Ice concentration is not shown, as the central Greenland Sea was completely ice free during the whole winter.

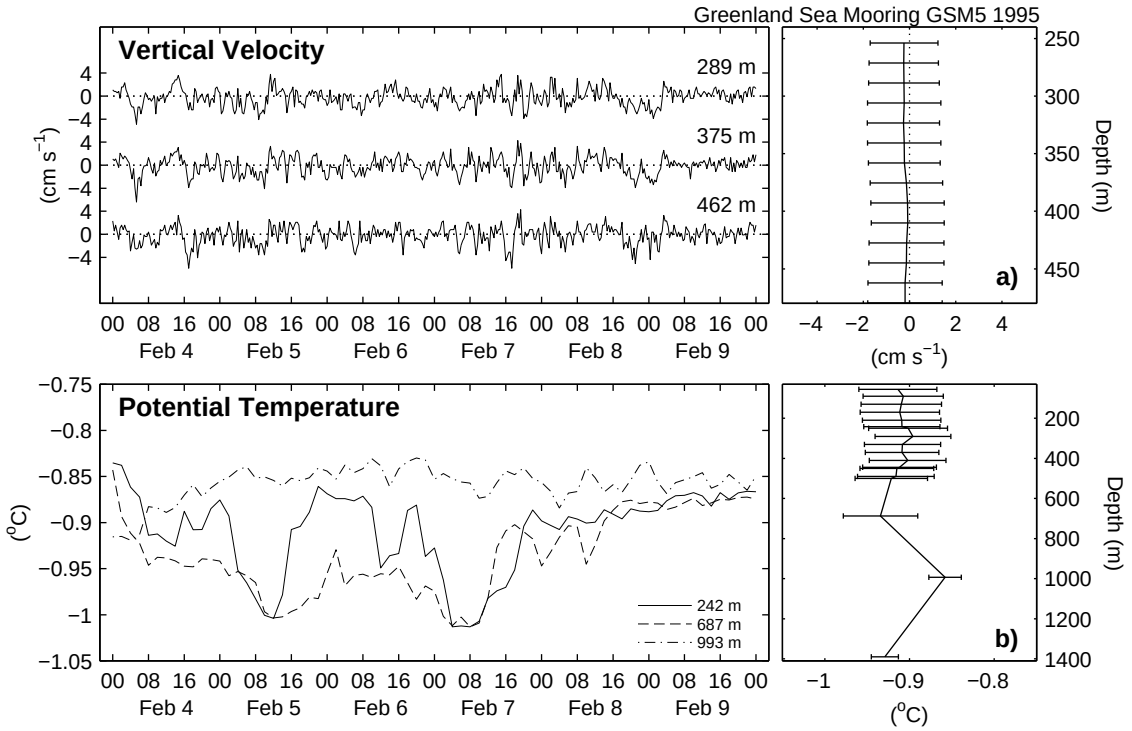


FIG. 5.5: Time series of vertical velocity (a) and potential temperature (b) at Greenland Sea mooring GSM5 during the convection period of 4–9 February 1995. The right hand side graphs show the corresponding mean profiles and the standard deviation as bars.

underlying level at 993 m was not affected and stayed relatively warm during this period.

Between 16 February and 11 March the surface forcing was weak and the temperature in the upper 600 m stayed nearly constant. Large temperature fluctuations as in the previous winters were not observed, indicating that the early mixing of the upper water column was probably more complete, leaving only small horizontal inhomogeneities.

The next period of strong surface forcing was during 11 – 16 March. Extremly high fluctuations of vertical velocity occurred, but they may partly result from the continuous sampling mode of the ADCP (Appendix A.2). Considerable cooling or deepening of the mixed layer did not take place. Further cooling of the mixed layer below -1 °C occurred during the last forcing period from 23 to 27 March. Subsequently the temperature variability at the 993 m level increased and the temperature reached mixed layer values by the end of April. The vertical velocity variability increased slightly between 16 and 22 April, although the surface forcing was rather weak.

### 5.1.2 Labrador Sea

#### Winter 1994/95

The cycle of preconditioning, deep convection, and restratification as observed at the Labrador Sea mooring *Bravo* in combination with PALACE float data during the winter of 1994/95 is discussed at length in Lilly et al. (1999). The period of deep mixing is summerized here for comparison with the later observations from 1997 to 1999.

Time series of total surface buoyancy flux (NCEP/NCAR reanalysis), potential temperature, and vertical velocity from January to April 1995 at mooring *Bravo* are shown in Figure 5.6 (the figures dealing with the observations in the following winters are all shown on the sames scale for comparison). Two periods of intense vertical mixing (24 February to 1 March and 4 – 9 March) are shown as an expanded view in Figure 5.7.

Cold mixed layer water appeared at the topmost sensor by 8 January during a period of strong cooling, but the mixed layer depth remained fairly constant until the end of January. High frequency temperature fluctuations occurred at the 260 m level between 18 and 22 January and between 23 and 27 January. Afterwards the temperature returned to its early January level. Between 1 and 8 February the temperature variability at 260 m increased again and the temperature often dropped below 2.4 °C. During the same period the temperature at the next deeper sensor (510 m) rised to about 3.2 °C, which is the value previously found at 260 m. This slight warming is also visible at the deeper levels down to 1260 m.

First signs of downward motion appeared around 9 February in the vertical velocity records. This coincided with cooling at 510 m and warming at 210 m through entrainment of warmer water from below. Temperature fluctuations were high at 510 m between 10 and 23 February denoting the incorporation of this level into the mixed layer. Small events of downward motion are visible on 17 and 18 February. After the homogenization of the upper 500 m the number of captured vertical velocity events increased drastically between 24 February and 1 March (Figure 5.7a). On 27 February the mixed layer temperature increased rapidly from 2.6 °C to 3 °C, probably due to horizontal inhomogeneties. Immediately afterwards the 260 m temperature started decreasing again, but towards values below the previous mixed layer temperature, while at the 510 m level the temperature remained high. The active mixing continued during this restratification period, as visible in the vertical velocity and temperature fluctuations (Figure 5.7a, b). The restratification period lasted until 2 March.

Between 3 and 9 March the mixed layer rapidly deepened to the 1260 m level and its temperature reached 2.67 °C. The highest vertical velocities of this winter occurred during this period. After 10 March again some restratification occurred, but only at the deeper levels. Throughout the rest of March sporadic events of vertical mixing occurred. The deepest mixed layer of about 1800 m was found around 24 March. Afterwards the mixed patch collapsed rapidly, manifested

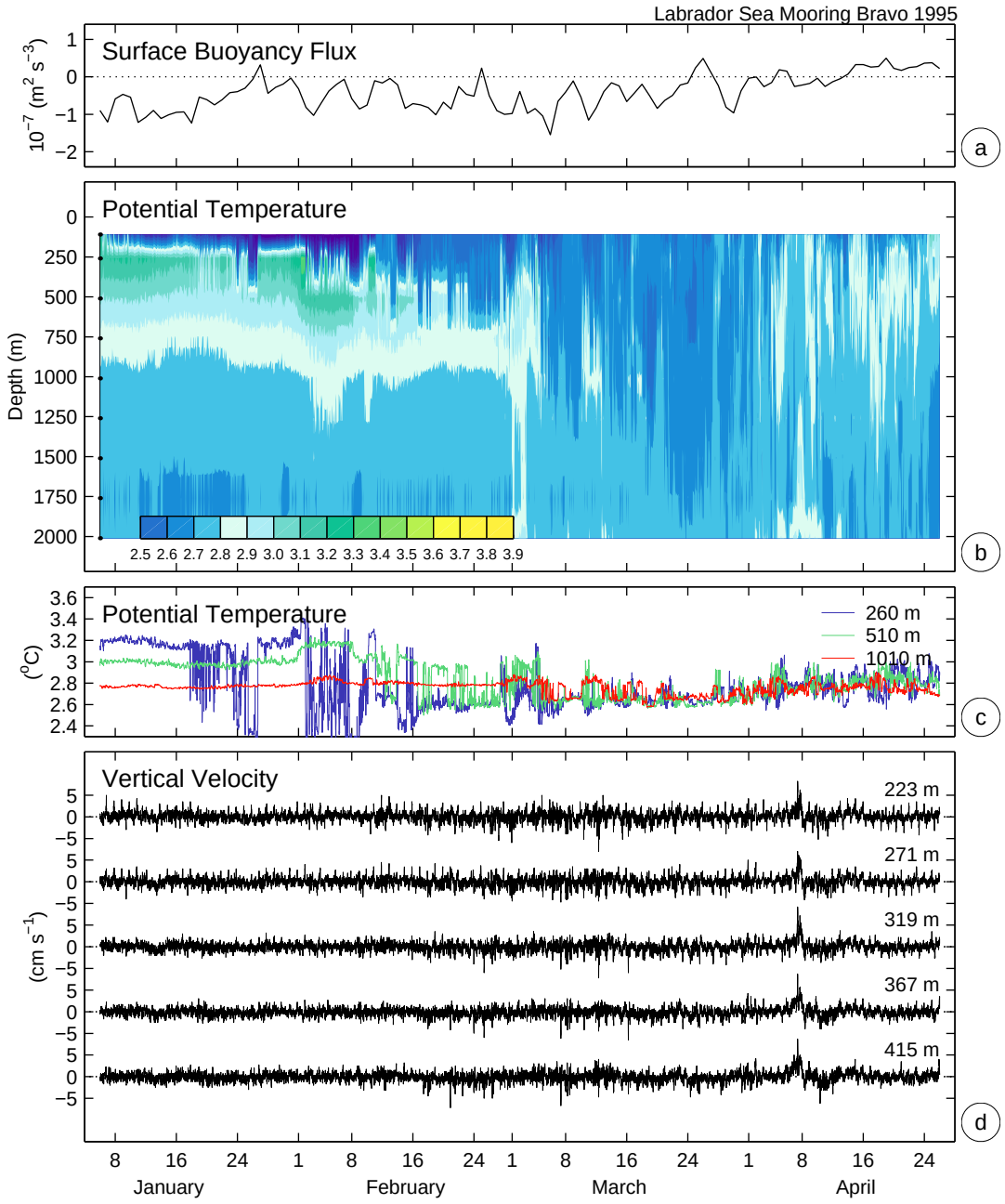


FIG. 5.6: Time series of (a) NCEP/NCAR reanalysis daily total surface buoyancy flux, (b) potential temperature contours with the depths of the sensors indicated as dots on the left hand side, (c) potential temperature at selected depths, and (d) vertical velocity at selected depths at Labrador Sea mooring *Bravo* from January to April 1995 (temperature data courtesy of J. Lazier and P. Rhines).

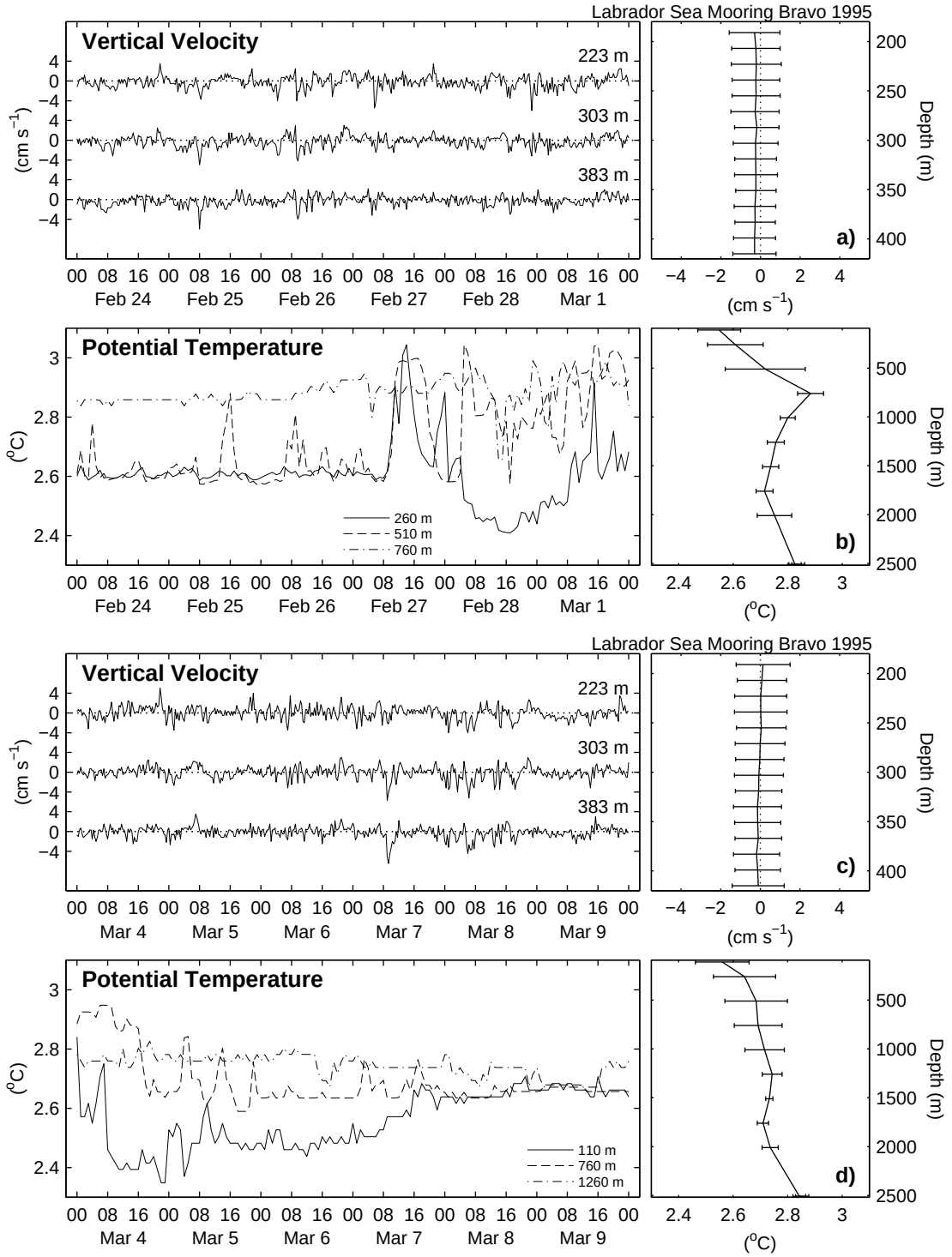


FIG. 5.7: Time series of vertical velocity (a, c) and potential temperature (b, d) at Labrador Sea mooring *Bravo* for the convection periods of 24 February to 1 March and 4 – 9 March 1995. The right hand side graphs show the corresponding mean profiles and the standard deviation as bars. (temperature data courtesy of J. Lazier and P. Rhines).

through increased temperature variability at all instrument levels.

*Winter 1996/97*

The meteorological conditions during the winter of 1996/97 showed a dramatic transition of the flow regime over the North Atlantic which resulted in a significant change in the magnitude of surface forcing in the Labrador Sea region. Until mid–January the presence of a blocking high over Europe and anomalously high pressure over Greenland caused a significant westward shift of cyclonic activity with the effect of rather low heat loss over the Labrador Sea. In contrast, February 1997 was a month in which the circulation pattern over the North Atlantic was significantly stronger than average, resulting in strong heat loss over the Labrador Sea (The Lab Sea Group, 1998). As a consequence, the buoyancy flux dropped from even positive values in early January to large negative values at the beginning of February (Figure 5.8a). The remaining winter was characterized by the highest buoyancy fluxes occurring over the whole observation period.

With the surface forcing increasing from mid–January onwards, the temperature at 75 m started to decrease from about 3 °C to 2.6 °C at the beginning of February (Figure 5.8c). The large temperature fluctuations around 24 February denote the passage of a cold–core eddy, causing the mooring to be towed down which brought the topmost sensor sporadically into the warmer Irminger Sea Water below the mixed layer. After 2 February, the temperature variability increased at the 425 m level and a few days later also at the 869 m level, both temperatures oscillated between warmer values and the background temperature.

The first plume activity appeared in the vertical velocity records around 10 February (Figure 5.8d), coinciding with the incorporation of the 425 m level into the mixed layer. A 14–day period of intense vertical mixing followed, during which the mixed layer deepened to 770 m. An expanded view of the period from 18 – 24 February is shown in Figure 5.9a, b. During this period the temperature at the upper 500 m stayed fairly homogeneous, while large variability occurred at the three temperature sensors below, showing the deepening of the mixed layer.

On 22 February the surface forcing weakened and arrived at an intermediate minimum on 24 February. There still occurred sporadic events of downward motion, but the homogeneity of the mixed layer down to 770 m lasted only for a few hours. Although the surface buoyancy loss increased from day to day immediately after 24 February, warming occurred at the mooring location through horizontal mixing until 1 March.

The first nine days of March show reinforced surface fluxes, which (although weaker than during the event in February) caused numerous plume events, the most impressive sequence of downward motion of all records (Figure 5.9c). The mixed layer deepened rapidly from 770 m to 1080 m, and for a few hours on 7 March low temperatures of about 2.6 °C appeared at the 1280 m sensor.

Between 4 and 20 April, low temperatures appeared over the whole instrument range, much

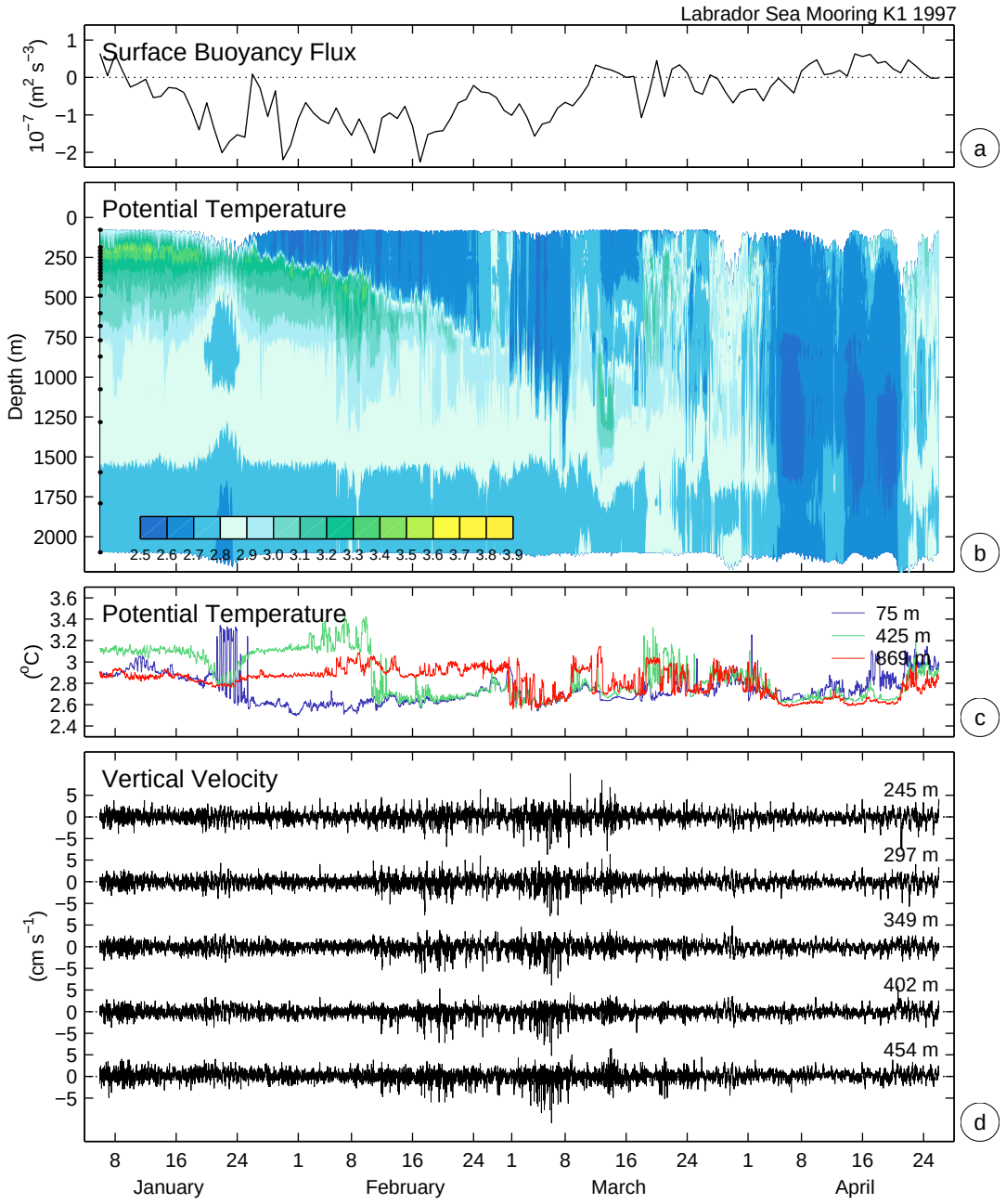


FIG. 5.8: Same as Figure 5.6 at Labrador Sea mooring K1 from January to April 1997.

deeper than the convection observed at the mooring location and deeper than the mixed patch mapped during the R/V *Knorr* cruise (The Lab Sea Group, 1998). The event occurred in several pulses, clearly not related to active convection at the mooring location. Neither do the vertical velocity records show any intense downward motion, nor did any significant surface cooling occur,

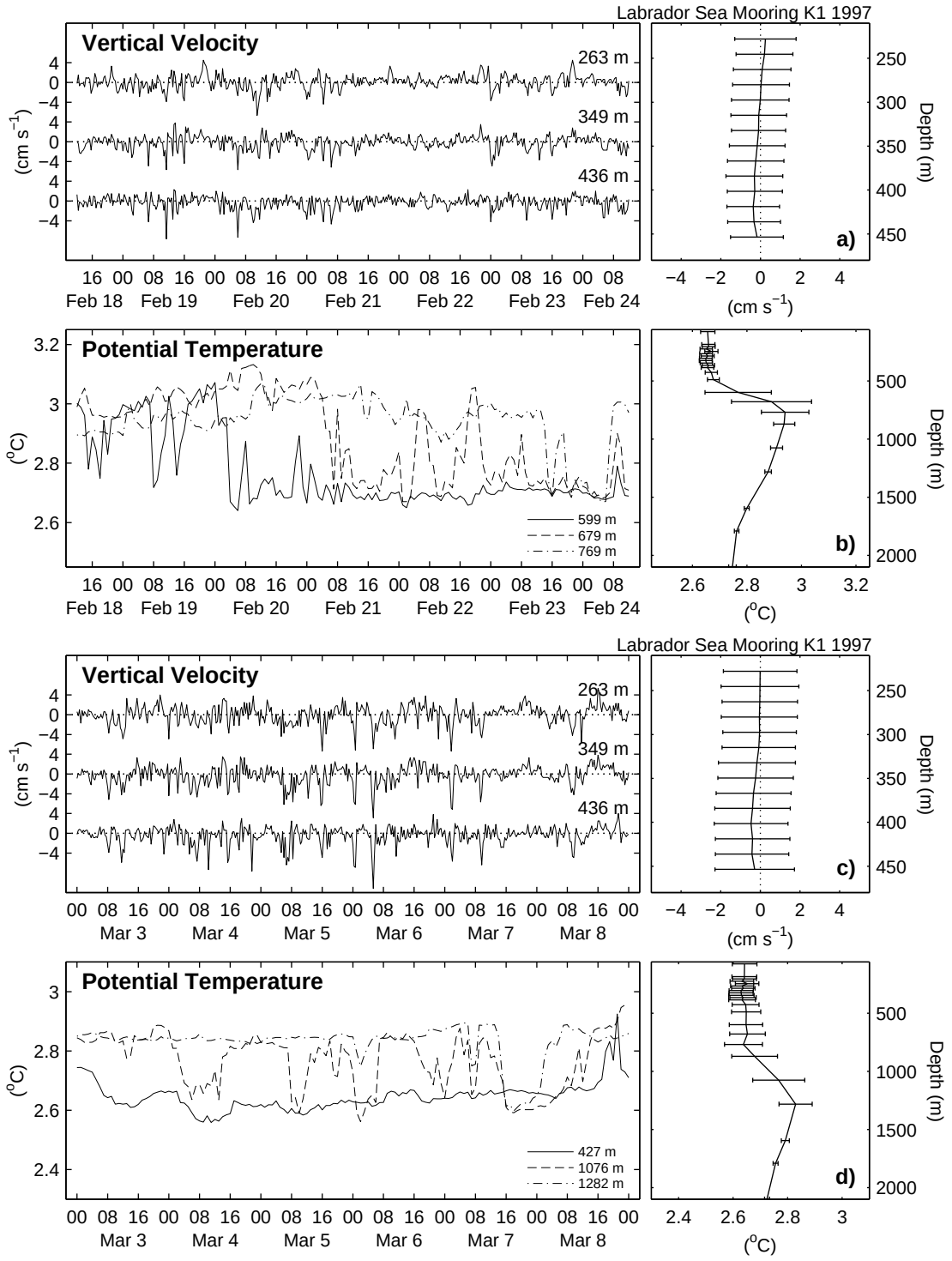


FIG. 5.9: Same as Figure 5.7 for the periods of 18–23 February and 3–8 March 1997 at Labrador Sea mooring K1.

as the cooling season had already ended. The coldest temperatures (below 2.6 °C) were found between 750 and 1750 m. The high–resolution temperature time series (Figure 5.8c) show that the water column was less homogeneous during these events than during the period of active convection at the beginning of March.

A possible explanation could be, that convection to below 1300 m might have occurred in the cold–core eddies observed in early winter, as suggested by Legg et al. (1998). The reduced vertical stability in the interior of such an eddy would allow deeper convection and its cyclonic rotation would efficiently trap the cold water inside, subsequently being advected past the mooring.

*Winter 1997/98*

At the beginning of January 1998, the near–surface temperatures at mooring K11 were relatively high compared to the previous winters, but dropped sharply around 8 January, indicating that the warm water was advected away from the mooring location (Figure 5.10). Another advective event was observed between 17 and 22 February, this time a cold–core eddy with minimum temperatures below 2.8 °C at 1300 m depth.

Several events of surface cooling occurred during the last week of January but the temperature at 76 m decreased only slowly. The next event of strong surface forcing occurred between 4 and 13 February. During this period the mixed layer deepened below 300 m, while its temperature stayed relatively constant at about 2.9 °C. For the following 13 days the temperatures at 76 and 300 m overlaid each other, with some warming between 14 and 16 February. The next cooling period was from 17 to 26 February and a number of downward motion events is visible in the vertical velocity records (Figure 5.10c).

This first period of moderate mixing activity was followed by two weeks of relatively calm conditions until 14 March. The temperature fluctuations at 300 m increased drastically during this period, and also the deeper levels show warming and high–frequency temperature fluctuations. Although the cooling weakened, the lowest near–surface temperatures (below 2.8 °C) occurred during this period. The high–frequency fluctuations quickly ceased after strong surface forcing set in on 14 March.

The period of intense surface forcing lasted for nine days until 22 March, with two days of relatively calm conditions inbetween. After a number of short events where increasing cold temperatures appeared at 550 m, the mixed layer deepened below this level on 20 March (Figure 5.11), while the next deeper level stayed unaffected. Although weaker than during the previous winters, a number of downward velocity events, of typically 3 – 4 cm $s^{-1}$, were measured during this period.

From 26 March onwards, strong horizontal mixing set in as indicated by the temperature fluctuations. On 6 and 9 April convectively generated water appeared for short periods at the 814 m sensor, but no corresponding vertical velocity was observed and the buoyancy flux was positive. Therefore deeper convection had probably occurred in the vicinity of the mooring.

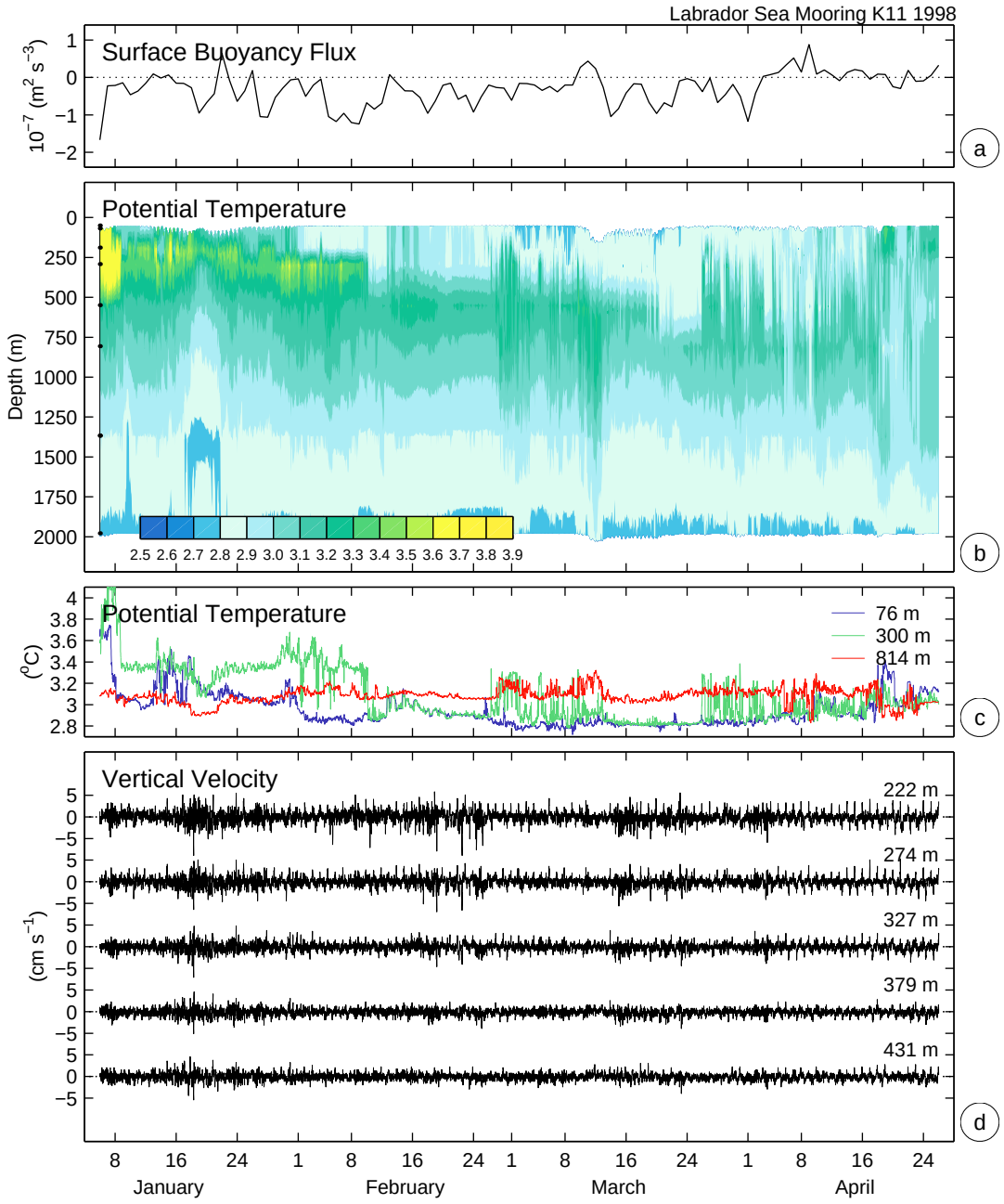


FIG. 5.10: Same as Figure 5.6 at Labrador Sea mooring K11 from January to April 1998.

*Winter 1998/99*

During the winter of 1998/99, strong surface forcing occurred in early January, and mixing below 290 m took place at the location of mooring K21 by 18 January (Figure 5.12). Thereafter the stratification was partly restored through major advection of warm water. After the advective event

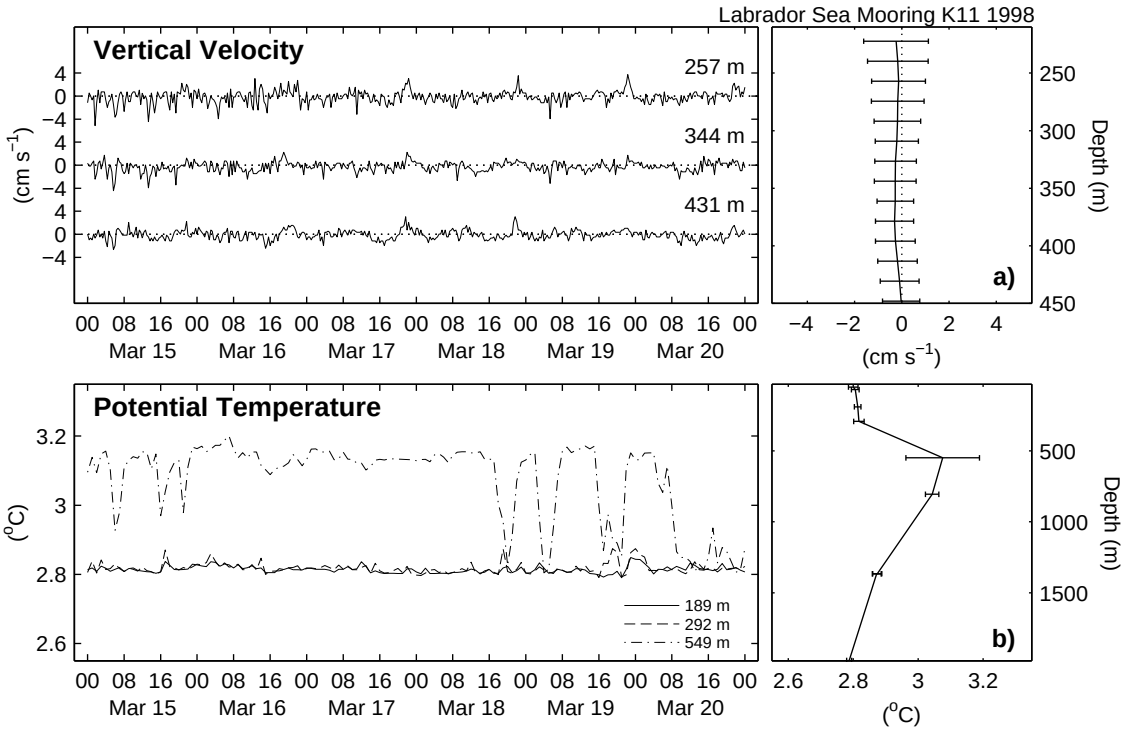


FIG. 5.11: Same as Figure 5.7 for the period of 15–20 March 1998 at Labrador Sea mooring K11.

had passed, the mixed layer was about 0.1 °C warmer and with 250 m depth also shallower than before.

Large buoyancy loss between 25 January and 4 February deepened the mixed layer again to about 300 m and its temperature decreased below 3 °C. During the following weeks, until 1 March, the mixed layer depth oscillated between 200 and 300 m. The near–surface temperature decreased slowly to about 2.8 °C, while several warming events were observed at the deeper instruments. Although the vertical velocity records are much noisier compared to the previous deployments, a number of downward motion events could be identified by the end of February (Figure 5.13). Sporadic events of decreasing temperature at the 560 m sensor, but without corresponding velocity signals, show that convection happened to mix the water column somewhat deeper in the vicinity of the mooring, as during the previous winter. Indeed, some profiles obtained with the moored CTD profiler at mooring K20 by the end of March indicate vertical mixing to 800 – 900 m depth (Figure 4.2).

The restratification in April 1999 was the most intense of all observations, as warm water of about 4 °C invaded the upper 500 m. As a consequence of the mainly barotropic flow, the mooring was towed down several times by hundreds of meters. On 2 April the top of the mooring went down to about 800 m.

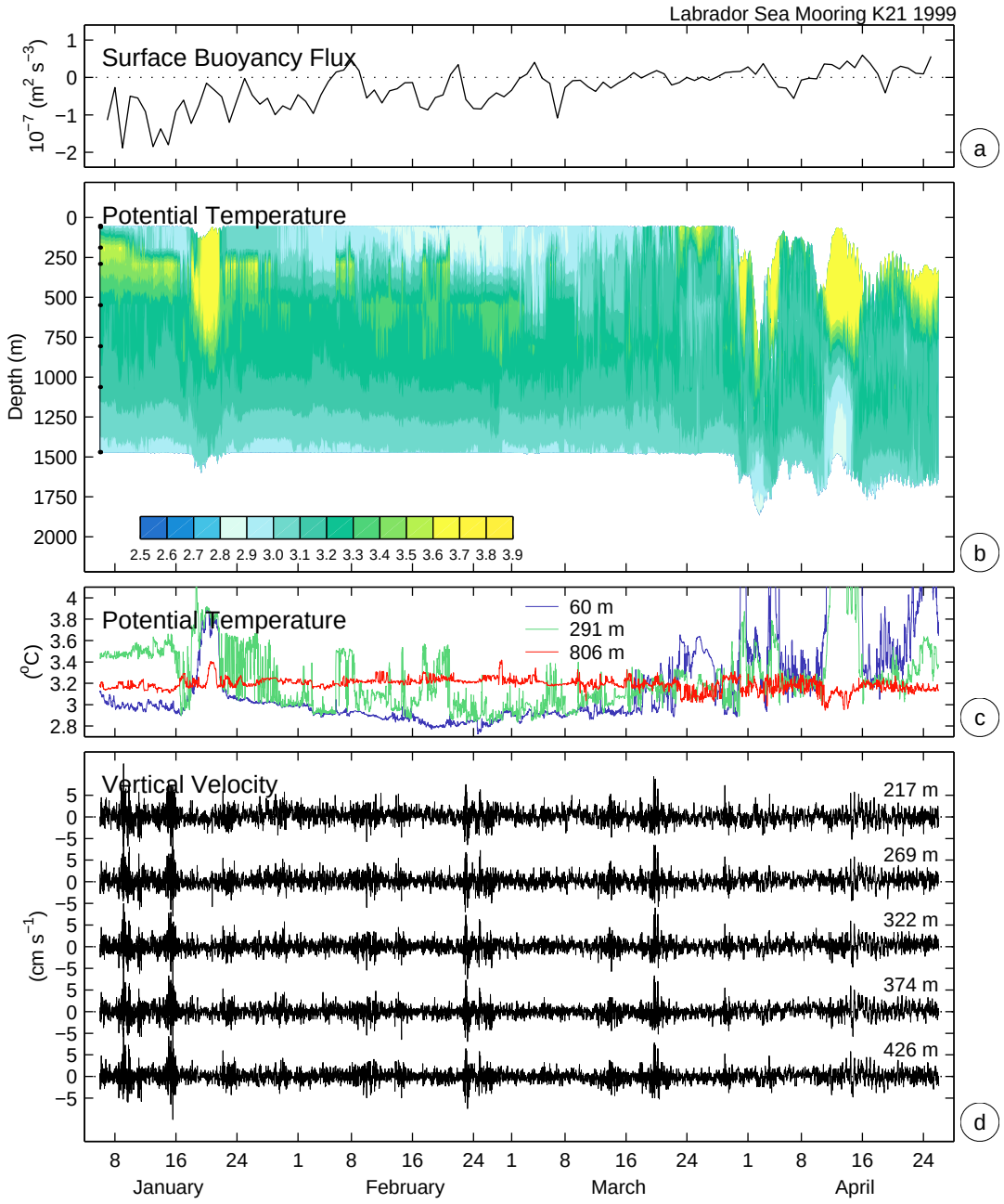


FIG. 5.12: Same as Figure 5.6 at Labrador Sea mooring K21 from January to April 1999.

### 5.1.3 Summary

In the Greenland Sea, convection together with substantial downward motion was observed only during the winters of 1988/89 and 1994/95. In March 1989 vertical mixing occurred to below 1300 m and in April 1995 a maximum mixed layer depth of about 1000 m was observed. The

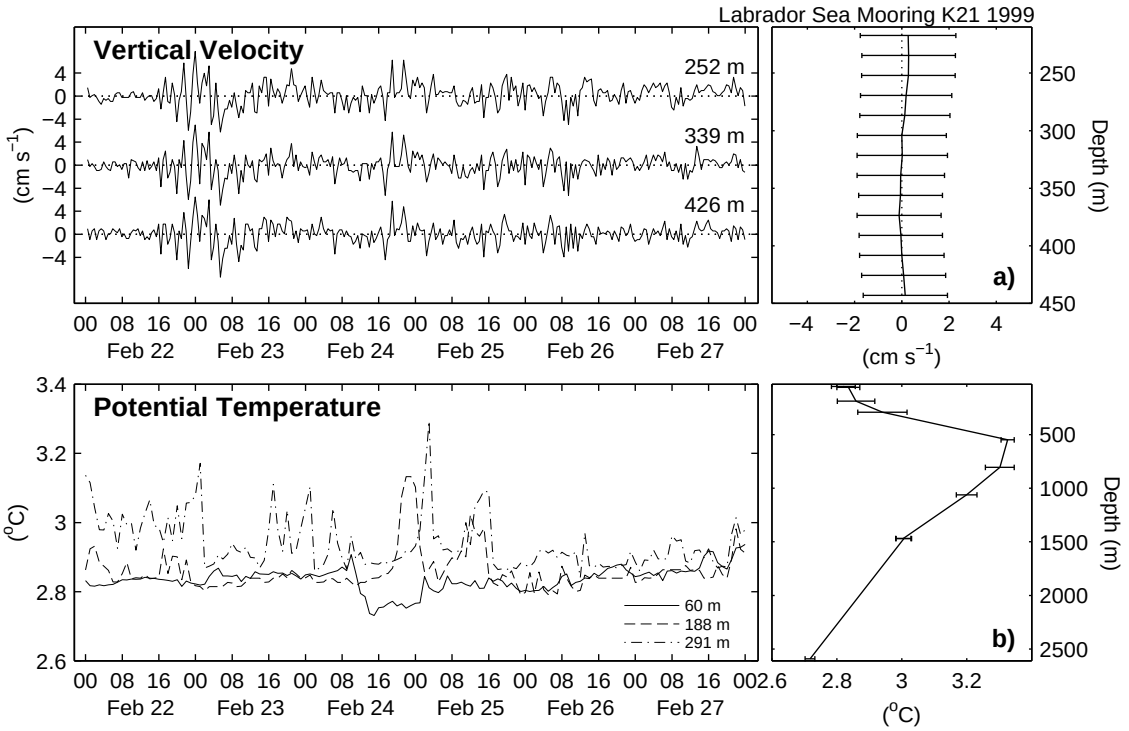


FIG. 5.13: Same as Figure 5.7 for the period of 22–27 February 1999 at Labrador Sea mooring K21.

winters of 1990/91 and 1992/93 showed only minor events of enhanced downward motion. A fundamental difference between the winters of 1988/89 and 1994/95 was the total absence of sea ice in the central Greenland Sea during winter. While in 1988/89 brine release through ice formation and subsequent ice export contributed to the buoyancy loss (Visbeck et al., 1995), the convection in winter 1995 was purely driven by air–sea fluxes.

In the Labrador Sea, the convection was deepest during the winter of 1995, while the surface buoyancy loss and the intensity of the vertical velocity events was largest during the winter of 1997. The convection activity was less intense during the last two winters, but still a small number of downward motion events were found in the vertical velocity records.

Cooling and deepening of the mixed layer often occurred concurrently to warming and increasing temperature fluctuations at the deeper instruments. This may be an indication of squeezing of the water column and the generation of anticyclonic vorticity below the deepening mixed layer. Nothing similar was observed in the Greenland Sea temperature records.

Violent mixing and lateral exchange between the convection site and the surroundings often occurred concurrently, but nevertheless horizontal mixing is most pronounced after the vertical mixing ceased.

## 5.2 Individual Plumes Events

To determine the physical properties, like vertical velocity and horizontal scale, of individual convection cells, the ADCP vertical velocity records obtained at the convection moorings were carefully inspected for the periods of plume events by eye. Examples of vertical velocity patterns that could be addressed to plume events are shown in Figure 5.14 for some of the convection moorings.

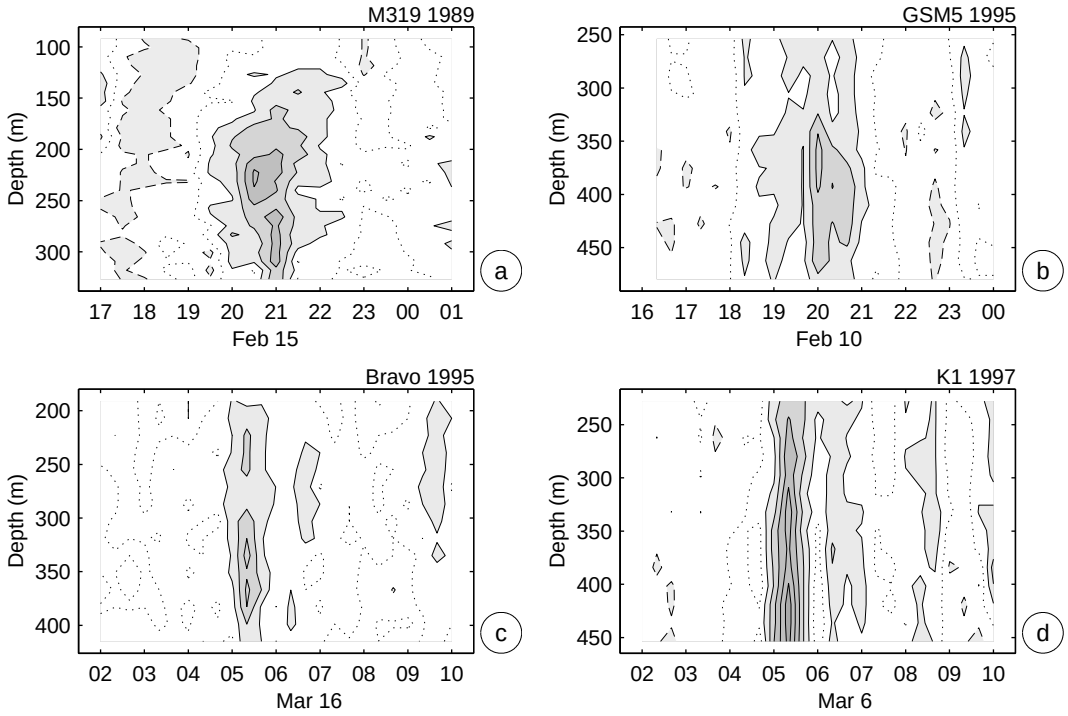


FIG. 5.14: Example vertical velocity contour plots of individual plume events observed at the moorings in the Greenland (a, b) and Labrador Seas (c, d). The contour interval is 2 cm $s^{-1}$ and the shading is proportional to the current speed. Downward velocity is contoured solid, upward velocity dashed, and zero contour is dotted.

Based on previous studies on the signature of plumes in ADCP time series (Schott and Leaman, 1991; Schott et al., 1993; Visbeck, 1993), several criteria were applied to identify vertical velocity events that are most likely associated with convection: Events should appear simultaneously over several bins of good data; the magnitude of the vertical velocity should exceed the magnitude of the error velocity; the error velocity should not show an organized pattern; symmetrical oscillations of comparable amplitude should not occur (internal waves); and events that occurred during the two hours just before sunrise were not considered because of possible contamination through plankton migration. Further it has been verified that no significant vertical excursions of the instruments occurred during the convection periods (Appendix A.2). The approximate location of the zero vertical velocity contours were then selected as boundaries for the individual plume events.

Although this selection process is somewhat subjective, it was chosen because attempts to apply automated selection criteria failed to deliver reliable results. Automated procedures, involving the increased variance and skewness of the vertical velocity distribution during convection periods (Figure 5.15), always resulted in the selection of events that were obviously not associated with convection activity when the chosen criteria were to weak, or failed to detect plume events under to strong criteria.

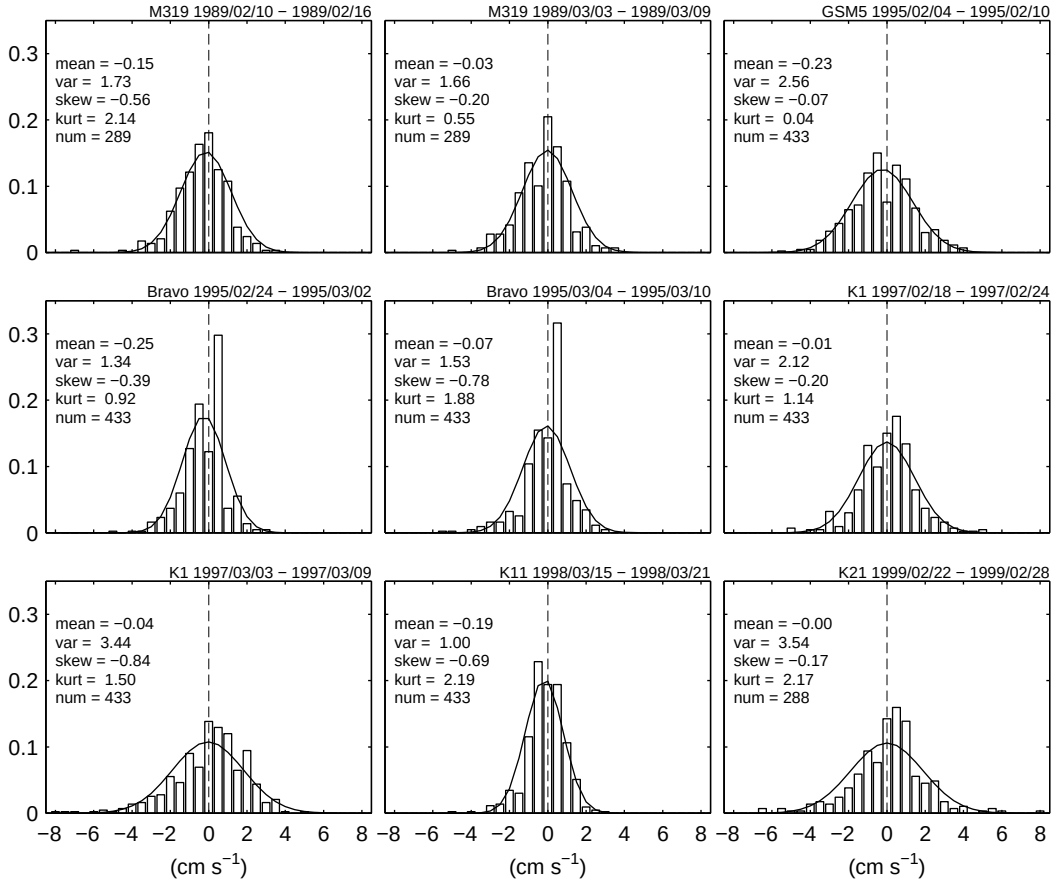


FIG. 5.15: Probability distribution of vertical velocity at 300 m depth during 6–day convection periods in the Greenland (M319 and GSM5) and Labrador Seas (Bravo, K1, K11, K21). The corresponding normal distribution (solid line) is computed from mean and variance of the vertical velocity distribution. Mean, variance, skewness, kurtosis, and the number of measurements is listed in each panel.

As already discussed above, convection activity is characterized by enhanced high–frequency variability of the vertical velocity (Figure 4.15 and Figure 4.16). In addition to the variance, Visbeck (1993) also discussed higher moments of the vertical velocity distributions obtained in the Greenland Sea (winter 1989) and the western Mediterranean (winters 1987 and 1992), and found negative skewness and increased kurtosis during periods of convection activity. The skewness

characterizes the degree of asymmetry of a distribution around its mean. The kurtosis measures the relative peakedness or flatness of a distribution. Both quantities are nondimensional, characterizing the shape of a distribution compared to a normal distribution. Increased skewness of the vertical velocity distribution is to be expected because of the intense downward motion in the plumes, that is compensated by moderate upward motion inbetween. The kurtosis of the vertical velocity distribution is a measure of the frequentness of plumes in the time series. A large number denotes many plumes with high downward velocity.

The duration of the vertical velocity events selected from the ADCP time series, i. e. the time it took for the events to pass the moorings with the background flow, is shown in Figure 5.16a. The typical transit times were between one and two hours. Only a small number of events appeared in the vertical velocity records for three hours or more. Events shorter than 40 minutes could not be resolved, due to the ADCP sampling rates of 20 to 40 minutes: at least two samples are necessary to gain confidence about a plume event. In the Greenland Sea the passage times are somewhat longer compared to the Labrador Sea, due to the weaker background currents.

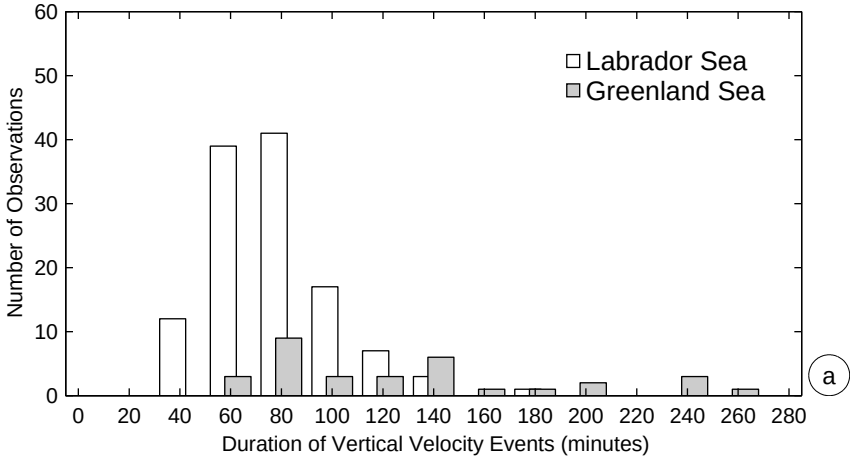


FIG. 5.16: (a) Transit time of plume events observed in the vertical velocity records at the convection moorings in the Greenland and Labrador Seas. The transit time is set by the horizontal size of the plumes and the strength of the background currents, advecting the plumes past the mooring.

The cumulative number of observed plume events for the months of February through April is shown in Figure 5.17 for the individual convection moorings. In general the number of plumes observed in the Labrador Sea was much greater than in the Greenland Sea. This results from the intense convection activity observed at the Labrador Sea moorings Bravo (1995) and K1 (1997). The number of plumes observed during the following winters of moderate convection activity at the Labrador Sea moorings K11 (1998) and K21 (1999) is comparable to the number of events found in the vertical velocity times series obtained at the moorings M319 (1989) and GSM5 (1995) in the Greenland Sea. Only two, respectively one event was found at the Greenland Sea moorings GSM2

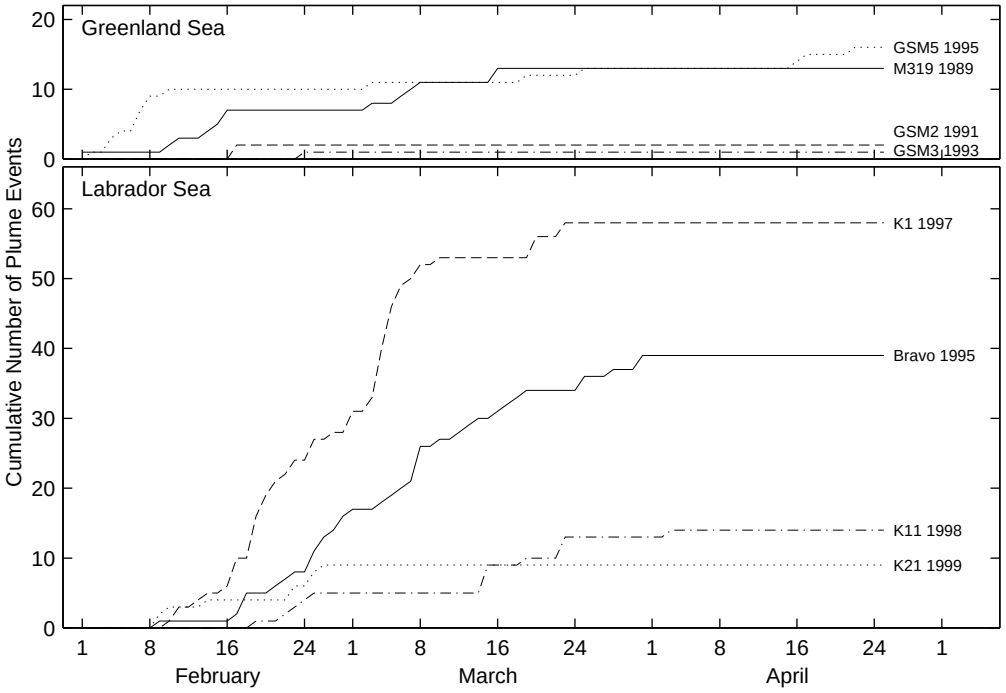


FIG. 5.17: Cumulative number of plume events observed at the Greenland Sea convection moorings M319 (1989), GSM2 (1991), GSM3 (1993), and GSM5 (1994) (upper panel), and at the Labrador Sea convection moorings Bravo (1995), K1 (1997), K11 (1998), and K21 (1999) (lower panel).

(1991) and GSM3 (1993).

### *5.2.1 Vertical Velocity and Horizontal Scale*

The maximum downward velocity is easily diagnosed from the ADCP measurements during the plume events. It is shown in Figure 5.18, plotted versus depth, for the individual observation periods. In the Greenland Sea values of 6 – 8 cm $s^{-1}$ are found during the winters 1988/89 (M319) and 1994/95 (GSM5). Schott et al. (1993) discussed the observations from the winter 1988/89 more thoroughly. They also detected downward velocity events exceeding 3 cm $s^{-1}$ at a depth of about 1400 m at mooring T6 (nearby M319). The vertical velocity records obtained at mooring GSM5 show even higher values than those shown in Figure 5.18, but these events could not be clearly identified as plumes. In the velocity records with sparse convection activity, obtained during the winters of 1990/91 (GSM2) and 1992/93 (GSM3), the maximum velocities were only 3 – 4 cm $s^{-1}$.

In the Labrador Sea the highest vertical velocity of up to 11 cm $s^{-1}$ occurred during the winter of most intense plume activity 1996/97 at mooring K1. During the other observation periods the downward motion reached velocity values of typically 6 – 8 cm $s^{-1}$. Lilly et al. (1999) discussed a plume event with a maximum velocity of 8 cm $s^{-1}$ in the *Bravo* time series of 1994/95. This

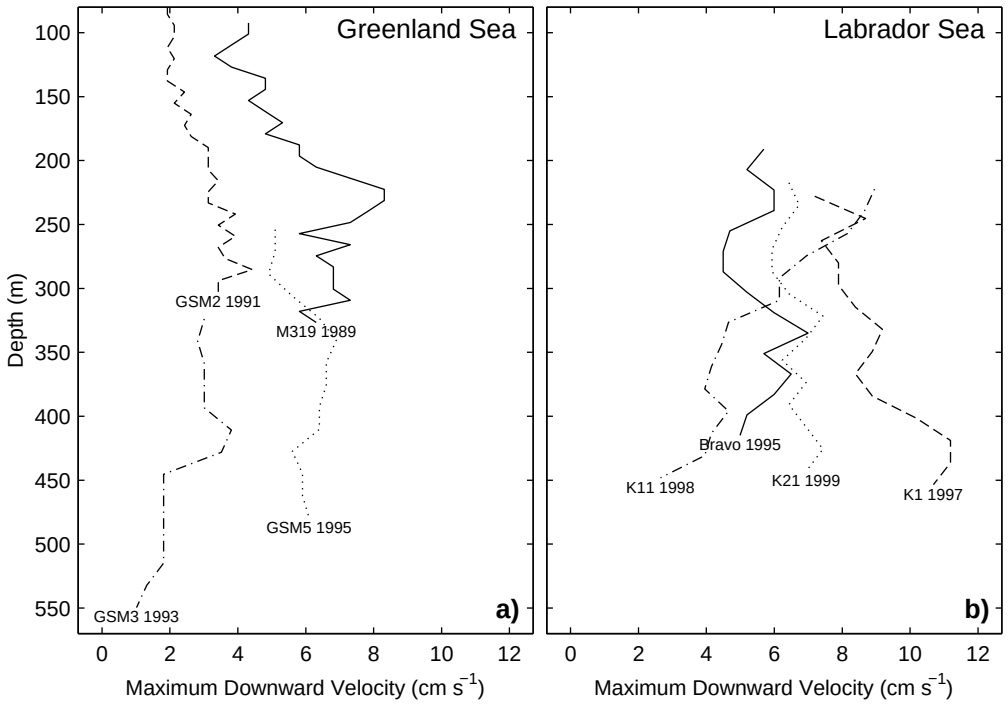


FIG. 5.18: Maximum downward velocity of the plumes observed in the Greenland Sea (a) and in the Labrador Sea (b) for the individual observation periods, as function of depth.

event does not appear in Figure 5.18, because it occurred shortly before sunrise and is therefore not considered here due to the possible contamination through plankton migration.

Figure 5.19 shows the frequency distribution of maximum downward velocity of all plume events. The observations obtained in the Labrador Sea show a smooth distribution between velocities of 3 and 9 cm s$^{-1}$. Vertical velocities below 3 cm s$^{-1}$ could hardly be identified as plume events in the ADCP measurements. Most of the events show vertical velocities between 3 – 5 cm s$^{-1}$ but also a large number of plumes with downward motion of 5 – 9 cm s$^{-1}$ was found. In the Greenland Sea the distribution of maximum vertical velocity observations is more irregular, probably due to the smaller number of events observed. Here most of the events show maximum vertical velocities of typically 4 – 5 cm s$^{-1}$, with only a small number of plumes with higher velocities.

Assuming the observed vertical velocity field to be quasi–stationary while being advected past the mooring with the background flow allows to estimate the horizontal scale of the individual convection cells (Schott and Leaman, 1991). If indeed the passage of the center of the plume has been observed, then the mean advection speed times the duration of the event gives the plume diameter.

Visbeck (1993) developed more sophisticated schemes to determine the physical properties of convective plumes from ADCP measurements. The methods were applied to the observations

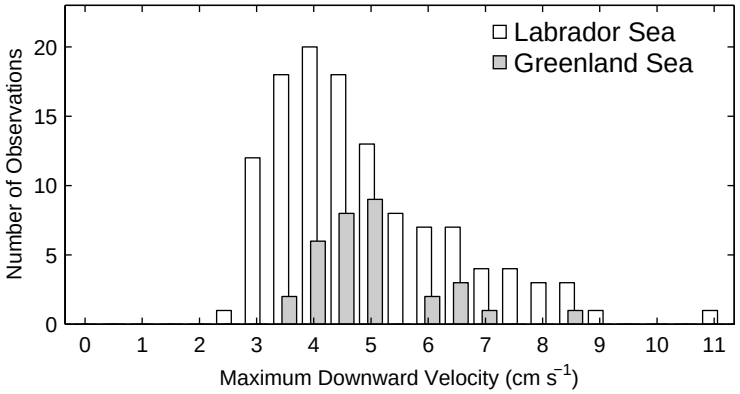


FIG. 5.19: Maximum downward velocity of individual plumes observed in the Labrador and Greenland Sea in bins of 0.5 cm s$^{-1}$.

obtained in the Greenland Sea during the winter of 1988/89, and to the observations obtained in the western Mediterranean from 1992. One of these schemes was to use the spreading of the ADCP beams with increasing distance from the transducer. At a distance of 300 m from the transducer the beams are horizontally separated by about 220 m (with 20° transducer angle). The horizontal scale was estimated from the increasing decorrelation of velocity measurements with increasing distance from the transducer, for cases where the plume diameter was of the same order as the beam separation. The second method was to fit an idealized three–dimensional velocity field to the ADCP measurements. The free parameters of this kinematic plume model were, among others: the background velocity, the horizontal distance of the ADCP section through the plume from its center, the rotation, the maximum vertical velocity, and the plume diameter. However, it turned out that the results of both methods were consistent with the frozen structure assumption, which will be used here to estimate horizontal plume scales, because of its ease of use.

To separate the background currents from the high–frequency oscillations that contain the plume signals, the spectra of horizontal current velocities in the Greenland and Labrador Seas are analyzed (Figure 5.20). In both regions, the spectra show a band of relatively low energy between periods of 5 to 10 hours, separating the tidal currents from the high–frequency oscillation. Therefore the 9–hour lowpassed horizontal velocity mean from all ADCP bins is assumed to be a good estimate of the background flow. Integrating the background velocity over the period of a plume passage results in an estimate of the plume diameter.

From the first observations of convective plumes with moored ADCPs in the western Mediterranean Schott and Leaman (1991) estimated the horizontal plume scale to be of order 1 km. The subsequent measurements carried out in the Greenland Sea suggested a horizontal scale of about 300 m (Schott et al., 1993). During the winter of 1991/92 a small–scale triangle of 2 km sidelength with four ADCPs (one of the moorings carried two instruments) was deployed in the convection

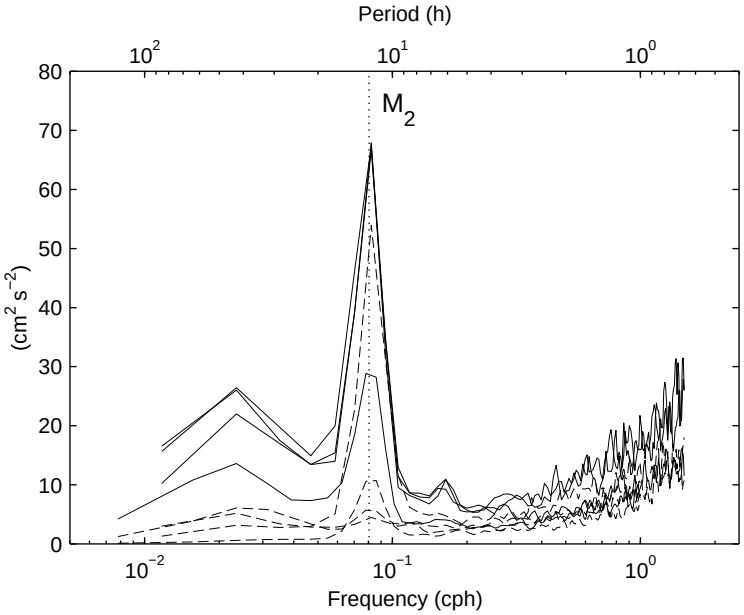


FIG. 5.20: Variance–preserving spectra of unfiltered horizontal current velocity at 300 m depth from the Labrador (solid) and the Greenland Sea (dashed) convection moorings for the period between 1 February and 1 May. The spectra were computed using 3–day segments with 50% overlap and Hanning–window tapering.

region of the western Mediterranean (Schott et al., 1996). An interesting results was that the horizontal currents on the timescale of the observed plumes were not correlated among the stations. Therefore, the horizontal plume scales again had to be estimated from individual station data. Typical values obtained were 300 – 600 m. In the central Labrador Sea Lilly et al. (1999) found the ADCP measurements obtained during the winter 1994/95 to be consistent with convective plumes of width 200 to 1000 m.

The number of observations of individual plume diameters in the Greenland and Labrador Seas is shown in Figure 5.21. In the Greenland Sea, most of the estimates fall between 200 and 600 m. Only three events of larger plume scale have been found, which may be considered as outliers. The mean horizontal plume size is of about 400 m. Larger horizontal scales occur in the Labrador Sea, ranging from 200 to 1200 m, again with some outliers at larger sizes. Here the mean horizontal size is about 700 m.

The maximum vertical velocities as well as the horizontal scales of convective plumes derived here generally confirm the earlier observations with moored ADCPs in convection regions, supporting them with a broader observational base. The large number of plumes found in the newer observations motivated to test theoretical scaling arguments of the velocity and length scales of plumes as discussed in section 5.3.

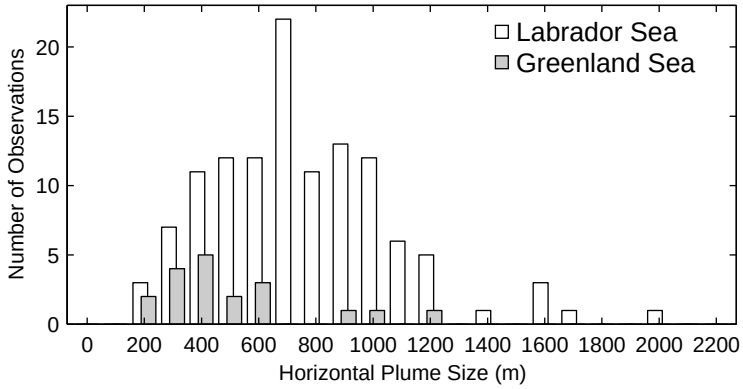


FIG. 5.21: Number of observations of plume diameters at the Labrador and Greenland Sea convection moorings in 100 m bins.

### *5.2.2 Three–dimensional Flow Field*

The question of whether there is a horizontal circulation associated with plumes has been addressed in all previous studies dealing with ADCP measurements in the convection regions of the western Mediterranean, the central Greenland Sea, and the central Labrador Sea. Considering a convection cell with inflow in the upper region and outflow in the lower region, cyclonic circulation on top and anticyclonic circulation at the bottom of the plume would be explainable by potential vorticity conservation of a water column stretched in the upper part and squeezed in the lower part.

During their observation in February 1987 in the western Mediterranean, Schott and Leaman (1991) found only one event where a clear horizontal current anomaly was detectable, but it could not be explained consistently with either cyclonic or anticyclonic rotation. Indications of a horizontal circulation were also found in the central Greenland Sea during a plume event observed on 16 March 1989 at mooring T6. In the upper layer currents rotated anticlockwise with the arrival of the plume, corresponding to cyclonic motion. In the deep layer clockwise rotation of the currents was observed, which corresponds to anticyclonic motion. An opposite rotation of the horizontal currents on the backside of the plume was not observed (Schott et al., 1993). As the horizontal currents observed at the triangular array in the western Mediterranean (1991/92) decorrelated among the stations, meaningful vorticity calculations could not be carried out (Schott et al., 1996). Rotation was analyzed for two cases using the kinematic plume model of Visbeck (1993). The first case yielded no detectable rotation, while the second was consistent with cyclonic rotation. Lilly et al. (1999) interpreted the horizontal current fluctuations associated with plume events in the *Bravo* 1994/95 time series as cyclonic vorticity.

It can be concluded that the evidence for a well organized horizontal circulation associated with individual convective plumes is sparse. A careful inspection of the plume events observed in the Greenland and Labrador Seas during the subsequent experiments brought no new evidence for

consistent horizontal circulation associated with them. Therefore a different approach is followed here.

Integrating the lowfrequency background velocity with respect to time allows to estimate the spatial structure from the Eulerian measurements, assuming that the flow field is quasi static while passing the mooring as described above. This results in one estimate of the highfrequency, three–dimensional flow field associated with each individual plume. Then the velocity measurements of several plume events from periods of intense convection activity could be averaged to determine the mean velocity structure.

If consistent structures of horizontal currents associated with plume events do exist, this should be revealed in the mean flow fields. Otherwise, if the horizontal currents on these short time scales are random structures, they should cancel each other. Figure 5.22 shows the mean three–dimensional flow field derived for a number of intense convection periods, one from the Greenland Sea during February 1995 (GSM5) and five from the Labrador Sea (*Bravo*, K1, and K11). The horizontal velocity parallel to the background flow and the vertical velocity are shown as vectors, while the component perpendicular to the background flow is shown as contours. The magnitude of the vertical velocity is emphasized by shading. Cyclonic rotation should reveal itself through positive contours on the lefthand side of the maximum downward velocity and negative contours on the righthand side. This is clearly not the case for the observations from the Labrador Sea, but could not completely be ruled out for the Greenland Sea case.

### *5.2.3 Diurnal Cycle of Vertical Velocity*

In the western Mediterranean a diurnal cycle of the occurance of downward motion has been found, corresponding to the diurnal cycle of the surface forcing (Schott et al., 1996). Plume generation occurred dominantly at night, at maximum buoyancy flux. Enhanced vertical mixing, at a level of about 300 m, typically set in four hours after the cooling started, and ended by the time the surface forcing was minimal. This sets a lower limit for the lifetime of the plumes that is at least not long compared to an inertial period.

The mean diurnal cycle of the heat flux over the Labrador Sea convection region (as derived from R/V *Knorr* cruise 147 shipboard meteorological observations) for the convection period from 10 February to 9 March 1997 is shown in Figure 5.23a. Although there is no heat gain during mid–day as in the western Mediterranean, the heat loss drops significantly between 10:00 UTC and 20:00 UTC due to insolation. The minimum at 15:00 UTC (corresponding to local noon) is about 250 W $m^{-2}$ lower than the values found at night.

The vertical velocities at mooring K1 displayed versus the time of day show a predominance of large downward motion during night and early morning hours (Figure 5.23b). No downward vertical velocity exceeding 4 cm $s^{-1}$ was observed between 17:00 UTC and 21:00 UTC at K1. The corresponding variance of the vertical velocity is shown in Figure 5.23c. The variance decreases

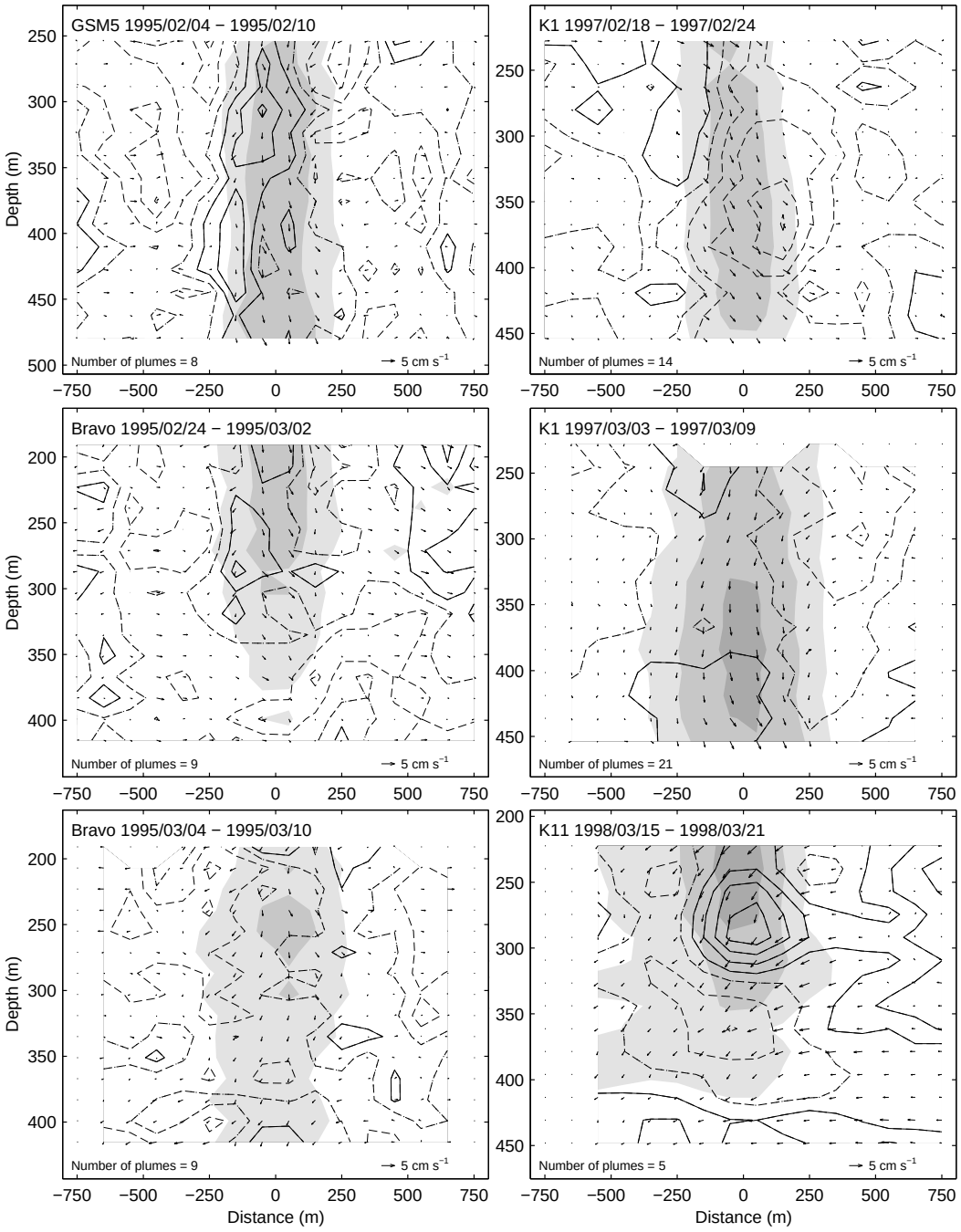


FIG. 5.22: Mean three–dimensional flow field associated with plume events during periods of intense convection in the Greenland Sea (GSM5) and the Labrador Sea (*Bravo*, K1, K11). The current vectors denote the vertical velocity and the horizontal component parallel to the lowfrequency background flow. The contour lines denote the horizontal velocity perpendicular to the background flow. Positive for flow out of the plane (solid) and negative for flow into the plane (dashed). The shading is proportional to the intensity of downward velocity. The contour interval is 1 cm $s^{-1}$, and the zero contour is not shown.

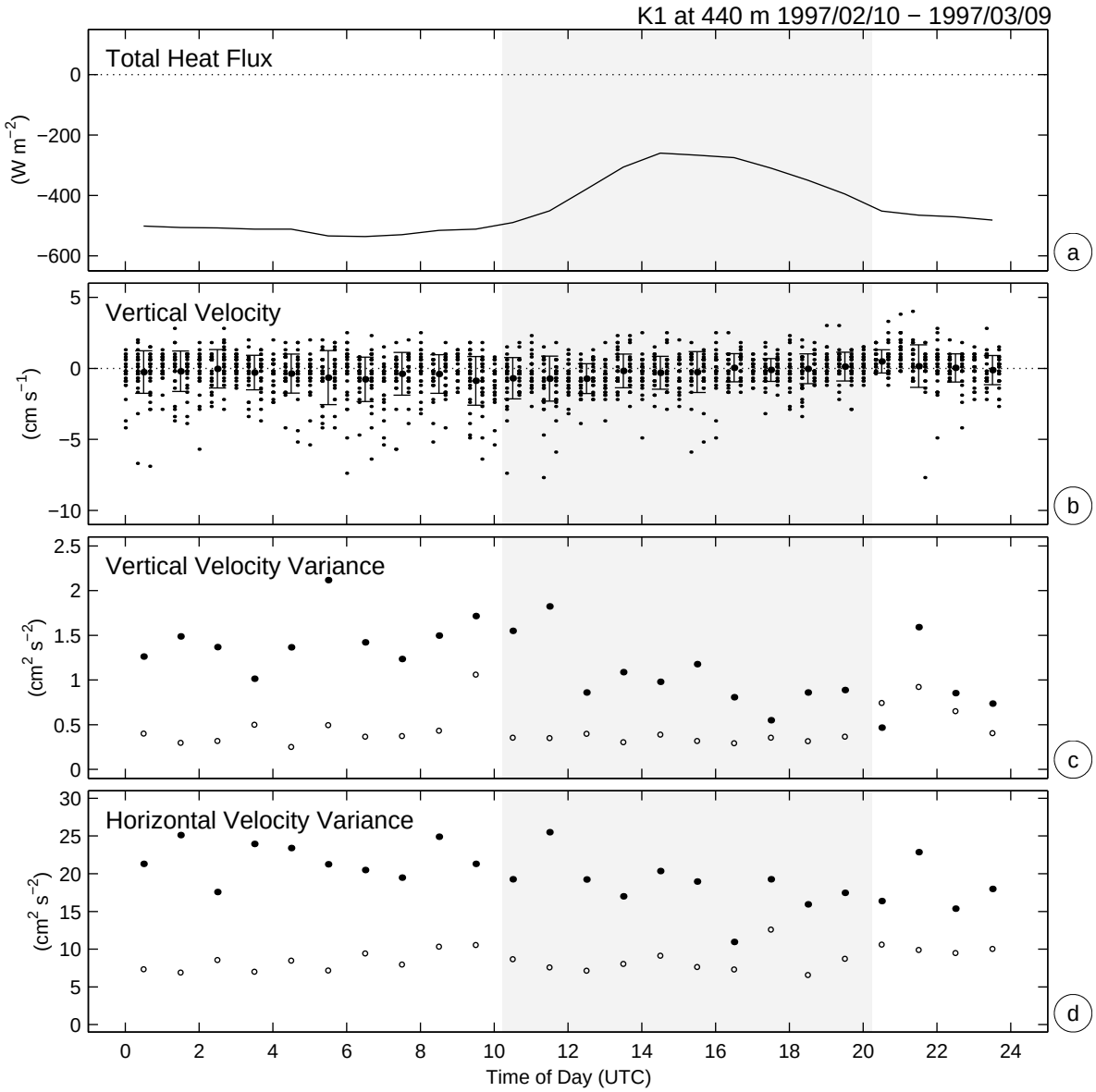


FIG. 5.23: (a) Mean diurnal heat flux from R/V *Knorr* shipboard measurements between 10 February and 9 March 1997 in the Labrador Sea. (b) Vertical velocities at Labrador Sea mooring K1 at 440 m versus time of day, as well as their hourly means and standard deviations for the same period. (c) Corresponding hourly mean variance of the vertical velocity (dots) and for a preconvection period from 1 October to 30 November 1996 (circles). (d) Same as (c) for the horizontal velocity variance. The time between sunrise and sunset is marked by shading.

after 12:00 UTC when the surface heat flux reduces, and has its minimum at 21:00 UTC with values comparable to the preconvection variance (October/November 1996). The horizontal velocity variance (Figure 5.23d) shows a similar behavior, although much less pronounced. The peak in the vertical velocity variance at 22:00 UTC results from plankton migration; plankton peaks also

appear in the preconvection time series at 09:00 UTC and 22:00 UTC.

Figure 5.24 shows the number of occurances of downward motion exceeding 3 cm $s^{-1}$ at 300 m depth versus time of day from the Labrador and Greenland Sea convection moorings during the months of February and March. Most remarkable is that the Labrador Sea time series do not show a single event of enhanced downward motion between 20:00 UTC and 22:00 UTC. This may partly result from upward motion of plankton, occurring at this time and compensating the downward motion. The largest number of events is found around 09:00 UTC, which is shortly before sunrise and therefore again contaminated by plankton migration. Thereafter the number of observations decreases continuously towards the 21:00 UTC minimum.

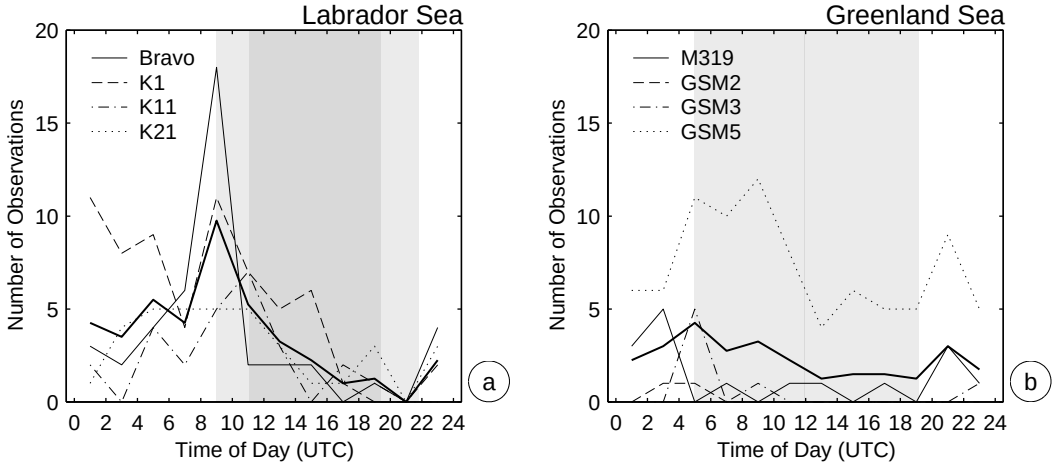


FIG. 5.24: Number of observations of downward motion exceeding 3 cm $s^{-1}$ versus time of day for 2–hour intervals during the months of February and March at 300 m depth from four ADCP time series obtained in (a) the Labrador Sea (Bravo, K1, K11, and K21) and (b) the Greenland Sea (M319, GSM2, GSM3, and GSM5) respectively. The mean is shown as heavy line. The shading denotes the the time between sunrise and sunset. Dark shading for 1 February (not in the Greenland Sea due to polar night) and light shading for 1 April.

Although the vertical velocity time series are partly contaminated by plankton motion, this could not explain the diurnal cycle of vertical velocity in Labrador Sea mooring records. The plankton migration occurs only during the two hours before sunrise and after sunset, while the vertical velocity cycle appears over the whole day, with extrema during the periods of plankton activity.

In the Greenland Sea the diurnal cycle of insolation restarts around mid–February, with the end of the polar night. Although the number of vertical velocity events in the Greenland Sea is much smaller compared to the Labrador Sea, most of the events are likewise found during nighttime. The diurnal cycle of vertical velocity intensity is not that pronounced in the Greenland and Labrador Seas compared to the observations obtained in the western Mediterranean in February 1992 (Schott et al., 1996). Nevertheless, there is evidence that intense downward motion occurs predominantly

at night, while it ceases when the surface forcing decreases due to insolation (Figure 5.24). This suggests an upper limit for the lifetime of plumes which would then be at least not long compared to the inertial period.

During the polar night a diurnal cycle of surface forcing does not exist in the Greenland Sea. This arises the possibility that plumes exist sufficiently long to be modified by the Earth's rotation and come under geostrophic control. This may be the case for the plumes in early February 1995 at mooring GSM5 where slightly consistent horizontal velocities structures were observed (Figure 5.22). On the other hand, plumes may be generated continuously throughout the day and decay before they come under rotational control. This cannot be distinguished by the ADCP measurements, because the plumes are only sliced for a rather short period as they pass the mooring location. The question of whether plumes are rotationaly controlled will be further discussed in the context of theoretical scaling arguments in section 5.3.

### *5.2.4 Vertical Heat Flux*

The number of direct measurements of turbulent heat flux in the ocean is sparse and limited to observations of small–scale turbulence (Moum, 1990; Yamazaki and Osborn, 1993; Fleury and Lueck, 1994; Gargett and Moum, 1995; Sun et al., 1996; Morison and McPhee, 1998). Estimating the vertical heat flux involves taking the covariance of the fluctuating vertical velocity and temperature $\langle w'\theta' \rangle$, the vertical heat flux by definition, which in general is difficult to observe. Conventionally the estimates are based on indirect methods, where the heat flux is inferred from the turbulent dissipation rates of temperature variance and kinetic energy (Osborn and Cox, 1972; Osborn, 1980).

In a deep convection regime the largest turbulent scale occurring is the plume scale. The vertical velocity fluctuations associated with plumes are evident in the ADCP measurements, but the vertical density gradient, driving the plumes, is small. Assuming that the vertical buoyancy flux should compensate the surface loss and manifests itself only in temperature changes, the magnitude of the expected temperature fluctuations can be estimated as follows:

$$B = g\alpha \frac{Q}{\rho_0 c_p} = w'b' = -\frac{g}{\rho_0} w'\rho' = g\alpha w'\theta', \tag{5.1}$$

where $B$ and $Q$ is the surface buoyancy and heat flux respectively, $\rho_0$ a reference density, $c_p$ the specific heat, $\alpha$ the thermal expansion coefficient, and $w'$, $b'$, $\rho'$, and $\theta'$ are the vertical velocity, buoyancy, density, and temperature fluctuations, respectively.

Typical conditions during convection in the Labrador Sea are $B \approx 1 \times 10^{-7}$ m$^2$ s$^{-3}$ (equivalent to a heat flux of approximately 400 W m$^{-2}$), $\alpha \approx 1 \times 10^{-4}$ K$^{-1}$, and $w' \approx 1 \times 10^{-1}$ m s$^{-1}$. The resulting temperature fluctuations are only $\theta' \approx 1 \times 10^{-3}$ °C, detectable, if at all, only with today's high–precision instruments (SeaCATs and MicroCATs). In the Greenland Sea, where $\alpha$ is only about $0.3 \times 10^{-4}$ K$^{-1}$, a measurable covariance of the vertical velocity and temperature fluctua-

tions is not expected. Salinity fluctuations and therewith density fluctuation are not detectable at all with state of the art instruments, due to even smaller signals and the larger uncertainties of the conductivity measurements.

At the depths where moored SeaCATs of MicroCATs are in the range of an ADCP, the calculation of the heat flux term or of the correlation coefficient $\rho_{w\theta} = \langle w'\theta' \rangle / \langle w'^2 \rangle^{1/2} \langle \theta'^2 \rangle^{1/2}$ is straightforward, but it is important to know whether the calculated values are statistically significant. In order to test the statistical significance, two methods are used here: First an F–test for the correlation coefficient during periods of strong vertical mixing at the Labrador Sea moorings K1 (1997) and K11 (1998), and second, as a nonparametric approach, confidence limits for the heat flux are computed with the bootstrap method (e. g. Tichelaar and Ruff, 1989).

The correlation coefficient $\rho_{w\theta}$ can be considered significant if it exceeds a critical value of

$$\rho_c^2 = \frac{F_{1,n_2,\alpha}}{F_{1,n_2,\alpha} + n_2}, \tag{5.2}$$

where $F_{1,n_2,\alpha}$ is the value of the $F$ distribution with one and $n_2$ = $n^*$ - 2 degrees of freedom at $100\alpha\%$ confidence. The number of independent observations or effective degrees of freedom $n^*$ is

$$\frac{1}{n^*} = \frac{1}{n} + \frac{2}{n^2} \sum_{j=1}^{n} (n-j) C(j\tau), \tag{5.3}$$

where $C(j\tau)$ is the autocorrelation of the measured quantity at lag $j\tau$, with $\tau$ the sampling interval, and $n$ the number of samples (Garrett and Petrie, 1981).

All convection moorings in the central Labrador Sea carried one SeaCAT or MicroCAT recorder within the range of the ADCP. The temperature fluctuations were obtained by subtracting the 9–hour low-passed time series from the measurements. Applying Equation 5.3 to the autocorrelation functions of the observed vertical velocity and temperature fluctuations results in time intervals between two independent values of 60 minutes for the vertical velocity and 40 minutes for the temperature fluctuations (the sampling interval is 20 minutes). As a conservative estimate, a time interval of 80 minutes will be used, corresponding to the typical transit times of plumes at the moorings (Figure 5.16).

Considering periods of strong mixing activity it turned out that at least three to four days of averaging are necessary to come up with significant correlation coefficients for a few periods. Therefore five–day sections of vertical velocity and temperature data were used to calculate the statistics. With the sampling interval of 20 minutes this results in 90 independent observations within each five–day period. Thus, at a 90% confidence level, the correlation coefficents have to exceed the critical value of $\rho_c$ = 0.17 to differ significantly from zero.

The three periods of vertical velocity and temperature fluctuations with highest correlation are shown in Figure 5.25. Two periods are from mooring K1 (1997), including the most intense

downward motion events from all records, one during the second half of February and one at the beginning of March. The third period shown corresponds to the strongest mixing activity found by mid–March of the following winter at mooring K11. The statistics for these periods are summerized in Table 5.1. The instantaneous heat flux values $w'\theta'$ show distinct positive spikes in all three sections, indicating upward flow of heat to compensate losses at the surface. The occurrence of these spikes corresponds to negative vertical velocity and negative temperature anomalies.

TABLE 5.1: Statistical summary of the correlation calculations, for the three periods shown in Figure 5.25.

| Mooring | | $\langle w'^2 \rangle^{1/2}$ $(\times 10^{-2}\ m\ s^{-1})$ | $\langle \theta'^2 \rangle^{1/2}$ $(\times 10^{-2}\ ^\circ C)$ | $\langle w'\theta' \rangle$ $(\times 10^{-4}\ ^\circ C\ m\ s^{-1})$ | $\rho_{w\theta}$ |
|---|---|---|---|---|---|
| K1 | 19–24 Feb. 1997 | 1.36 | 1.45 | 0.48 | 0.24 |
| K1 | 3–8 Mar. 1997 | 1.94 | 1.16 | 0.57 | 0.26 |
| K11 | 13–18 Mar. 1998 | 0.96 | 1.31 | 0.25 | 0.19 |

During the periods of active convection the vertical velocity distribution shows increased skewness, due to intense downward motion in the plumes compensated by moderate upward motion inbetween (Figure 5.15). Furthermore, the high–frequency temperature fluctuations also deviate from a normal distribution for the periods shown in Figure 5.25. In order to increase the confidence in the heat flux estimates nonparametric methods, where normality has not to be assumed, can be used to test the statistical significance.

Several authors employed a method apparently suggested by B. Ruddick and first published by Yamazaki and Osborn (1993), where the observed correlation coefficients are compared to the probability density function (pdf) of noise. The noise pdf is computed by calculating the correlation for many randomly shifted segments of vertical velocity and temperature data to assure that these two series are totally uncorrelated. Figure 5.26 shows the probability distribution of noise estimated from 2000 realizations during February and March 1997 at mooring K1. Comparing the correlation coefficients observed at K1 (Table 5.1) with the noise distribution reveals that the probability of accepting noise is very small.

To obtain time series of vertical heat fluxes, 5–day running averages of $w'\theta'$ were computed for the months of February and March at the convection moorings in the central Labrador Sea (Figure 5.27). The confidence limits for the heat flux averages were estimated with the bootstrap method. As a nonparametric method boostrapping provides freedom from the assumption of a normal data distribution, but the number of effective degrees of freedom still has to be considered. Therefore 80–minute averages were computed before resampling the data to ensure that the samples are statistically independent. Since the method of Garrett and Petrie (1981) used to estimated the number of degrees of freedom is a parametric approach, and normality has to be assumed, the confidence limits might be underestimated if the number of degrees of freedom has been overestimated.

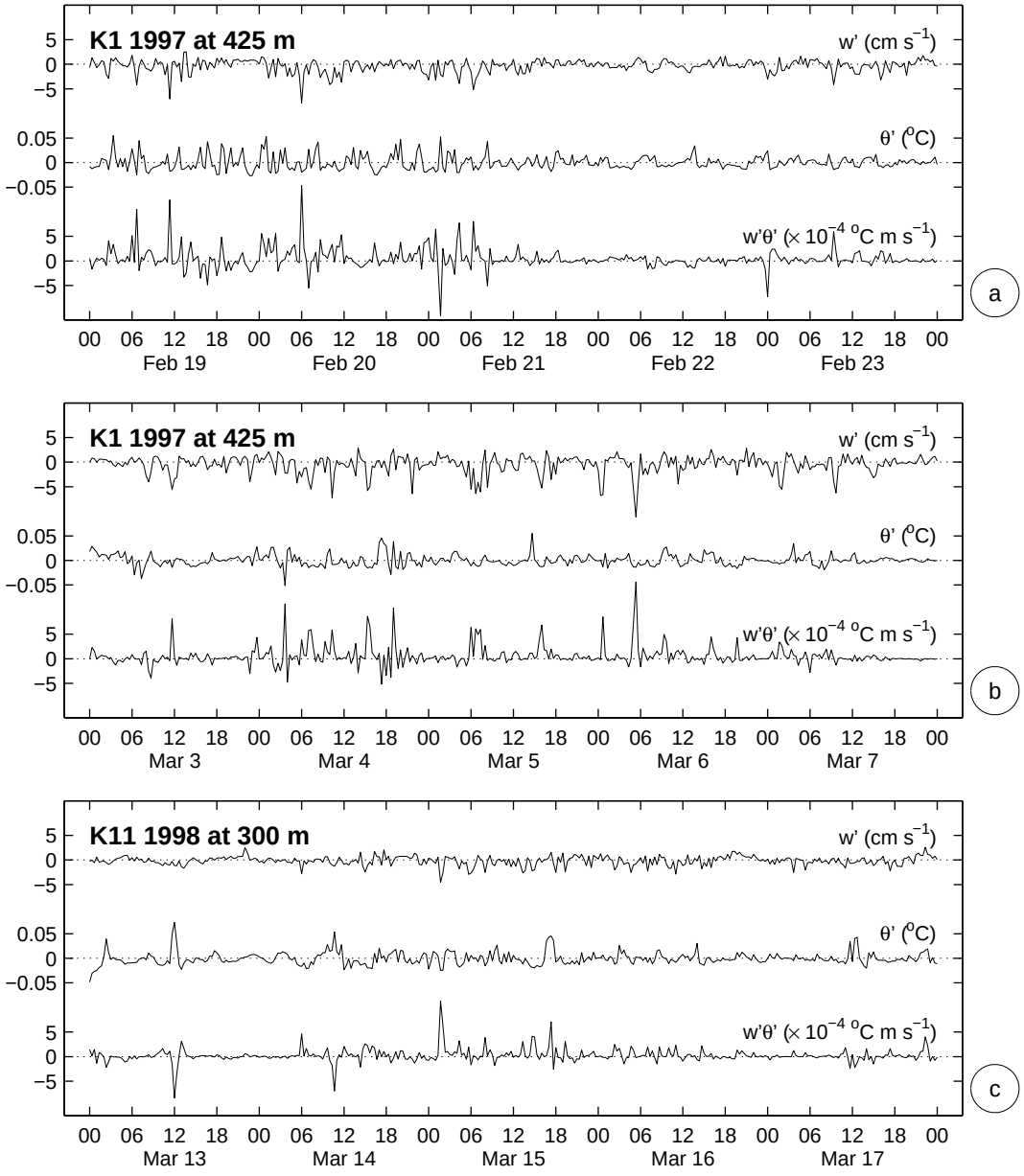


FIG. 5.25: Time series of vertical velocity, temperature, and instantaneous heat flux signals for three 5–day sections of data from the moorings K1 (1997) and K11 (1998) in the central Labrador Sea, where the correlation of vertical velocity and temperature fluctuations is statistically significant. Positive values of instantaneous heat flux indicate upward flow of heat to compensate losses at the surface.

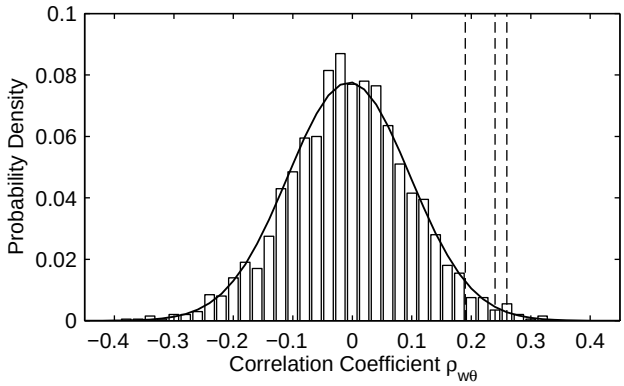


FIG. 5.26: Probability distribution of the correlation coefficient between vertical velocity and randomly shifted temperature fluctuations for the months of February and March at Labrador Sea mooring K1 (1997). The corresponding normal distribution (solid line) is computed from mean and variance of the noise distribution. The dashed lines indicate the correlation coefficients obtained for the time series shown in Figure 5.25 and listed in Table 5.1.

The time series of vertical heat flux at the Labrador Sea moorings show that most of the time the heat flux is not significantly different from zero. The large errorbars at the beginning of the *Bravo* (1995) time series are associated with the passage of the base of the mixed layer. During this time the temperature sensor is, due to horizontal inhomogeneties, sometimes below the mixed layer and sometimes in it, causing large temperature fluctuations. In the remaining time three short events of slightly significant heat flux occurred.

As already discussed above, the most remarkable events of upward heat flux associated with convection activity are found in the time series obtained at mooring K1. The two events, one in mid–February and one at the beginning of March 1997, lasted for several days each and show mean heat fluxes of about 200 W $m^{-2}$. This value compares well with results from the 3D Lagrangian floats operating in this area at the same time (E. Steffen, personal communication). During the period between mid–February and mid–March, the heat flux observed at depth even appears to be roughly correlated with the surface forcing.

The event of significant upward heat flux in the time series of mooring K11 in mid–March 1998 amounts to an average of about 100 W $m^{-2}$. No significant results were found at K21 (1999), probably resulting from the less precise vertical velocity measurements during this deployment period (due to lower battery capacity less pings were averaged into the ensemble means, see Appendix A.2). A similar analysis has been carried out for the time series obtained in the Greenland Sea, but no significant correlation was found in any of them. This is most likely due to the smaller temperature fluctuations caused by the same amount of surface heat flux, as stated above.

Considering the heat flux estimates listed in Table 5.1, it is tempting to speculate on the corre-

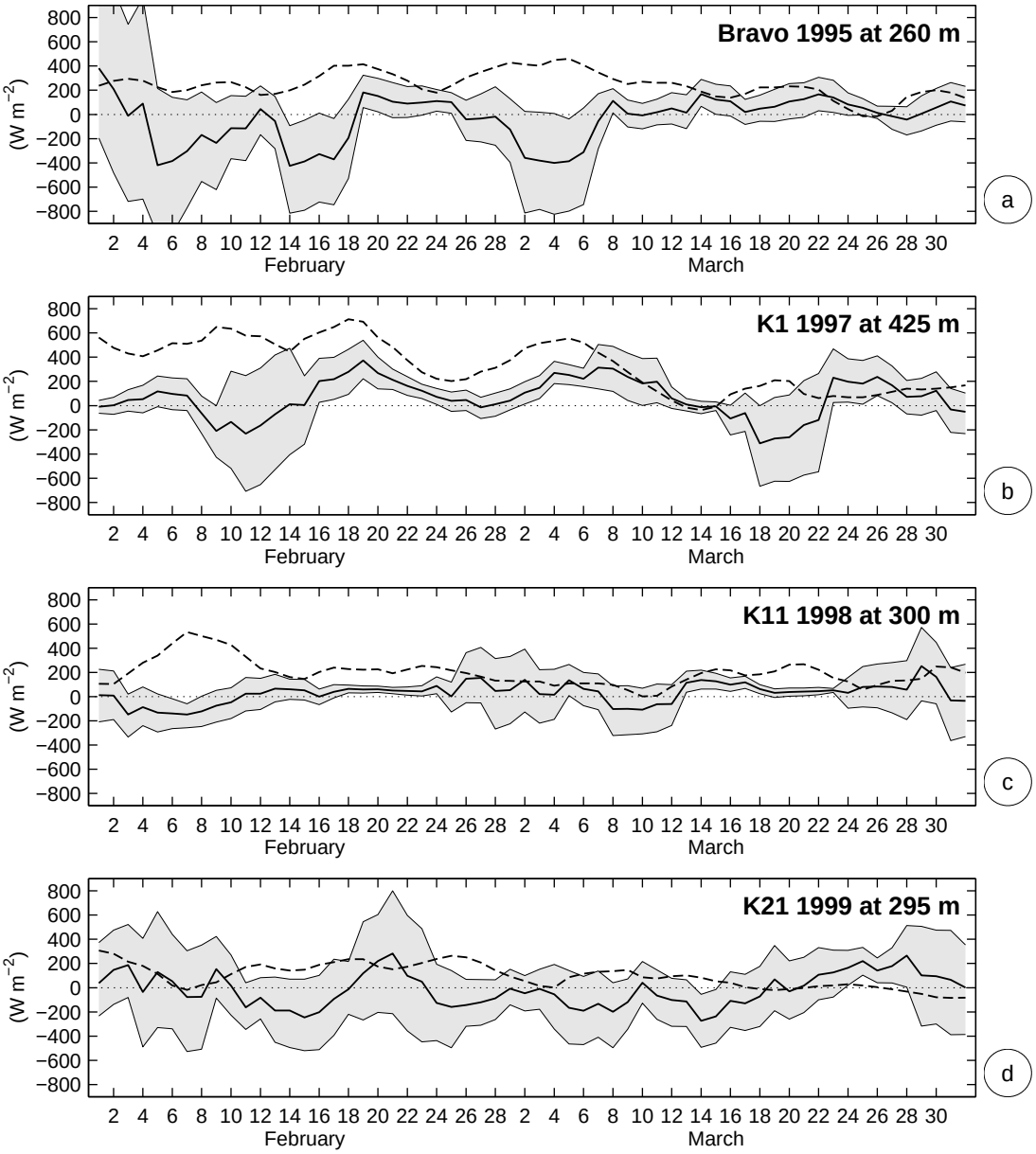


FIG. 5.27: 5–day running averages of vertical heat flux $\rho_0 c_p \langle w'\theta' \rangle$ (solid) and NCEP/NCAR reanalysis surface heat flux (dashed) for the months of February and March at the convection moorings in the central Labrador Sea. The shading denotes 90% confidence limits computed with the bootstrap method.

sponding eddy diffusivity

$$K_T = \frac{\langle w'\theta' \rangle}{d\bar{\theta}/dz}. \tag{5.4}$$

Estimates of the mean vertical temperature gradient can be gained from CTD profiles obtained in the convection area during the winter cruise of R/V *Knorr* in 1997 (Figure 5.28a,b). The *Knorr* cruise carried out in the following winter of 1998 already ended in early February, therefor no CTD profiles for the mixing period in mid–March are available.

During the first period of intense mixing in February 1997 the *Knorr* did not operate near mooring K1, and therefor temperature profiles obtained about 130 nm northwestward were used (stations 45 – 48). For the second period at the beginning of March CTD cast were carried out in the vicinity of mooring K1 (stations 99 – 103). The mean vertical temperature gradient in the mixed layer was estimated by fitting a straight line to the upper 550 m and 600 m, respectively. The resulting eddy diffusivities are shown as cumulative averages in Figure 5.28c,d. The values are of about 1 – 1.5 $m^2\ s^{-1}$, large compared to typical open–ocean values (away from boundaries) of $10^{-5}\ m^2\ s^{-1}$ (e. g. Munk and Wunsch, 1998). The vertical temperature gradient in the upper water column was rather surprising as nothing similar was observed during convection in the western Mediterranean (Leaman and Schott, 1991; Schott et al., 1996). However, it should be noted that the Labrador Sea CTD profiles show no corresponding density gradient.

## 5.3 Scaling of Plumes

### 5.3.1 Theory: Scaling Arguments

Conventionally, the parameter ranges in which laboratory and numerical experiments of convection in homogeneous and rotating fluids were conducted are classified by the flux Rayleigh number

$$Ra_f = \frac{Bh^4}{\kappa^2 \nu}, \tag{5.5}$$

and the Taylor number

$$Ta = \frac{1}{Ek^2} = \frac{f^2 h^4}{\nu^2}, \tag{5.6}$$

where $B$ is the buoyancy flux, $h$ the depth of the convective layer, $\kappa$ and $\nu$ the thermal diffusivity and kinematic viscosity respectively, $Ek$ the vertical Ekman number, and $f$ the Coriolis parameter. The flux Rayleigh number $Ra_f$ is the ratio of the destabilizing effect of the buoyancy flux to the stabilizing effect of diffusion. The Taylor number $Ta$ is a measure of the importance of rotation to diffusion. The ratio between kinematic viscosity and thermal diffusivity is the Prandtl number:

$$Pr = \frac{\nu}{\kappa}. \tag{5.7}$$

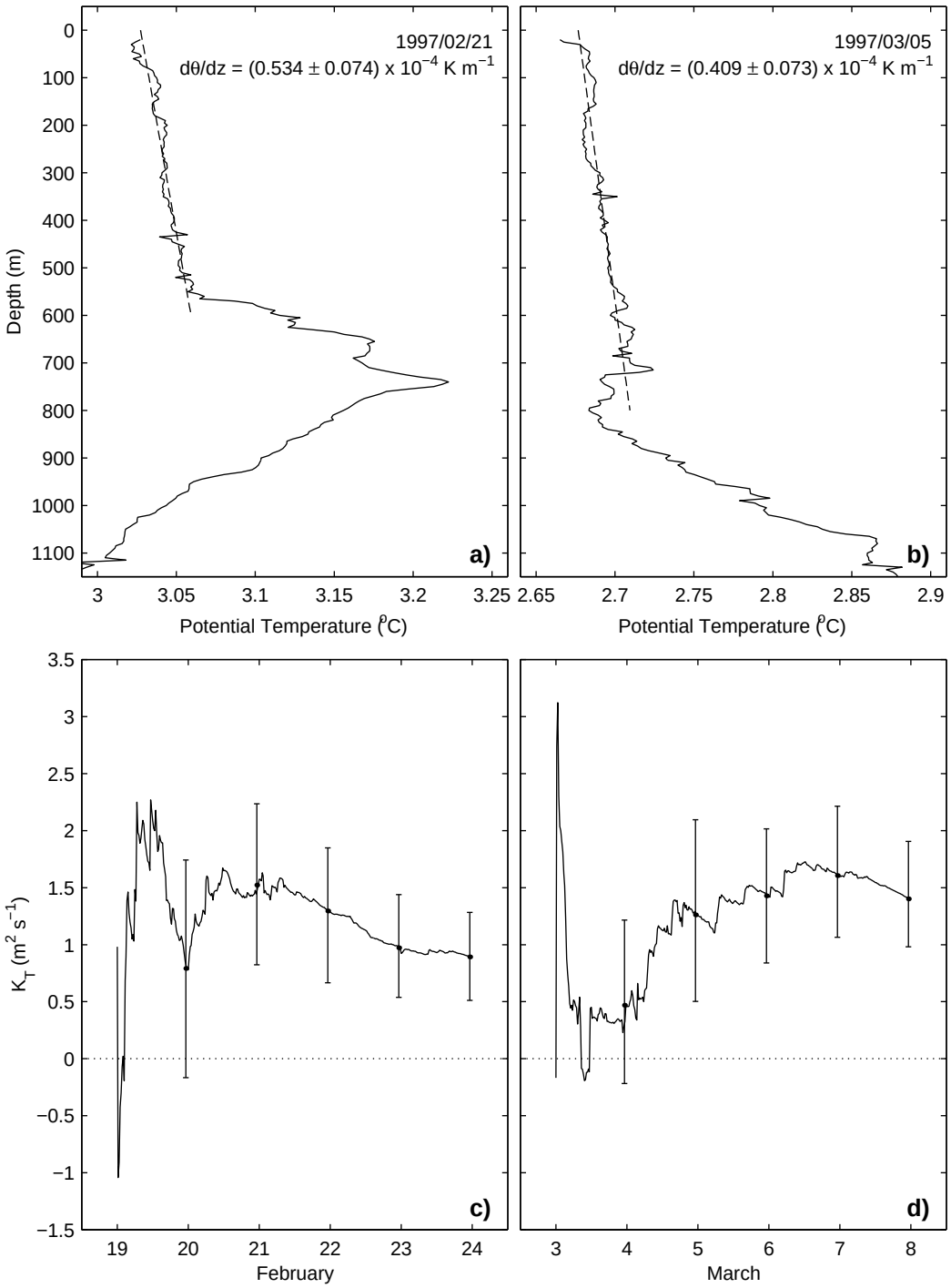


FIG. 5.28: (a, b) Mean potential temperature profiles from R/V *Knorr* cruise 147 in the central Labrador Sea for two periods where intense mixing was observed. The fitted vertical temperature gradient is shown as dashed line. (c, d) Cumulative mean of the eddy diffusivity $K_T = \int (w'\theta'/\overline{\theta}_z)dt / \int dt$ estimated from heat flux time series at mooring K1 using the vertical temperature gradients $\overline{\theta}_z$ from (a, b), respectively (assumed to be constant). The errorbars are 90% confidence limits computed with the bootstrap method. (CTD data courtesy of R. Pickart)

Boubnov and Golitsyn (1990, their Figure 2) divided the ($Ra_f$–$Ta$) plane into four regions: (1) a thermoconductivity regime, in which diffusion suppresses the convective instability, (2) a regime of regular cells, (3) a geostrophic turbulence regime, and (4) a fully turbulent regime. Maxworthy and Narimousa (1994, their Figure 18) expanded the figure to larger values of both $Ra_f$ and $Ta$, and added regions appropriate to a number of laboratory and numerical experiments, as well as for some observations from the western Mediterranean and the Arctic, apparently using molecular values of $\kappa$ and $\nu$.

In the case of open–ocean convection the flow is certainly turbulent, and the molecular values of $\kappa$ and $\nu$ have to be replaced with the corresponding eddy viscosity and diffusivities. Therefore appropriate values for $Ra_f$ and $Ta$ are not known with any certainty. To characterize the convective process solely through external parameters, velocity, space, and buoyancy scales independent of assumptions concerning eddy viscosity and diffusivities were developed (Jones and Marshall, 1993; Marshall et al., 1994; Maxworthy and Narimousa, 1994; Marshall and Schott, 1999). These scaling laws for an unstratified fluid, as far as they concern the plume dynamics, are summerized in the following.

The scaling arguments are based on the picture of convection driven into a homogeneous mixed layer of depth $h$ by a surface buoyancy flux of magnitude $B$, (illustrated schematically in Figure 5.29), assuming that the potential energy increase caused by the buoyancy flux is transferred into kinetic energy. At early stages after the start of the surface forcing ($t \ll f^{-1}$), isotropic turbulence will develop below a thermal boundary layer $\delta$ at the surface. The developing plumes are so small in scale that they cannot feel the finite depth of the mixed layer and rotation is apparently unimportant. At this stage the surface buoyancy flux $B$ remains the only controlling parameter, and the scales for the depth, velocity, and buoyancy of the plumes can be expressed in terms of the buoyancy flux $B$ and the time $t$ (Jones and Marshall, 1993; Marshall and Schott, 1999):

$$\begin{aligned} l &\sim (Bt^3)^{1/2}, \\ u \sim w &\sim (Bt)^{1/2}, \\ b &\sim \left(\frac{B}{t}\right)^{1/2}. \end{aligned} \tag{5.8}$$

Evolving in time the turbulent cells grow and become constrained either by the depth of the convective layer or the Earth's rotation. With the depth $h$ as the limiting length scale of the plumes, putting $l = h$ in equation (5.8) results in the following scales (e. g. Maxworthy and Narimousa, 1994, and references therein):

$$\begin{aligned} l \sim l_{norot} &= h, \\ u \sim u_{norot} &= (Bh)^{1/3}, \end{aligned}$$

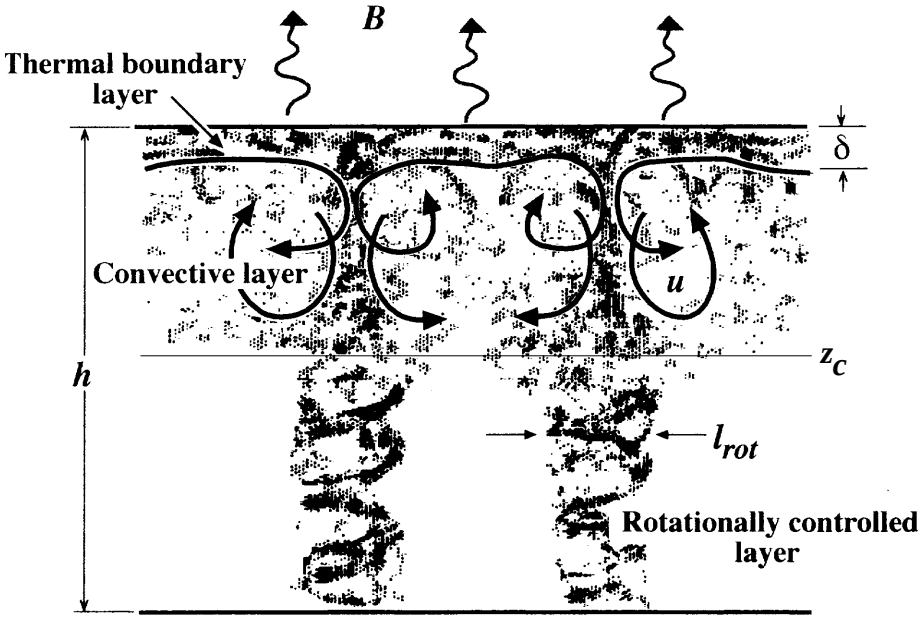


FIG. 5.29: Schematic representation of the evolution of a population of plumes under rotational control sinking in to a fluid of depth $h$, triggered by buoyancy loss $B$. If the depth of the fluid exceeds the critical depth $z_c$ (as drawn here) the plumes that make up the convective layer will come under rotational control on the scale $l_{rot}$ (modified version of Marshall and Schott, 1999, their Figure 19).

$$b \sim b_{norot} = \left(\frac{B^2}{h}\right)^{1/3}. \tag{5.9}$$

The subscript *norot* indicates that these scales are independent of rotation. From these a Rossby number of the turbulent fluctuations in the mixed layer can be constructed as (e. g. Coates and Ivey, 1997):

$$Ro = \frac{u}{fl} \sim \frac{u_{norot}}{f l_{norot}} = \left(\frac{B}{f^3 h^2}\right)^{1/3} \tag{5.10}$$

The rightmost term is often called the convective Rossby number $Ro_c$ (e. g. Raasch and Etling, 1991; Julien et al., 1996).

With further preceding time the plumes may become sufficiently large for their turnover timescale $l/u$ to arrive at the same order as the rotational timescale $f^{-1}$. At the critical depth $z_c$, a transition from the three–dimensional plumes to quasi two–dimensional, rotationally dominated motions will occur. In this case the ocean has to be sufficiently deep ($z_c < h$) for the plumes to come under geostrophic control before they reach the bottom. Replacing $t$ by $f^{-1}$ in equation (5.8), the turbulent length, velocity and buoyancy scales become (Fernando et al., 1991; Maxworthy and

Narimousa, 1994, and references therein):

$$\begin{aligned} l \sim z_c \sim l_{rot} &= \left(\frac{B}{f^3}\right)^{1/2}, \\ u \sim u_{rot} &= \left(\frac{B}{f}\right)^{1/2}, \\ b \sim b_{rot} &= (Bf)^{1/2}, \end{aligned} \tag{5.11}$$

where the subscript *rot* denotes the scales for turbulence dominated by rotation. At these scales the turbulent Rossby number is invariant:

$$Ro = \frac{u}{fl} \sim \frac{u_{rot}}{fl_{rot}} = 1. \tag{5.12}$$

The transition to rotational control of the turbulence, beneath an upper convective layer, might be expected, if the ratio between the rotational length scale $l_{rot}$ and the total depth of the convective layer $h$ is small. The natural Rossby number

$$Ro^* = \frac{l_{rot}}{h} = \frac{u_{rot}}{fh} = \left(\frac{B}{f^3h^2}\right)^{1/2} \sim \frac{z_c}{h} \tag{5.13}$$

is a measure of this ratio (Marshall and Schott, 1999). The critical depth of the upper convective layer $z_c$ is related to the rotational scale $l_{rot}$. Therefore the natural Rossby number $Ro^*$ at which the transition occurs can be deduced from the coefficient of proportionality between $z_c$ and $l_{rot}$ and vice versa. Thus plumes come under rotational control, if the natural Rossby number is less than the reciprocal value of the scaling factor for $z_c$.

### 5.3.2 Results from Laboratory and Numerical Studies

The problem of convection in a rotating fluid has been addressed in a number of laboratory and numerical experiments. A wide range of aspects of the convection problem has been covered in these experiments, not limited to the dynamics on the plume scale. Another major subject, for instance, was the dynamics of a convectively generated homogeneous patch of dense water. In the following the focus is on experiments that arrived at quantitative results for the scaling factors in Equations 5.9 and 5.11. A broad review of laboratory and numerical experiments is given in Marshall and Schott (1999).

Laboratory and numerical experiments are generally performed over a wide range of buoyancy fluxes and rotation rates. The experiments of Fernando et al. (1991) were carried out in a bottom–heated, rotating tank filled with a homogeneous salt solution. Maxworthy and Narimousa (1994) used a source of denser saltwater released into the underlying fluid. Coates et al. (1995) again employed a source of bottom heating and examined the development of plumes into a thermally

stratified fluid. In a later experiment they used a larger range of rotation rates, and compared runs in stratified fluid with unstratified runs (Coates and Ivey, 1997). Jones and Marshall (1993) employed a numerical model based on the nonhydrostatic Boussinesq equations. The grid spacing of 250 m horizontally and 100 m in the vertical was small enough to resolve gross aspects of plumes.

The resulting scaling factors from the different experiments are summarized in Table 5.2. All laboratory experiments agree in the rotational velocity scale of $u \approx 2.2u_{rot}$, confirming earlier results of Boubnov and Golitsyn (1990). In the numerical experiment of Jones and Marshall (1993) the velocity fluctuations were of about the same order as the rotational scale. Maxworthy and Narimousa (1994) also found that the maximum velocity occurring in rotating plumes scales with $l_{rot}$, and estimated a scaling factor of 4.

TABLE 5.2: Nonrotational and rotational scaling factors, and the critical depth where the transition to rotational controlled convection occurs.

| nonrotational | rotatinonal scaling | critical depth |
|---|---|---|
| Fernando et al. (1991): bottom–heated rotating tank | | |
| | $l = (3.2 \pm 0.3)l_{rot}$* | $z_c = (12.7 \pm 1.3)l_{rot}$ |
| $u = (0.5 \pm 0.07)u_{norot}$† | $u = (2.4 \pm 0.2)u_{rot}$ | |
| Jones and Marshall (1993): 250 m horizontal resolution nonhydrostatic model | | |
| | $u \approx 0.9u_{rot}$‡ | |
| Maxworthy and Narimousa (1994): rotating tank, dense water released on top | | |
| | $l = (15.0 \pm 1.5)l_{rot}$ | $z_c = (12.7 \pm 1.5)l_{rot}$ |
| | $u = (2.0 \pm 0.2)u_{rot}$ | |
| | $u_{max} = (4.0 \pm 0.4)u_{rot}$ | |
| Coates et al. (1995): bottom–heated rotating tank, with thermally stratified fluid | | |
| $l = (0.38 \pm 0.06)l_{norot}$ | | |
| $u \approx 0.3u_{norot}$ | | |
| Coates and Ivey (1997): bottom–heated rotating tank | | |
| $u = (0.8 \pm 0.1)u_{norot}$† | $u = (2.2 \pm 0.2)u_{rot}$ | $z_c = (35 \pm 15)l_{rot}$ |
| This study: observations with moored ADCPs (see Section 5.3.3) | | |
| $l \sim h$ | | |
| $u = (0.6 \pm 0.2)u_{norot}$ | | |
| $u_{max} = (1.5 \pm 0.6)u_{norot}$ | | |

* using $l = 0.25z_c$ (Hunt, 1984)
† runs carried out with rotation switched off ($f = 0$)
‡ estimated from values given in their Table 3

Fernando et al. (1991) and Coates and Ivey (1997) carried out a number of runs with rotation switched off ($f = 0$), resulting in nonrotational scaling factors for the velocity fluctuations

of 0.5 and 0.8, respectively. In their experiments, Coates and Ivey (1997) demonstrated that with increasing rotation the nonrotational scaling factor for velocity decreases, thus explaining their earlier results (Coates et al., 1995) of a relatively small scaling factor of about 0.3. Both experiments showed, that the nonrotational scaling stays valid in the presence of rotation, and also in the presence of an initial thermal stratification.

Considering the critical depth $z_c$, where the plumes come under rotational control, Maxworthy and Narimousa (1994) confirmed the results of Fernando et al. (1991) of a scaling factor of 12.7 for $z_c$, but came to a quite different length scale for the rotating plumes. They found that the mean diameter of the convective cells is about the same as the depth of the upper convective layer. But while the results of Maxworthy and Narimousa (1994) were drawn from direct observations in the tank, the result of Fernando et al. (1991) was derived from earlier results of Hunt (1984). Coates and Ivey (1997) did not find a sudden transition from three–dimensional turbulence to rotationally controlled flow, but a rather smooth asymptotic one from one state to the other. They found a mean scaling factor of 35 for the critical depth, and a maximum scaling factor of 50 below which the turbulence was fully rotationally controlled.

The corresponding natural Rossby numbers for the scaling factors of $z_c$ found in the laboratory experiments are $Ro^* < 1/12.7 = 0.08$ for the results of Fernando et al. (1991) and Maxworthy and Narimousa (1994), and $Ro^* < 1/35 = 0.03$ for the results of Coates and Ivey (1997). This is much smaller than the value of about 0.7 suggested by the (apparently rather more diffusive (Marshall and Schott, 1999)) numerical experiments of Jones and Marshall (1993).

### *5.3.3 Observational Results Compared with Theory*

Despite the technical limitations of oberserving 3-D turbulence in the ocean, the attempt is made in the following to test the above scaling arguments with the field observations. Considering that a natural Rossby number of at least less than 0.1 appears to be necessary for a transition to rotationally controlled turbulence, it seems unlikely that this regime is appropriate for deep convection in the ocean. With a buoyancy flux of $B \approx 1 \times 10^{-7}$ m$^2$ s$^{-3}$ and a Coriolis parameter of $f \approx 1 \times 10^{-4}$ s$^{-1}$, the depth of the upper convective layer has to exceed 3200 m in order for the natural Rossby number to be less than 0.1. This is close to the water depth in the convection regions of the Greenland and Labrador Seas.

Figure 5.30 shows a contour plot of the natural Rossby number as function of buoyancy flux, mixed layer depth, and the Coriolis parameter in the Labrador Sea and the Greenland Sea, together with the conditions found during the plume events. The buoyancy flux during plume events is taken from NCEP/NCAR reanalysis data and the mixed layer depth is estimated from the temperature records obtained at the moorings. The uncertainties in the mixed layer depth may be up to several hundred meters depending on the actual spacing of temperature sensors in the mooring. Most of the events occurred at natural Rossby numbers well above the critical value of 0.1 and only a few

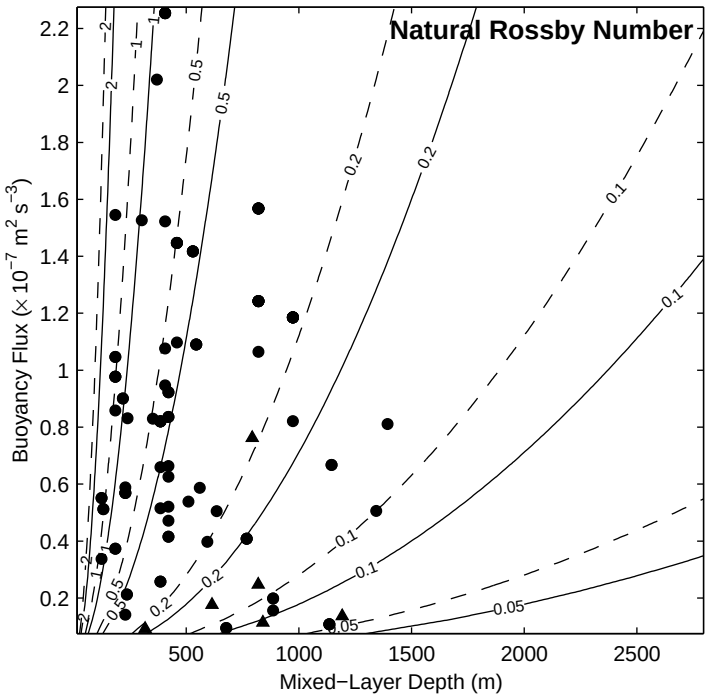


FIG. 5.30: Natural Rossby number $Ro^* = (B/f^3h^2)^{1/2}$ as function of surface buoyancy flux $B$, mixed layer depth $h$, and Coriolis parameter $f = 1.2 \times 10^{-4}$ s$^{-1}$ for the central Labrador Sea (solid) and $f = 1.4 \times 10^{-4}$ s$^{-1}$ for the central Greenland Sea (dashed). Points corresponding to observations of plumes are shown as dots for the Labrador Sea and as triangles for the Greenland Sea.

events show small values of $Ro^*$, especially during periods of weak forcing.

The maximum downward velocity and the rms vertical velocity of the individual plumes nondimensionalized with both the nonrotational scale $(Bh)^{1/3}$ and the rotational scale $(B/f)^{1/2}$ are shown in Figure 5.31. The scaled velocity measurements are plotted against the depth, nondimensionalized with the mixed layer depth, where the maximum downward velocity was found. The means and standard deviations for depth bins of $z/h = 0.2$ are shown as errorbars.

It is evident that for the maximum downward velocity as well as for the rms vertical velocity the nonrotational scaling is the better description of the observations. The scatter of the velocity data nondimensionalized with the rotational scale is at least twice that of the nonrotational scaling. Thus, the rotation clearly does not control the turbulence and the rms vertical velocity can be related to the nonrotational scale as

$$\langle w^2 \rangle^{1/2} = (0.6 \pm 0.2)(Bh)^{1/3}. \tag{5.14}$$

For the maximum downward velocity the observations suggest the relation

$$w_{max} = (1.5 \pm 0.5)(Bh)^{1/3}. \tag{5.15}$$

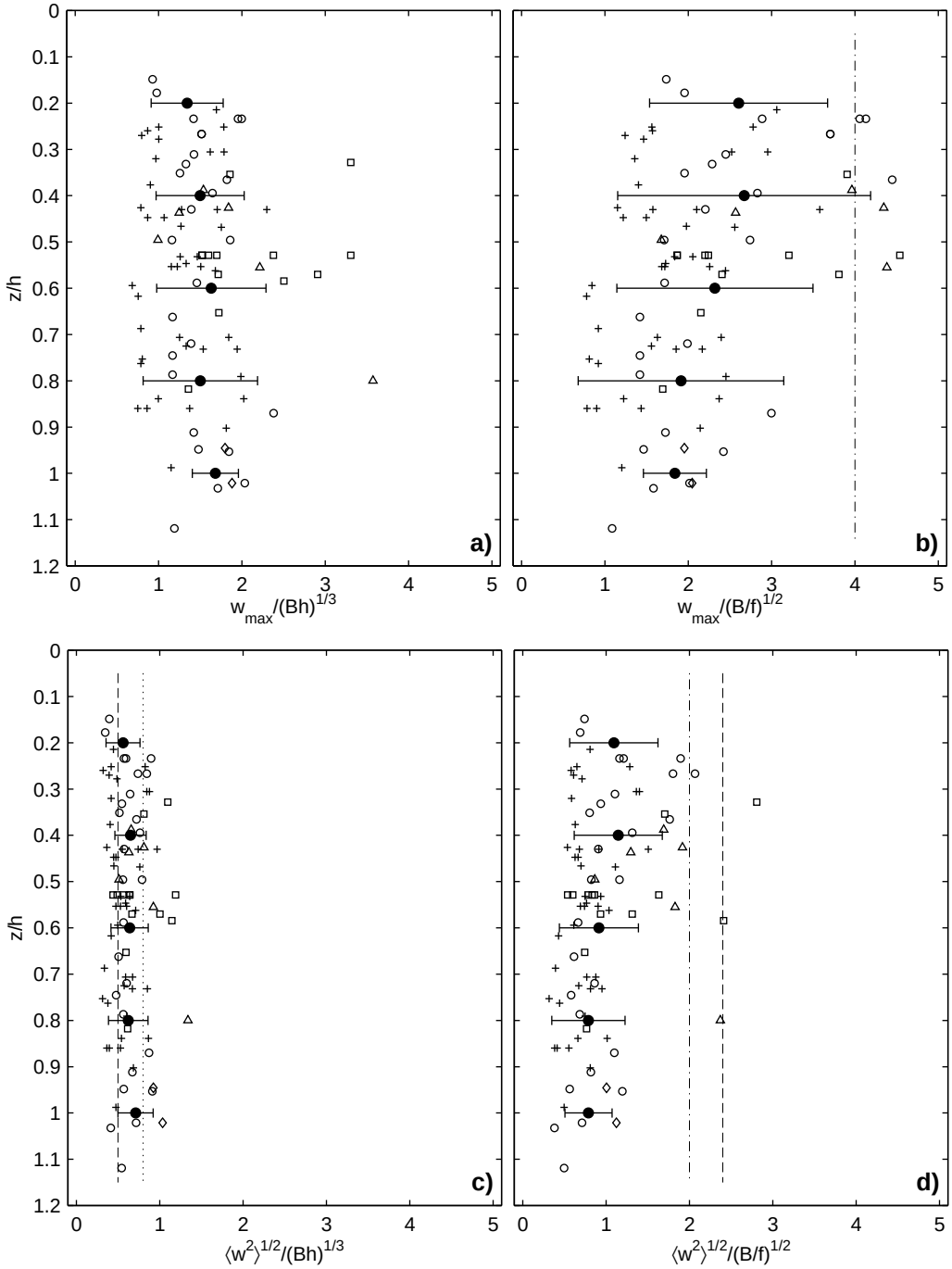


FIG. 5.31: Maximum downward velocity of individual plumes nondimensionalized with the nonrotational scale $(Bh)^{1/3}$ (a), and nondimensionalized with the rotational scale $(B/f)^{1/2}$ (b), plotted against the observation depth nondimensionalized with the mixed layer depth. (c) and (d) are the same for the rms vertical velocity. The data are from the Labrador Sea moorings Bravo 1994/95 (circles), K1 1996/97 (plus), K11 1997/98 (squares), K21 1998/99 (diamonds), and the Greenland Sea mooring GSM5 1994/95 (triangles). Means and standard deviations for $z/h$ = 0.2 intervals are shown as solid dots and errorbars. Results from laboratory experiments of Fernando et al. (1991) (dashed), Maxworthy and Narimousa (1994) (dashdot), and Coates and Ivey (1997) (dotted) are shown for comparison.

With a typical Labrador Sea buoyancy flux of $B$ = $1\times10^{-7}$ m$^2$ s$^{-3}$ and a mixed layer depth of $h$ = 1000 m this scaling results in a vertical velocity of $\langle w^2\rangle^{1/2} = (3 \pm 1)$ cm s$^{-1}$ and maximum values of $w_{max} = (7 \pm 2)$ cm s$^{-1}$.

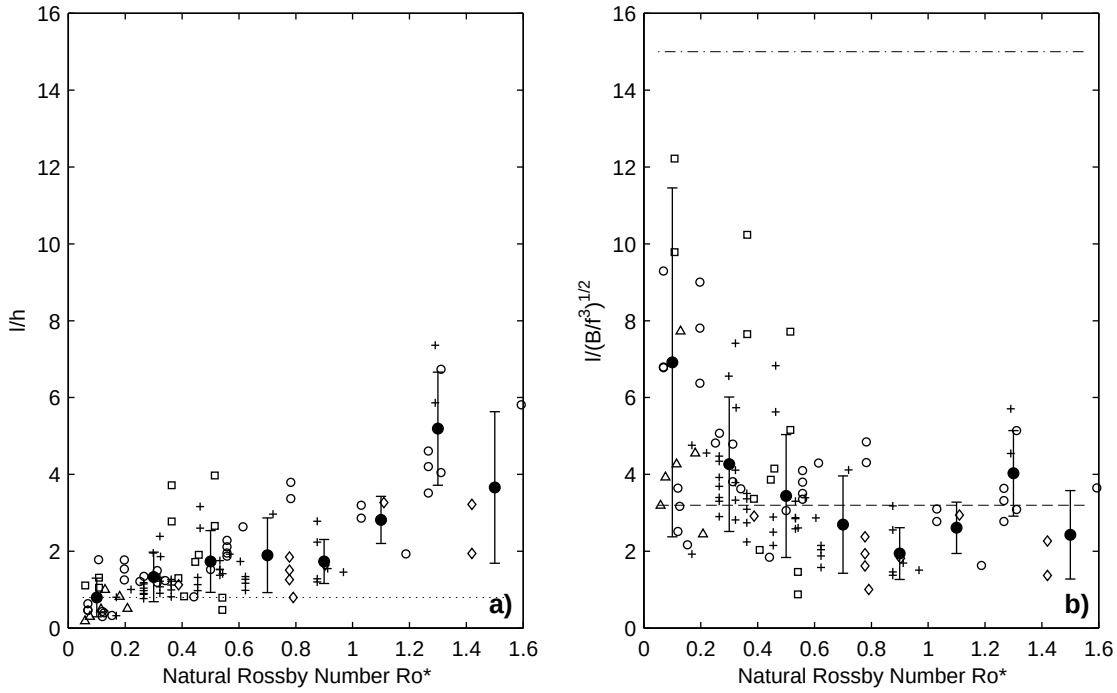


FIG. 5.32: Observed plume diameter nondimensionalized with the mixed layer depth (a), and nondimensionalized with the rotational scale $(B/f^3)^{1/2}$, plotted against the natural Rossby number $Ro^* = (B/f^3h^2)^{1/2}$. Markers are the same as in Figure 5.31. Means and standard deviations for $Ro^* = 0.2$ intervals are shown as solid dots and errorbars. Results from laboratory experiments of Fernando et al. (1991) (dashed), Maxworthy and Narimousa (1994) (dashdot), and Coates and Ivey (1997) (dotted) are shown for comparison.

Figure 5.32 shows the diameter of individual plumes scaled with the mixed layer depth and with the rotational scale $(B/f^3)^{1/2}$, plotted against the natural Rossby number $Ro^*$. In case of a transition to rotationally controlled turbulence, one would expect a decreasing scatter of the plume diameters scaled with $l_{rot}$ towards small natural Rossby numbers. This is obviously not the case. Instead the scatter increases dramatically towards small values of $Ro^*$.

Compared to the vertical velocity measurements, which are very accurate, the plume diameters are only rough estimates obtained from contour plots of vertical velocity. Although the nonrotational scaling of the plume diameters clearly describes the observations better than the rotational scaling, an appropriate scaling factor cannot be determined. At least the observed horizontal scales appear to be of the same order as the mixed layer depth.

Concurrent measurements of three–dimensional currents were carried out in the context of the *Labrador Sea Deep Convection Experiment* with 3–D Lagrangian floats, employed to track indi-

vidual water parcels. During the first winter (1997) the horizontal tracking of the floats failed, and only pressure records were obtained. In February and March 1998 three–dimensional trajectories were obtained, and rotation was observed on the 3–7 km scale. Evidence for rotation on smaller scales was found, but beyond the tracking accuracy. A downward spiraling of water parcels was not observed (E. Steffen, personal communication).

Assuming that the density anomalies caused by buoyancy loss at the surface are carried downward by the plumes, it takes a time of order $t_{mix} \sim h/w_{plume}$ to bring the dense fluid to the base of the mixed layer. Since in a diffusive system it takes a time of order $h^2/K_v$ to propagate a signal over a distance $h$, the magnitude of the diffusivity $K_v$ can be deduced from the knowledge of $t_{mix}$ (Send and Marshall, 1995; Klinger et al., 1996; Send and Käse, 1998)

$$K_v = \frac{h^2}{t_{mix}} = h w_{plume} \tag{5.16}$$

Using the vertical velocity scaling derived from the observations (Equation 5.14), a vertical mixing timescale can be defined as

$$t_{mix} = \frac{h}{\langle w^2 \rangle^{1/2}} = \frac{h}{0.6(Bh)^{1/3}} = \frac{1}{0.6}\left(\frac{h^2}{B}\right)^{1/3}, \tag{5.17}$$

and the corresponding eddy diffusivity results in

$$K_v = h\langle w^2 \rangle^{1/2} = 0.6(Bh^4)^{1/3}. \tag{5.18}$$

For the typical conditions of $B = 1\times10^{-7}$ m$^2$ s$^{-3}$ and $h$ = 1000 m, this results in a mixing timescale $t_{mix}$ of about 10 hours and a diffusivity of about 30 m$^2$ s$^{-1}$. These values, appropriate for effects of plumes, have to be compared with the thermal diffusivity derived from the heat flux estimates in Section 5.2.4. As the diffusivity of $K_T$ = 1 m$^2$ s$^{-1}$ resulted from 5–day vertical heat flux averages, it can be regarded as an estimate of the effective mixing carried out through an ensemble of plumes over several days. The corresponding mixing timescale of 11.5 days is then the time it takes to completely homogenize a convective patch by a large number of convective plumes. The other way round, the instantaneous heat flux time series (Figure 5.25) show peak values of 5 – 15 $\times$ 10$^{-4}$ K m s$^{-1}$ during individual plume event, with the vertical temperature gradient in the near–surface layer of about 0.5 $\times$ 10$^{-4}$ K m$^{-1}$ this gives diffusivities of $K_T$ = 10 – 30 m$^2$ s$^{-1}$, which corresponds well to the diffusivity resulting from the vertical velocity scaling.

In summary, the observations of individual plumes with moored ADCPs in the Greenland and Labrador Seas clearly support the nonrotational regime. This is consistent with the laboratory experiments that suggested a transition to rotationally controlled turbulence at natural Rossby numbers at least less than 0.1, while the natural Rossby numbers corresponding to the observed plume

events were generally larger. The scaling factor for the rms vertical velocity is remarkably close to the values obtained in the tank experiments where rotation has been switched off. One uncertainty arises from the fact that at large mixed layer depths only the upper part of the plumes is observed with the moored ADCPs, and one might argue that a transition to rotationally controlled flow occurs in the deeper part. On the other hand there is no indication in the observed horizontal scales of the plumes to follow the rotational scaling at small natural Rossby numbers.

# 6. SUMMARY AND CONCLUSIONS

In this study, observations at the known convection sites of the central Greenland and Labrador Seas were analyzed. The measurements carried out at moored stations in the Greenland Sea covered the period from June 1988 to October 1995 with a gap between April 1991 and August 1992. In the Labrador Sea the first mooring array was deployed in August 1996 and, while the observations are presently continued, the measurements up to summer 1999 were analyzed and compared to earlier observations from the winter 1994/95.

The convection activity observed in the central Labrador and Greenland Seas showed considerable interannual variability throughout the observational periods. In the Labrador Sea, the maximum depth of convection decreased from about 1800 m during the winter of 1994/95 to only 600 m in 1999. The water mass properties of the winter mixed layer showed increasing temperature and density and decreasing salinity. It has been shown that the variability of the convection activity cannot be attributed to variations of the surface forcing alone, but that the prevailing stratification is of similar importance. The most remarkable difference was between the winters of 1994/95 and 1996/97. The winter of 1996/97 was one of rather strong surface forcing, but the initial buoyancy content of the water column observed during summer 1996 was the highest within the observational period. A considerable amount of the additional buoyancy was located in the near–surface layer and caused by low salinity. Thus the convection in 1996/97 was less deep than in 1994/95, where the stratification was weaker and the less intense surface forcing could cause deeper convection. Nevertheless, probably more new Labrador Sea Water was formed during the winter of 1996/97, because a larger amount of water was transformed to the typical LSW density class.

One–dimensional budgets of heat and freshwater were evaluated at the Labrador Sea convection moorings and compared to the NCEP/NCAR reanalysis surface fluxes. The magnitude of the NCEP/NCAR freshwater fluxes turned out to be too small to explain the observed salinity of the winter mixed layer. The heat fluxes of the NCEP/NCAR data were typically 20 – 50% larger than the observed heat loss of the water column between summer and winter, but it cannot be separated to which degree this imbalance is due to overestimations of the heat fluxes or the lateral advection of heat. Between summer 1996 and summer 1999 the temperature time series showed a general warming of the upper 2000 m. The mean annual warming rate was of 0.13 °C/yr, corresponding to a net heat flux of about 34 W $m^{-2}$. The annual mean air–sea heat loss in the central Labrador Sea was of 60 W $m^{-2}$ for this period, resulting in 95 W $m^{-2}$ that have to be supplied by lateral

advection. This is most likely an upper limit, because of the possible overestimation of heat loss in the NCEP/NCAR data.

In the Greenland Sea, ongoing convection to the ocean bottom has not been directly observed at present, although it is suspected to occur at least occasionally. During the period of observations at moored stations, convection was only observed to reach intermediate depths. Yet, the observations revealed an interesting difference between the convection during the winter of 1988/89 and the winters of 1993/94 and 1994/95. In 1988/89, ice formation and its subsequent export out of the convection region contributed substantially to the buoyancy loss of the surface layer during the preconditioning (Visbeck et al., 1995), while during the later winters the central Greenland Sea remained ice free and the convection was purely driven by air–sea fluxes.

Regarding the impact of NAO variability on the convection intensity in the Greenland and Labrador Seas as suggested by Dickson et al. (1996), there is no obvious relation between the convection intensity during a particular winter and the winter mean NAO index. While the convection intensity decreased in the Labrador Sea over the observational period, the winter mean NAO index increased between 1996 and 1999. However, such a direct link was presumably not implied by the authors, and the relation between the NAO and the convection intensity should be considered on a longer time scale than year to year changes.

At least in the Labrador Sea, where about 30% of the variability of the winter time surface buoyancy loss are explained by the NAO index, several years of positive NAO, as during the late 1980s and early 1990s, increase the likelyhood that deep convection has taken place during such a period. If the restratification occurs on time scales longer than one year, convection could more easily reach larger depths during subsequent winters. This was probably the case for the winter of 1994/95. On the other hand, during a multi–year period of negative or moderate NAO, intense convection probably occurs only sporadically. The restratification of the water column through lateral advection, indicated by the warming trend observed in the Labrador Sea temperature records, then prevents deep convection during a subsequent mild winter. This was likely the case for the winter of 1996/97 and also for the winter of 1971/72, which showed the largest buoyancy loss in the NCEP/NCAR reanalysis data, but where convection reached to only 1500 m depth at OSW *Bravo* due to the low salinity of the near surface layer (Lazier, 1980).

In the Greenland Sea, the situation is more complicated due to the interaction with sea ice. A relation between the winter mean NAO index and the buoyancy loss to the atmosphere does not exist, at least in the NCEP/NCAR reanalysis data. Further, convection to large depths appears to be a rare event, while convection to intermediate depths occurs more regularly and either with sea ice interaction or purely driven by the atmosphere.

In addition to the observations in the central Labrador Sea, moorings were also deployed in the boundary current region. They were equipped as convection moorings in order to register eventually happening convection in the Labrador Current as suggested by Pickart et al. (1997). Both

the vertical velocity measurements as well as the temperature development over the winter period showed no evidence of convection activity at these mooring locations. Instead, rather instantaneous cooling over several hundred meters was observed during winter, followed by increased fluctuations between cold and warm conditions. The large vertical range of the temperature fluctuations suggests a lateral advection of the anomalies. The temperature and salinity time series indicate that the cold and fresh water in the boundary current region can be a result of horizontal mixing with convectively generated water from the interior Labrador Sea.

Interestingly, the water mass properties of the winter mixed layer observed in 1999 at the central convection mooring corresponded to the source properties of the so called upper LSW (Pickart et al., 1996), indicating the possibility of its formation in the central Labrador Sea during rather mild winters. This is in contrast to the suggestion by Pickart et al. (1997) of upper LSW being formed by convection in the main branch of the Labrador Current.

The vertical velocity measurements from the Labrador and Greenland Seas were carefully analyzed for individual plume events. The resulting number of observed events by far exceeds those of previous studies, thus allowing the first thoroughly test of theoretical scaling laws, developed from numerical and laboratory experiments, against field observations.

The spatial and velocity structure of the convective plumes observed in the Labrador and Greenland Seas generally confirm the earlier observations with moored ADCPs in convection regions, supporting them with a broader observational base. The plumes observed in the Greenland Sea showed horizontal scales of typically 200 – 600 m, based on the horizontal background flow and assuming that plumes are advected as frozen structures. The maximum downward velocities were of 4 – 5 cm $s^{-1}$ with peak values of up to 9 cm $s^{-1}$. In the Labrador Sea, plumes with larger diameters of 200 – 1200 m were diagnosed. The average horizontal size was of about 700 m and the vertical velocities ranged between 3 and 9 cm $s^{-1}$. During the winter of 1996/97 it was possible to directly measure the vertical heat flux associated with plumes over two periods of intense convection. Both events lasted for several days and showed statistically significant mean heat fluxes of about 200 W $m^{-2}$ at a depth of 430 m. A further period of significant heat flux of about 100 W $m^{-2}$ was observed during the following winter in mid–March 1998.

A major question addressed was whether convective plumes come under rotational control, and hence if their growth is constrained by the Earth's rotation. The observed maximum and rms vertical velocities agree with the scaling arguments for the nonrotational regime, and the determined scaling factor for the rms vertical velocity is remarkably close to the values obtained in tank experiments where rotation has been switched off. The natural Rossby numbers corresponding to the observed plume events were generally larger then 0.1, which is consistent with the laboratory experiments that suggest a transition to rotationally controlled turbulence for smaller Rossby numbers. The results for the horizontal plume scale are less clear, but still the nonrotational scaling describes the observations better than the rotational scaling, and the observed horizontal scales appear to be

of the same order as the mixed layer depth.

Previous studies brought no clear evidence for a well organized horizontal circulation associated with convective plumes and the larger number of events analyzed here also showed no consistent horizontal currents, even when several events where averaged. Instead, it seems that the horizontal currents on short time scales are random structures, at least in the Labrador Sea. For the Greenland Sea, due to the fewer observations, it cannot be ruled out that sporadically convective plumes become rotationally controlled. Further, the buoyancy flux in the Greenland Sea is generally weaker than in the Labrador Sea and convection was observed only to intermediate depths. A weak surface forcing of $B = 0.1 \times 10^{-7}$ m$^2$ s$^{-3}$ and a deep mixed layer of about 3000 m gives a natural Rossby number of about 0.02 and thus would result in rotationally controlled turbulence, according to the results of Coates and Ivey (1997). Nevertheless, these authors showed that the nonrotational scaling, which was found to be consistent with the observations, stays valid even in a state of transition where the rotation affects but does not control the turbulence. Thus it can be concluded that the nonrotational scaling applies for the majority of oceanic conditions, while rotationally controlled convection occurs only rarely in the ocean.

Regarding the net effect of individual plumes and their representation in numerical models, Klinger et al. (1996) showed that the gross properties of plumes seen in their nonhydrostatic, plume–resolving model are adequately represented by a slow convective adjustment scheme. A slow adjustment scheme is equivalent to employing a large vertical diffusion for statically unstable conditions. The vertical velocity scaling derived from the observations indicates that a vertical diffusivity of $K_v = 0.6(Bh^4)^{1/3}$ is appropriate for the effects of convective plumes. The corresponding mixing time scale is typically of the order of several hours. On the larger scale, the measurements of the vertical heat flux suggest that it takes several days for the plumes to homogenize a convective patch. An appropriate diffusivity to represent the net effect of an ensemble of plumes is probably one order of magnitude smaller than on the plume scale.

# APPENDIX

# A. MOORINGS AND DATA QUALITY

## *A.1 Moored Instruments*

Throughout the years of convection observations in the Greenland and Labrador Seas, a multitude of different instruments was deployed in the moorings. A listing of the instruments deployed in the Greenland Sea moorings is given in Table A.1 (including the moored array from the winter of 1988/89 for completeness), and the instruments deployed in the Labrador Sea are listed in Table A.2. The three–dimensional flow field was recorded using RD instruments acoustic Doppler current profilers (ADCPs), discussed in more detail in Appendix A.2. Horizontal currents were measured with Aanderaa rotor current meters (RCMs) and in the Labrador Sea also with FSI acoustic current meters (ACMs). The ACMs were initially intended to measure all three velocity components, but the vertical velocity turned out to be unreliable. All current meters were further equipped with temperature sensors.

Additional temperature records from four types of instruments were used to measure the changes of the thermal stratification: Aanderaa thermistor strings with a thermistor spacing of 20 m for the 200 m long strings and 40 m spacing for the 400 m strings, FSI temperature recorders, temperature/pressure recorders developed at the IfM Kiel, and Sea–Bird temperature/conductivity recorders (SeaCATs, MicroCATs). The temperature measurements were compared to CTD casts obtained in the vicinity of the moorings and most of the instruments needed offset corrections of typically 0.02 – 0.20 °C, except for the high–precision SeaCATs and MicroCATs and the IfM Kiel instruments. The accuracy of the temperature/conductivity recorders was further improved by lowering the instruments together with the CTD probe before deployment and after recovery. The rms differences were typically 0.001 °C and 0.003 mS/cm. The IfM Kiel recorders were laboratory calibrated and have a nominal accuracy of 0.005 – 0.010 °C.

The determination of salinity and density from conductivity and temperature measurements with SeaCATs and MicroCATs may be considerably affected if a constant pressure is used (i. e. the nominal instrument depth). An increase of pressure of 100 dbar, due to vertical excursions of the instruments, results in a decrease of 0.05 in salinity and 0.04 in density. The error on the computation of potential temperature is about one order of magnitude smaller. In order to account for the vertical excursions of sometimes several hundred meters in the central Labrador Sea, pressure records were constructed using a mooring model. The model determines the equilibrium response

TABLE A.1: Greenland Sea moorings

| Instrument Type | Depth (m) | Duration (days) | Sampling Rate (minutes) | Remarks |
|---|---|---|---|---|
| *Mooring: M250, 73° 21.5' N 0° 48.0' W, Water Depth: 3008 m* | | | | |
| *1988/07/02 09:37 – 1989/05/18 18:18* | | | | |
| THS (200 m) | 78 | 320 | 120 | |
| ADCP (upward) | 361 | 320 | 30 | |
| RCM-4 | 371 | 320 | 60 | |
| RCM-4 | 827 | 320 | 60 | |
| RCM-4 | 1437 | 320 | 60 | |
| RCM-5 | 2442 | 320 | 60 | |
| *Mooring: M319, 74° 57.0' N 4° 59.0' W, Water Depth: 3554 m* | | | | |
| *1988/06/17 19:50 – 1989/05/28 06:06* | | | | |
| THS (200 m) | 60 | 385 | 120 | |
| ADCP (upward) | 344 | 385 | 30 | |
| RCM-4 | 347 | 385 | 60 | |
| RCM-5 | 807 | 385 | 60 | no data |
| RCM-5 | 1345 | 385 | 60 | |
| *Mooring: T5, 75° 34.0' N 6° 7.0' W, Water Depth: 3374 m* | | | | |
| *1988/09/14 13:42 – 1989/08/30* | | | | |
| Tomo | 97 | | | (SIO/WHOI) |
| ADCP (downward) | 141 | 344 | 30 | |
| *Mooring: T6, 75° 3.0' N 2° 58.0' W, Water Depth: 3624 m* | | | | |
| *1988/09/20 14:05 – 1989/08/20* | | | | |
| RCM/SeaCAT | 60 | | | (NOAA/PMEL) |
| Tomo | 88 | | | (SIO/WHOI) |
| RCM/SeaCAT | 197 | | | (NOAA/PMEL) |
| ADCP (downward) | 200 | 333 | 60 | |
| ADCP (upward) | 1400 | 333 | 60 | |
| RCM/SeaCAT | 1402 | | | (NOAA/PMEL) |
| *Mooring: GSM1, 75° 0.1' N 4° 0.0' W, Water Depth: 3600 m* | | | | |
| *1989/05/28 13:17 – 1990/06/27* | | | | |
| THS (200 m) | 68 | 329 | 120 | until 1990/04/23 |
| ADCP (upward) | 321 | 0 | 30 | no data |
| RCM-4 | 332 | 177 | 60 | until 1989/11/22 |
| RCM-4 | 795 | 394 | 60 | |
| RCM-5 | 1410 | 336 | 60 | until 1990/04/30 |
| RCM-5 | 3087 | 0 | 60 | no data |

Instrument types are: ADCP, RDI acoustic Doppler current profiler; RCM, Aanderaa current meter; THS, Aanderaa thermistor string; SeaCAT, Sea–Bird temperature/conductivity recorder.

TABLE A.1:(continued)

| Instrument Type | Depth (m) | Duration (days) | Sampling Rate (minutes) | Remarks |
|---|---|---|---|---|
| *Mooring: GSM2, 75° 1.2' N 4° 4.9' W, Water Depth: 3600 m* | | | | |
| *1990/07/13 18:18 – mooring lost* | | | | |
| ADCP (upward) | 324 | 264 | 30 | found in summer 1995 |
| *Mooring: GSM3, 74° 59.3' N 3° 3.6' W, Water Depth: 3520 m* | | | | |
| *1992/08/20 01:22 – 1993/04/09 07:38* | | | | |
| SeaCAT | 58 | 232 | 20/5* | bad conductivity |
| RCM-4 | 79 | 232 | 120 | (IfM Hamburg) |
| THS (200 m) | 100 | 0 | 120 | no data |
| RCM-4 | 324 | 232 | 120 | (IfM Hamburg) |
| SeaCAT | 346 | 232 | 20/5* | bad conductivity |
| THS (400 m) | 568 | 0 | 120 | no data |
| ADCP (upward) | 570 | 232 | 20 | |
| SeaCAT | 572 | 232 | 20/5* | |
| RCM-5 | 1101 | 232 | 120 | (IfM Hamburg) |
| SeaCAT | 1408 | 232 | 20/5* | |
| RCM-5 | 2456 | 232 | 120 | (IfM Hamburg) |
| *Mooring: GSM4, 74° 59.4' N 2° 53.9' W, Water Depth: 3630 m* | | | | |
| *1993/05/21 21:52 – 1994/07/30 12:48* | | | | |
| SeaCAT | 170 | 434 | 20/5* | |
| RCM-8 | 195 | 434 | 120 | |
| THS (200 m) | 216 | 434 | 120 | |
| SeaCAT | 442 | 434 | 20/5* | |
| THS (400 m) | 463 | 434 | 120 | |
| ADCP (upward) | 869 | 0 | 20 | no data |
| SeaCAT | 874 | 434 | 20/5* | |
| RCM-8 | 1076 | 434 | 120 | |
| SeaCAT | 1477 | 434 | 20/5* | |
| RCM-8 | 2548 | 434 | 120 | |
| *Mooring: GSM5, 75° 2.3' N 2° 54.8' W, Water Depth: 3563 m* | | | | |
| *1994/07/30 17:58 – 1995/10/17 12:07* | | | | |
| SeaCAT | 45 | 443 | 20/5* | |
| THS (400 m) | 90 | 228 | 120 | until 1995/05/05 00:00 |
| SeaCAT | 242 | 443 | 20/5* | |
| SeaCAT | 444 | 443 | 20/5* | |
| ADCP (upward) | 500 | 443 | 20 | |
| SeaCAT | 687 | 443 | 20/5* | |
| SeaCAT | 993 | 443 | 20/5* | |
| RCM-7 | 1390 | 443 | 60 | |

* higher sampling rate during winter months

TABLE A.2: Labrador Sea moorings

| Instrument Type | Depth (m) | Duration (days) | Sampling Rate (minutes) | Remarks |
|---|---|---|---|---|
| *Mooring K1, 56° 33.6' N 52° 39.5' W, Water Depth: 3492 m* | | | | |
| *1996/08/10 22:20 – 1997/05/25 15:16* | | | | |
| SeaCAT | 75 | 288 | 10 | |
| Tomo | 132 | | | |
| THS (200 m) | 182 | 288 | 60 | |
| SeaCAT | 425 | 288 | 10 | |
| ADCP (upward) | 487 | 288 | 20 | |
| MiniT | 596 | 288 | 10 | |
| MiniT | 677 | 288 | 10 | |
| MiniT | 768 | 288 | 10 | |
| SeaCAT | 869 | 288 | 10 | 1996/11/22 temp./cond. jump |
| MiniT | 972 | 288 | 10 | until 1996/10/23 |
| ACM | 1074 | 288 | 30 | |
| SeaCAT | 1281 | 288 | 10 | no conductivity |
| MiniT | 1595 | 288 | 10 | from 1996/10/22 |
| MiniT | 1739 | 288 | 10 | only 1996/10/20 – 1996/11/10 |
| ACM | 1790 | 288 | 30 | |
| SeaCAT | 2096 | 288 | 10 | |
| *Mooring K2, 55° 19.5' N 53° 53.6' W, Water Depth: 2385 m* | | | | |
| *1996/08/09 15:35 – 1997/08/07 20:40* | | | | |
| SeaCAT | 110 | 363 | 10 | |
| THS (200 m) | 135 | 363 | 180 | |
| SeaCAT | 388 | 363 | 10 | |
| ADCP (upward) | 440 | 363 | 20 | |
| THS (400 m) | 476 | 363 | 180 | |
| Current Meter | 880 | 363 | 17 | (SIO) temperature only |
| SeaCAT | 985 | 363 | 10 | |
| ACM | 1149 | 363 | 30 | |
| RCM-8 | 1385 | 363 | 60 | |
| SeaCAT | 1761 | 363 | 10 | |
| ACM | 1762 | 363 | 30 | |
| ACM | 2118 | 363 | 30 | |
| *Mooring K3, 56° 15.1' N 48° 42.0' W, Water Depth: 3690 m* | | | | |
| *1996/08/13 21:06 – 1997/07/12 10:05* | | | | |
| Tomo | 120 | | | |

Instrument types are: ADCP, RDI acoustic Doppler current profiler; RCM, Aanderaa current meter; ACM, FSI acoustic current meter; THS, Aanderaa thermistor string; SeaCAT/MicroCAT, Sea–Bird temperature/conductivity recorder; MiniT, FSI temperature recorder; MiniTD, IfM Kiel temperature/pressure recorder.

TABLE A.2:(continued)

| Instrument Type | Depth (m) | Duration (days) | Sampling Rate (minutes) | Remarks |
|---|---|---|---|---|
| *Mooring K4, 58° 30.0' N 50° 34.2' W, Water Depth: 3530 m* | | | | |
| *1996/08/12 15:05 – 1997/07/10 21:28* | | | | |
| Tomo | 130 | | | |
| ACM | 590 | 332 | 30 | |
| *Mooring K5, 57° 29.8' N 51° 39.6' W, Water Depth: 3539 m* | | | | |
| *1996/08/11 18:07 – 1997/05/27 10:00* | | | | |
| ADCP (downward) | 80 | 289 | 30 | |
| CTD Profiler | 100 | 0 | 2880 | no data |
| *Mooring K6, 55° 09.1' N 54° 06.9' W, Water Depth: 1220 m* | | | | |
| *1996/08/08 22:32 – 1997/07/08 18:31* | | | | |
| ADCP (upward) | 350 | 334 | 20 | |
| ACM | 460 | 0 | 30 | no data |
| ACM | 660 | 334 | 30 | |
| *Mooring K11, 56° 33.6' N 52° 39.5' W, Water Depth: 3490 m* | | | | |
| *1997/07/22 23:39 – 1998/07/10 10:47* | | | | |
| MiniTD | 56 | 352 | 20 | |
| SeaCAT | 71 | 352 | 10 | |
| ADCP (downward) | 192 | 352 | 20 | |
| SeaCAT | 295 | 352 | 10 | |
| ACM | 550 | 352 | 30 | |
| SeaCAT | 809 | 352 | 10 | |
| MiniTD | 1150 | 0 | 20 | no data |
| SeaCAT | 1370 | 352 | 10 | |
| ACM | 1371 | 352 | 30 | |
| SeaCAT | 1980 | 352 | 10 | |
| RCM-8 | 2590 | 352 | 60 | |
| *Mooring K12, 55° 19.5' N 53° 53.6' W, Water Depth: 2380 m* | | | | |
| *1997/07/21 19:48 – 1998/07/11 14:04* | | | | |
| MiniTD | 54 | 355 | 20 | |
| Tomo | 123 | | | |
| ADCP (downward) | 186 | 355 | 30 | until 1998/05/02 |
| MicroCAT | 339 | 355 | 10 | |
| MiniTD | 768 | 355 | 20 | |
| ACM | 1471 | 355 | 30 | |
| SeaCAT | 1472 | 355 | 10 | |
| RCM-8 | 1979 | 355 | 30 | |
| ACM | 2277 | 355 | 60 | |

TABLE A.2:(continued)

| Instrument Type | Depth (m) | Duration (days) | Sampling Rate (minutes) | Remarks |
|---|---|---|---|---|
| *Mooring K14, 58° 30.0' N 50° 34.2' W, Water Depth: 3530 m* | | | | |
| *1997/07/23 22:35 – 1998/08/05 09:15* | | | | |
| Tomo | 130 | | | |
| ACM | 1315 | 377 | 30 | |
| *Mooring K15, 57° 06.1' N 54° 40.0' W, Water Depth: 3231 m* | | | | |
| *1997/07/20 09:44 – 1998/07/09 18:00* | | | | |
| ADCP (downward) | 70 | 354 | 30 | |
| CTD Profiler | | 354 | 2880 | incomplete |
| RCM-8 | 3023 | 354 | 60 | |
| *Mooring K17, 57° 24.8' N 55° 40.0' W, Water Depth: 2965 m* | | | | |
| *1997/07/20 19:09 – 1998/07/09 10:31* | | | | |
| Tomo | 134 | | | |
| ADCP (downward) | 261 | 354 | 30 | |
| MiniTD | 400 | 354 | 20 | |
| MicroCAT | 871 | 354 | 15 | |
| ACM | 872 | 0 | 30 | no data |
| ACM | 1380 | 0 | 30 | no data |
| *Mooring K20, 56° 58.8' N 54° 34.8' W, Water Depth: 3230 m* | | | | |
| *1998/08/03 13:08 – 1999/07/21 15:03* | | | | |
| MiniTD | 53 | 352 | 15 | |
| ADCP (downward) | 67 | 352 | 30 | |
| CTD Profiler | | 352 | 2880 | incomplete |
| RCM-8 | 3121 | 352 | 60 | |
| *Mooring K21, 56° 33.6' N 52° 39.5' W, Water Depth: 3490 m* | | | | |
| *1998/08/06 20:50 – 1999/07/18 10:22* | | | | |
| MiniTD | 69 | 346 | 20 | |
| MicroCAT | 73 | 346 | 15 | start 1998/08/07 00:00 |
| Tomo | 136 | | | |
| ADCP (downward) | 200 | 346 | 30 | |
| MicroCAT | 303 | 346 | 15 | |
| RCM-8 | 561 | 346 | 60 | |
| MicroCAT | 818 | 346 | 15 | |
| SeaCAT | 1074 | 346 | 15 | |
| SeaCAT | 1481 | 346 | 15 | |
| RCM-8 | 1482 | 346 | 60 | |
| SeaCAT | 2296 | 346 | 15 | offset 1998/09 – 1999/04 |
| ACM | 2601 | 346 | 30 | u, v bad after 1998/10/01 |

TABLE A.2:(continued)

| Instrument Type | Depth (m) | Duration (days) | Sampling Rate (minutes) | Remarks |
|---|---|---|---|---|
| *Mooring K22, 55° 27.2' N 53° 43.3' W, Water Depth: 2775 m* | | | | |
| *1998/08/01 20:33 – 1999/07/19 11:42* | | | | |
| Argonaut | 73 | 261 | 60 | until 1999/04/19 16:00 |
| Tomo | 131 | | | |
| ADCP (downward) | 195 | 0 | 30 | no data |
| SeaCAT | 348 | 352 | 15 | |
| MiniT | 607 | 0 | 10 | no data |
| MiniT | 758 | 0 | 10 | no data |
| MiniT | 909 | 0 | 10 | no data |
| MiniTD | 1000 | 352 | 20 | |
| MiniT | 1060 | 0 | 10 | no data |
| MiniT | 1211 | 0 | 10 | no data |
| MiniT | 1353 | 0 | 10 | no data |
| SeaCAT | 1517 | 352 | 15 | |
| RCM-8 | 1518 | 352 | 60 | |
| RCM-8 | 1916 | 352 | 60 | |
| RCM-8 | 2565 | 352 | 60 | |
| SeaCAT | 2751 | 352 | 15 | |
| ACM | 2752 | 352 | 30 | |
| *Mooring K23, 57° 24.8' N 56° 34.3' W, Water Depth: 2770 m* | | | | |
| *1998/08/04 00:23 – 1999/07/22 11:05* | | | | |
| MiniTD | 65 | 352 | 20 | |
| Tomo | 136 | | | |
| ADCP (downward) | 209 | 352 | 30 | |
| SeaCAT | 1329 | 352 | 15 | |
| RCM-8 | 1328 | 352 | 60 | |

of the mooring to a given velocity profile, from the drag coefficients and the buoyancy of each mooring component. The results were further improved by fitting them to pressure records and ADCP surface distance measurements. However, uncertainties of up to 100 dbar remained during periods of extreme vertical excursions.

## *A.2 ADCP Current Measurements*

All ADCPs operated at 153.6 kHz and had a 20° beam angle configuration. The setup parameters have been changed over the years depending on data storage capacity and battery power available. The observational range of the instruments and the depths of the individual vertical depth cells (bins) are shown in Figure A.1. The ADCP vertical velocity records all show a mean bias between

0.2 and 0.8 cm $s^{-1}$, that is always negative and probably results from the internal data processing. Assuming that the mean vertical velocity should vanish over the deployment period, the bias has been removed from each time series.

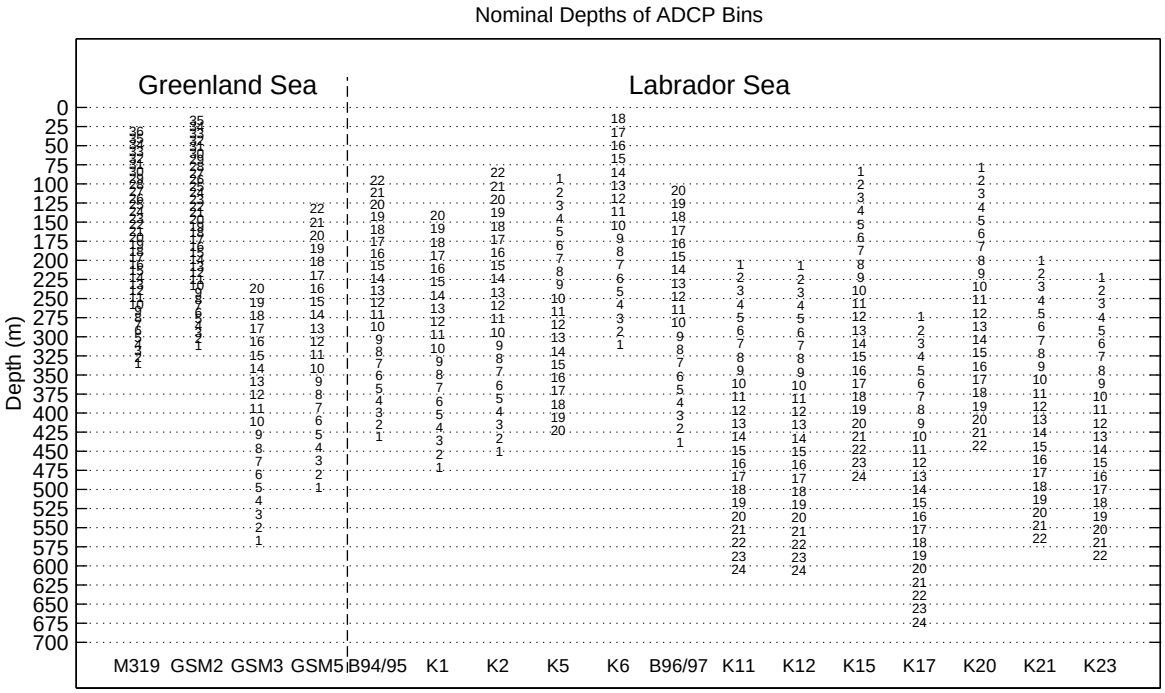


FIG. A.1: Observational range and the depths of the individual bins for all ADCPs in the Greenland and Labrador Seas.

For the first deployments in the Greenland Sea, up to the GSM2 mooring, bins of 8.6 m length were used, with 125 pings transmitted every 30 minutes at 1 second intervals vector averaged into ensembles (burst sampling). According to the manufacturer the random error of the horizontal velocity components, using 20° transducers, is approximately:

$$\sigma = \frac{1}{FD}\,\frac{2.4 \times 10^5}{\sqrt{N}} \tag{A.1}$$

where $\sigma$ is the standard deviation (m $s^{-1}$), $F$ is the frequency (Hz), $D$ is the bin length (m), and $N$ is the number of pings averaged (RD Instruments, 1989). For the vertical velocity component the error reduces by a factor of $sin20^\circ/cos20^\circ \approx 0.36$. The above parameter settings yield a nominal accuracy of 1.7 cm $s^{-1}$ for the horizontal ensemble velocity and of 0.6 cm $s^{-1}$ for the vertical velocity. The parameter settings for all ADCPs and the implied nominal accuracy is summarized in Table A.3.

During the later Greenland Sea ADCP deployments (GSM3, GSM5) the emsemble interval was reduced to 20 minutes and the instruments operated with 17.4 m bin length. The GSM3 instrument

TABLE A.3: ADCP parameter settings for all instruments and the implied nominal accuracy of the horizontal and vertical velocity components.

| Mooring | Bin Length (m) | Pings per Ensemble | Ping Interval (sec) | Ensemble Interval (min) | Horizontal Accuracy (cm $s^{-1}$) | Vertical Accuracy (cm $s^{-1}$) |
|---|---|---|---|---|---|---|
| *Greenland Sea* | | | | | | |
| M319 1988/89 | 8.2 | 125 | 1 | 30 | 1.7 | 0.6 |
| GSM2 1990/91 | 8.2 | 125 | 1 | 30 | 1.7 | 0.6 |
| GSM3 1992/93 | 17.4 | 60 | 1.5 | 20 | 1.3 | 0.5 |
| GSM5 1994/95 | 17.4 | 34 | 31.82 | 20 | 1.7 | 0.6 |
| *Labrador Sea* | | | | | | |
| Bravo 1994/95 | 17.4 | 35 | 2 | 20 | 1.7 | 0.6 |
| K1 1996/97 | 17.4 | 60 | 1 | 20 | 1.3 | 0.4 |
| K2 1996/97 | 17.4 | 60 | 1 | 20 | 1.3 | 0.4 |
| K5 1996/97 | 17.4 | 25 | 1 | 30 | 2.0 | 0.7 |
| K6 1996/97 | 17.4 | 60 | 1 | 20 | 1.3 | 0.4 |
| Bravo 1996/97 | 17.4 | 18 | 1 | 40 | 2.3 | 0.8 |
| K11 1997/98 | 17.4 | 70 | 1 | 20 | 1.2 | 0.4 |
| K12 1997/98 | 17.4 | 30 | 1 | 20 | 1.8 | 0.6 |
| K15 1997/98 | 17.4 | 30 | 1 | 30 | 1.8 | 0.6 |
| K17 1997/98 | 17.4 | 30 | 1 | 30 | 1.8 | 0.6 |
| K20 1998/99 | 17.4 | 30 | 54.00 | 30 | 1.8 | 0.6 |
| K21 1998/99 | 17.4 | 30 | 54.00 | 30 | 1.8 | 0.6 |
| K23 1998/99 | 17.4 | 30 | 54.00 | 30 | 1.8 | 0.6 |

used averaging of 60 pings at 1.5 second intervals, thus compensating the trade off due to fewer pings per ensemble by increasing the bin length. This gives a nominal accuracy of 1.3 cm $s^{-1}$ for the horizontal and 0.4 cm $s^{-1}$ for the vertical velocities. Due to less battery capacity only 34 pings per ensemble were possible for the GSM5 instrument, giving a nominal accuracy comparable to the earlier deployments. The GSM5 instrument was not operating in the burst sampling mode, but used pings evenly distributed over the ensemble interval.

The ADCPs deployed in the Labrador Sea all used a bin length of 17.4 m. The ensemble intervals range from 20 to 40 minutes. In the winter of 1994/95, 35 pings were transmitted at 2 second intervals, giving an accuracy comparable to the early Greenland Sea measurements. During the following two Labrador Sea deployment periods the convection moorings had ADCPs averaging 60 (K1, K2) and 70 (K11) pings per ensemble at 1 second intervals. For the remaining instruments only 18 to 30 pings were used due to lower battery capacity. The last deployment period so far was the winter of 1998/99. Here three ADCPs were employed, all with an ensemble interval of 30 minutes in continuous sampling mode.

Measuring vertical velocity associated with convection events was one of the main tasks of the moored ADCPs. As the Labrador Sea moorings were subject to large horizontal and vertical excursions, the vertical velocity of the instrument itself through the water has to be considered (the effect of vertical excursions on the velocity measurements in the Greenland Sea can be neglected). Figure A.2 shows the rate of change of the instrument depths as determined from the surface distance measurements of the upward–looking ADCPs (Visbeck and Fischer, 1995) or, in the case of moorings K11 and K21, from pressure records of the sensors mounted on the uppermost float.

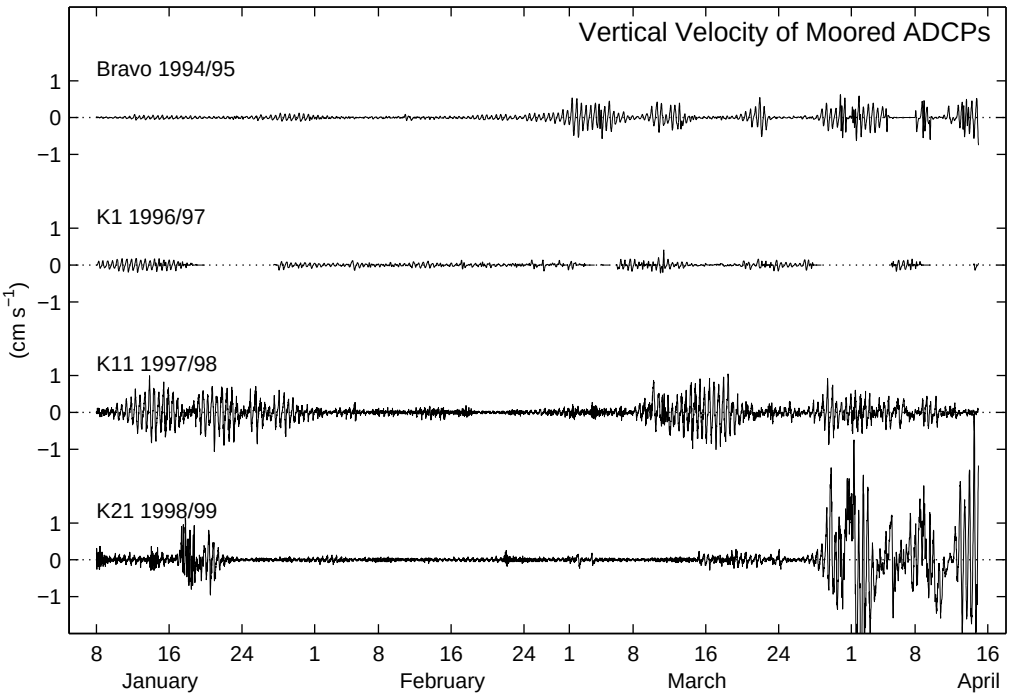


FIG. A.2: Vertical velocity through the water of ADCPs due to mooring excursions for the convection moorings in the Labrador Sea. The rate of change of the instrument depths was determined from the surface distance measurements of the upward–looking ADCPs or from pressure sensors mounted on the uppermost float (K11 and K21).

During most of the time the vertical velocity of the ADCPs through the water is vanishingly small, but some periods exist where velocities of more than 1 cm s$^{-1}$ occurred. The *Bravo* record from 1994/95 shows considerable vertical excursions between 1 and 14 March 1995 that coincide with convection activity, but the instrument velocity did not exceed 0.5 cm s$^{-1}$ while the downward motion in the observed plumes was of several centimeters per second. The ADCP record from the winter of 1996/97 shows very small instrument velocities, but for some periods the ADCP lost the contact to the sea surface making it impossible to determine the velocity. One of this periods was at the beginning of March where strong plume activity occurred. Fortunately these gaps were rather short compared to the larger ones at the end of January and at the beginning of April. As large

vertical excursions typically occur over several days and the instrument velocity is small before and after the gaps, it appears unlikely that major vertical excursions occurred.

A period of larger disturbance of the vertical velocity measurements was around 16 March 1998 at mooring K11. This period coincided with convection activity at the mooring location, but although the velocity of the instrument was of up to 1 cm $s^{-1}$ this is still rather small compared to the measured vertical velocities of 4 – 5 cm $s^{-1}$. During the winter of 1998/99 no considerable instrument excursion occurred during the convection period.

*Acknowledgements*

This work was guided by Prof. Friedrich Schott, who provided valuable advice and encouragement, which is gratefully appreciated.

Thanks are also due to my colleagues from the Department of Regional Oceanography at the Institut für Meereskunde in Kiel. Discussions with Uwe Send and Monika Rhein were very useful. I am especially grateful to Jürgen Fischer for countless discussions on convection and ocean circulation and never–ending interest in my work.

J. Lazier (Bedford Institute of Oceanography, Halifax) and P. Rhines (University of Washington, Seattle) shared their moored station data. R. Pickart (Woods Hole Oceanographic Institution), J. Meincke (Institut für Meereskunde, Hamburg), and D. Quadfasel (Niels Bohr Institute for Astronomy, Physics and Geophysics, Copenhagen) allowed the use of their hydrographic data. K. Bumke (Institut für Meereskunde, Kiel) provided meteorological data from the R/V *Knorr* cruise 147 and REMO heat flux data. L. Toudal (Technical University of Denmark, Lyngby) kindly provided Greenland Sea sea ice analysis data. Labrador Sea ice concentration data were obtained from the NCEP Ocean Modelling Branch (http://polar.wwb.noaa.gov/seaice/). NCEP/NCAR reanalysis data have been provided through the NOAA–CIRES Climate Diagnostics Center, Boulder, Colorado (http://www.cdc.noaa.gov/).

I am indepted to Maren Walter for critical reading and helpful comments on draft versions, and for thorough proofreading of the final manuscript.

This work was supported by the *Deutsche Forschungsgemeinschaft* through Sonderforschungsbereich 460 *Dynamik Thermohaliner Zirkulationsschwankungen* at the University of Kiel.

# BIBLIOGRAPHY


Aagaard, K., Swift, J. H., and Carmack, E. C. (1985). Thermohaline circulation in the Arctic Mediterranean Seas. *J. Geophys. Res.*, 90(C3):4833–4846.

Barnston, A. G. and Livezey, R. E. (1987). Classification, seasonality and persistence of low–frequency atmospheric circulation patterns. *Mon. Wea. Rev.*, 115(6):1083–1126.

Böning, C. W., Bryan, F. O., Holland, W. R., and Döscher, R. (1996). Deep–water formation and meridional overturning in a high–resolution model of the North Atlantic. *J. Phys. Oceanogr.*, 26:1142–1164.

Boubnov, B. M. and Golitsyn, G. S. (1990). Temperature and velocity field regimes of convective motion in a rotating plane fluid layer. *J. Fluid Mech.*, 219:215–239.

Budéus, G., Maul, A.-A., and Krause, G. (1993). Variability in the Greenland Sea as revealed by a repeated high spatial resolution conductivity–temperature–depth survey. *J. Geophys. Res.*, 98(C6):9985–10000.

Budéus, G., Schneider, W., and Krause, G. (1998). Winter convective events and bottom water warming in the Greenland Sea. *J. Geophys. Res.*, 103(C9):18513–18527.

Bullister, J. L. and Weiss, R. F. (1983). Anthropogenic chlorofluoromethanes in the Greenland and Norwegian Seas. *Science*, 221:265–268.

Carmack, E. and Aagaard, K. (1973). On the deep water of the Greenland Sea. *Deep–Sea Res.*, 20:687–715.

Cayan, D. R. (1992). Latent and sensible heat flux anomalies over the northern oceans: Driving the sea surface temperature. *J. Phys. Oceanogr.*, 22:859–881.

Clarke, R. A. and Gascard, J.-C. (1983). The formation of Labrador Sea Water. Part I: Large-scale processes. *J. Phys. Oceanogr.*, 13:1764–1778.

Clarke, R. A., Swift, J. H., Reid, J. L., and Koltermann, K. P. (1990). The formation of Greenland Sea Deep Water: Double diffusion or deep convection? *Deep–Sea Res.*, 37(9):1385–1424.

Coates, M. J. and Ivey, G. N. (1997). On convective turbulence and the influence of rotation. *Dyn. Atmos. Oceans*, 25:217–232.

Coates, M. J., Ivey, G. N., and Taylor, J. R. (1995). Unsteady, turbulent convection into a rotating, linearly stratified fluid: Modeling deep ocean convection. *J. Phys. Oceanogr.*, 25:3032–3050.

Curry, R. G., McCartney, M. S., and Joyce, T. M. (1998). Oceanic transport of subpolar climate signals to mid–depth subtropical waters. *Nature*, 391:575–577.

DeCosmo, J., Katsaros, K. B., Smith, S. D., Anderson, R. J., Oost, W. A., Bumke, K., and Chadwick, H. (1996). Air–sea exchange of water vapor and sensible heat: The humidity exchange over the sea (HEXOS) results. *J. Geophys. Res.*, 101:12001–12016.

Delworth, T., Manabe, S., and Stouffer, R. J. (1993). Interdecadal variations of the thermohaline circulation in a coupled ocean–atmosphere model. *J. Climate*, 6:1993–2011.

Dickson, R. R., Lazier, J. R. N., Meincke, J., Rhines, P., and Swift, J. (1996). Long-term coordinated changes in the convective activity of the North Atlantik. *Prog. Oceanogr.*, 38:241–295.

Dickson, R. R., Meincke, J., Malmberg, S.-A., and Lee, A. J. (1988). The "Great Salinity Anomaly" in the northern north Atlantic 1968–1982. *Prog. Oceanogr.*, 20:103–151.

Doherty, K. W., Frye, D. E., Liberatore, S. P., and Toole, J. M. (1999). A moored profiling instrument. *J. Atmos. Oceanic Technol.*, 16(11):1816–1829.

Döscher, R. and Redler, R. (1997). The relative importance of the northern overflow and subpolar deep convection for the North Atlantic thermohaline circulation. *J. Phys. Oceanogr.*, 27:1894–1902.

Fernando, H. J. S., Chen, R.-R., and Boyer, D. L. (1991). Effects of rotation on convective turbulence. *J. Fluid Mech.*, 228:513–547.

Fine, R. A. and Molinari, R. L. (1988). A continuous deep western boundary current between Abaco (26.5°N) and Barbados (13°N). *Deep–Sea Res.*, 35(9):1441–1450.

Fischer, J. and Schott, F. (2000). Labrador Sea Water tracked by profiling floats – from the boundary current into the open North Atlantic. *J. Phys. Oceanogr.* (submitted).

Fischer, J. and Visbeck, M. (1993). Seasonal variation of the daily zooplankton migration in the Greenland Sea. *Deep–Sea Res.*, 40:764–774.

Fleury, M. and Lueck, R. G. (1994). Direct heat flux estimates using a towed vehicle. *J. Phys. Oceanogr.*, 24:801–818.

Gargett, A. E. and Moum, J. N. (1995). Mixing efficiencies in turbulent tidal fronts: Results from direct and indirect measurements of density flux. *J. Phys. Oceanogr.*, 25:2583–2608.

Garrett, C. and Petrie, B. (1981). Dynamical aspects of the flow through the strait of Belle Isle. *J. Phys. Oceanogr.*, 11:376–393.

Gascard, J.-C. (1978). Mediterranean deep water formation, baroclinic instability and oceanic eddies. *Oceanol. Acta*, 1:315–330.

Gascard, J.-C. and Clarke, R. A. (1983). The formation of Labrador Sea Water. Part II: Mesoscale and smaller-scale processes. *J. Phys. Oceanogr.*, 13:1779–1797.

GSP Group (1990). Greenland Sea project: A venture toward improved understanding of the oceans' role in climate. *Eos Trans. AGU*, 71(24):750–755.

Häkkinen, S. (1987). Upwelling at the ice edge: A mechanism for deep water formation? *J. Geophys. Res.*, 92(C5):5031–5034.

Hunt, J. C. R. (1984). Turbulence structure in thermal convection and shear–free boundary layers. *J. Fluid Mech.*, 138:161–184.

Hurrell, J. W. (1995). Decadal trends in the North Atlantic Oscillation: Regional temperature and precipitation. *Science*, 269:676–679.

Hurrell, J. W. and van Loon, H. (1997). Decadal variations in climate associated with the North Atlantic Oscillation. *Climatic Change*, 36:301–326.

Isemer, H.-J. and Hasse, L. (1987). *The Bunker Climate Atlas of the North Atlantic Ocean. Vol. 2: Air–Sea Interactions.* Springer–Verlag, Berlin Heidelberg.

Jones, H. and Marshall, J. (1993). Convection with rotation in a neutral ocean, a study of open ocean deep convection. *J. Phys. Oceanogr.*, 23:1009–1039.

Jones, P. D., Jónsson, T., and Wheeler, D. (1997). Extension to the North Atlantic Oscillation using early instrumental pressure observations from Gibraltar and south–west Island. *Int. J. Climatol.*, 17:1433–1450.

Julien, K., Legg, S., McWilliams, J., and Werne, J. (1996). Rapidly rotating turbulent Rayleigh–Bénard convection. *J. Fluid Mech.*, 322:243–273.

Kalnay, E., Kanamitsu, M., Kistler, R., Collins, W., Deaven, D., Gandin, L., Iredell, M., Saha, S., White, G., Woollen, J., Zhu, Y., Chelliah, M., Ebisuzaki, W., Higgins, W., Janowiak, J., Mo, K. C., Ropelewski, C., Wang, J., Leetmaa, A., Reynolds, R., Jenne, R., and Joseph, D. (1996). The NCEP/NCAR 40–year reanalysis project. *Bull. Amer. Meteor. Soc*, 77(3):437–471.

Klinger, B. A., Marshall, J., and Send, U. (1996). Representation of convective plumes by vertical adjustment. *J. Geophys. Res.*, 101(C8):18175–18182.

Large, W. G. and Pond, S. (1982). Sensible and latent heat flux measurements over the ocean. *J. Phys. Oceanogr.*, 11:324–336.

Lazier, J. R. N. (1980). Oceanographic conditions at Ocean Weather Ship BRAVO, 1964–1974. *Atmos.–Ocean*, 18:227–238.

Lazier, J. R. N. (1995). The salinity decrease in the Labrador Sea over the past thirty years. In Martinson, D. G., Bryan, K., Ghil, M., Hall, M. M., Karl, T. M., Sarachik, E. S., Sorooshian, S., and Talley, L. D., editors, *Natural Climate Variability on Decade–to–Century Time Scales*, pages 295–302. National Academy Press, Washington, D. C.

Leaman, K. D. and Schott, F. (1991). Hydrographic structure of the convection regime in the Gulf of Lions: Winter 1987. *J. Phys. Oceanogr.*, 21:573–596.

Legg, S., McWilliams, J., and Gao, J. (1998). Localization of deep ocean convection by a mesoscale eddy. *J. Phys. Oceanogr.*, 28:944–970.

Lherminier, P., Gascard, J.-C., and Quadfasel, D. (1999). The Greenland Sea in winter 1993 and 1994: Preconditioning for deep convection. *Deep–Sea Res. II*, 46:1199–1235.

Lilly, J. M., Rhines, P. B., Visbeck, M., Davis, R., Lazier, J. R. N., Schott, F., and Farmer, D. (1999). Observing deep convection in the Labrador Sea during winter 1994–1995. *J. Phys. Oceanogr.*, 29:2065–2098.

Marotzke, J. and Scott, J. R. (1999). Convective mixing and the thermohaline circulation. *J. Phys. Oceanogr.*, 29:2962–2970.

Marshall, J. and Schott, F. (1999). Open–ocean convection: Oberservations, theory, and models. *Rev. Geophys.*, 37(1):1–64.

Marshall, J., Whitehead, J. A., and Yates, T. (1994). Laboratory and numerical experiments in oceanic convection. In Malanotte-Rizzoli, P. and Robinson, A. R., editors, *Ocean Processes in Climate Dynamics: Global and Mediterranean Examples*, pages 173–201. Kluwer Academic Publishers, Netherlands.

Maxworthy, T. and Narimousa, S. (1994). Vortex generation by convection in a rotating fluid. *J. Phys. Oceanogr.*, 24:865–887.

McDougall, T. J. (1983). Greenland Sea bottom water formation: A balance between advection and double–diffusion. *Deep–Sea Res.*, 30(11A):1109–1117.

MEDOC Group (1970). Observations of formation of deep water in the Mediterranean Sea, 1969. *Nature*, 227:1037–1040.

Meincke, J., Jónsson, S., and Swift, J. H. (1992). Variability of convective conditions in the Greenland Sea. *ICES mar. Sci. Symp.*, 195:32–39.

Morawitz, W. M. L., Sutton, P. J., Worcester, P. F., Cornuelle, B. D., Lynch, J. F., and Pawlowicz, R. (1996). Three–dimensional observations of a deep convective chimney in the Greenland Sea during the winter 1988/89. *J. Phys. Oceanogr.*, 26:2316–2343.

Morison, J. H. and McPhee, M. G. (1998). Lead convection measured with an autonomous underwater vehicle. *J. Geophys. Res.*, 103(C2):3257–3281.

Moum, J. N. (1990). The quest for $K_\rho$–preliminary results from direct measurements of turbulent fluxes in the ocean. *J. Phys. Oceanogr.*, 20:1980–1984.

Munk, W. and Wunsch, C. (1998). Abyssal recipes II: Energetics of tidal and wind mixing. *Deep–Sea Res. I*, 45:1977–2010.

Niiler, P. P. and Kraus, E. B. (1977). One-dimensional models of the upper ocean. In Kraus, E. B., editor, *Modeling and Prediction of the Upper Layers of the Ocean*, pages 143–172. Pergamon Press, Oxford.

Osborn, T. R. (1980). Estimates of the local rate of vertical diffusion from dissipation measurements. *J. Phys. Oceanogr.*, 10:83–89.

Osborn, T. R. and Cox, C. S. (1972). Oceanic fine structure. *Geophys. Fluid Dyn.*, 3:321–345.

Pawlowicz, R. (1995). A note on seasonal cycles of temperature and salinity in the upper waters of the Greenland Sea gyre from historical data. *J. Geophys. Res.*, 100(C3):4715–4726.

Pawlowicz, R., Lynch, J. F., Owens, W. B., Worcester, P. F., Morawitz, W. M. L., and Sutton, P. J. (1995). Thermal evolution of the Greenland Sea gyre in 1988-1989. *J. Geophys. Res.*, 100(C3):4727–4750.

Peterson, W. H. and Rooth, C. G. H. (1976). Formation and exchange of deep water in the Greenland and Norwegian seas. *Deep–Sea Res.*, 23:273–283.

Pickart, R. S. (1992). Water mass components of the North Atlantic deep western boundary current. *Deep–Sea Res.*, 39(9):1553–1572.

Pickart, R. S., Smethie, Jr., W. M., Lazier, J. R. N., Jones, E. P., and Jenkins, W. J. (1996). Eddies of newly formed upper Labrador Sea water. *J. Geophys. Res.*, 101(C9):20711–20726.

Pickart, R. S., Spall, M. A., and Lazier, J. R. N. (1997). Mid–depth ventilation in the western boundary current system of the sub–polar gyre. *Deep–Sea Res. I*, 44(6):1025–1054.

Raasch, S. and Etling, D. (1991). Numerical simulation of rotating turbulent thermal convection. *Contrib. Atmos. Phys.*, 64(3):185–199.

RD Instruments (1989). *Acoustic Doppler Current Profilers; Principles of Operation: A Practical Primer*. San Diego, California.

Renfew, I. A., Moore, G. W. K., Guest, P. S., and Bumke, K. (1999). A comparison of surface–layer, surface heat flux and surface momentum flux observations over the Labrador Sea with ECMWF analysis and ncep reanalysis. *J. Climate*. (submitted).

Roach, A. T., Aagaard, K., and Carsey, F. (1993). Coupled ice–ocean variability in the Greenland Sea. *Atmosphere–Oceans*, 31(3):319–337.

Rogers, J. C. (1984). The association between the North Atlantic Oscillation and the Southern Oscillation in the Northern Hemisphere. *Mon. Wea. Rev.*, 112(10):1999–2015.

Rudels, B. (1990). Haline convection in the Greenland Sea. *Deep–Sea Res.*, 37(9):1491–1511.

Rudels, B., Quadfasel, D., Friedrich, H., and Houssais, M.-N. (1989). Greenland Sea convection in the winter of 1987–1988. *J. Geophys. Res.*, 94(C3):3223–3227.

Schlosser, P., Bönisch, G., Rhein, M., and Bayer, R. (1991). Reduction of deepwater formation in the Greenland Sea during the 1980s: Evidence from tracer data. *Science*, 251:1054–1056.

Schott, F. and Leaman, K. D. (1991). Observations with moored acoustic Doppler current profilers in the convection regime in the Golfe du Lion. *J. Phys. Oceanogr.*, 21:558–574.

Schott, F., Visbeck, M., and Fischer, J. (1993). Observations of vertical currents and convection in the central Greenland Sea during the winter of 1988–89. *J. Geophys. Res.*, 98(C8):14401–14421.

Schott, F., Visbeck, M., Send, U., Fischer, J., Stramma, L., and Desaubies, Y. (1996). Observations of deep convection in the Gulf of Lions, Northern Mediterranean, during the winter of 1991/92. *J. Phys. Oceanogr.*, 26:505–524.

Send, U. and Käse, R. H. (1998). Parameterization of processes in deep convection regimes. In Chassignet, E. P. and Verron, J., editors, *Ocean Modeling and Parameterizations*, pages 191–214. Kluwer Academic Publishers, Netherlands.

Send, U. and Marshall, J. (1995). Integral effects of deep convection. *J. Phys. Oceanogr.*, 25:855–872.

Shuchman, R. A., Josberger, E. G., Russel, C. A., Fischer, K. W., Johannessen, O. M., Johannessen, J., and Gloersen, P. (1998). Greenland Sea Odden sea ice feature: Intra–annual and interannual variability. *J. Geophys. Res.*, 103(C6):12709–12724.

Smethie, Jr., W. M., Ostlund, H. G., and Loosli, H. H. (1986). Ventilation of the deep Greenland and Norwegian Seas: Evidence from krypton-85, tritium, carbon-14 and argon-39. *Deep–Sea Res.*, 33(5):675–703.

Smith, S. D. (1988). Coefficients for sea surface wind stress, heat flux, and wind profiles as a function of wind speed and temperature. *J. Geophys. Res.*, 93(C12):15467–15472.

Smith, S. D. (1989). Water vapor flux at the sea surface. *Boundary Layer Meteorol.*, 47:277–293.

Sun, H., Kunze, E., and Williams III, A. J. (1996). Vertical heat–flux measurements from a neutrally buoyant float. *J. Phys. Oceanogr.*, 26:984–1001.

Swallow, J. C. and Caston, G. F. (1973). The preconditioning phase of MEDOC 1969. part I: Observations. *Deep–Sea Res.*, 20:429–448.

The Lab Sea Group (1998). The Labrador Sea deep convection experiment. *Bull. Amer. Meteor. Soc.*, 79(10):2033–2058.

Tichelaar, B. W. and Ruff, L. J. (1989). How good are our best models? jackknifing, bootstrapping, and earthquake depth. *Eos Trans. AGU*, 70(20):593, 605–606.

Timmermann, A., Latif, M., Voss, R., and Grötzner, A. (1998). Nothern hemispheric interdecadal variability: A coupled air–sea mode. *J. Climate*, 11:1906–1931.

Toudal, L. (1999). Ice extent in the Greenland Sea 1978–1995. *Deep–Sea Res. II*, 46:1237–1254.

Toudal, L., Hansen, K. Q., Valeur, H., Wadhams, P., Aldworth, E., and Comiso, J. C. (1999). Mapping of ice in the Odden by satellite and airborne remote sensing. *Deep–Sea Res. II*, 46:1255–1274.

van Loon, H. and Rogers, J. C. (1978). The seesaw in winter temperatures between Greenland and northern Europe. Part I: General description. *Mon. Wea. Rev.*, 106:296–310.

Visbeck, M. (1993). *Konvektion im offenen Ozean.* PhD thesis, Institut für Meereskunde, Kiel, 187 pp.

Visbeck, M. and Fischer, J. (1995). Sea surface conditions remotely sensed by upward-looking ADCPs. *J. Atmos. Oceanic Technol.*, 12(1):141–149.

Visbeck, M., Fischer, J., and Schott, F. (1995). Preconditioning the Greenland Sea for deep convection: Ice formation and ice drift. *J. Geophys. Res.*, 100(C9):18489–18502.

Voorhis, A. and Webb, D. C. (1970). Large vertical currents observed in a winter sinking region of the northwestern Mediterranean. *Cah. Oceanogr.*, 22(6):571–580.

Wadhams, P. (1986). The ice cover. In Hurdle, B. G., editor, *The Nordic Seas*, pages 21–84. Springer–Verlag, New York.

Wadhams, P., Comiso, J. C., Prussen, E., Wells, S., Brandon, M., Aldworth, E., Viehoff, T., Allegrino, R., and Crane, D. R. (1996). The development of the Odden ice tongue in the Greenland Sea during the winter 1993 from remote sensing and field observations. *J. Geophys. Res.*, 101(C8):18213–18235.

Wallace, J. M. and Gutzler, D. S. (1981). Teleconnections in the geopotential height field during the northern hemisphere winter. *Mon. Wea. Rev.*, 109(4):784–812.

Wang, J., Mysak, L. A., and Ingram, R. G. (1994). Interannual variability of sea–ice cover in Hudson Bay, Baffin Bay and the Labrador Sea. *Atmos.–Ocean*, 32(2):421–447.

Wood, R. A., Keen, A. B., Mitchell, J. F. B., and Gregory, J. M. (1999). Changing spatial structure of the thermohaline circulation in response to atmospheric $CO_2$ forcing in a climate model. *Nature*, 399:572–575.

Worcester, P., Lynch, J. F., Morawitz, W. M. L., Pawlowicz, R., Sutton, P. J., Cornuelle, B. D., Johannessen, O. M., Munk, W. H., Owens, W. B., Shuchman, R., and Spindel, R. C. (1993). Evolution of the large–scale temperature field in the Greenland Sea during 1988–89 from tomographic measurements. *Geophys. Res. Lett.*, 20(20):2211–2214.

Yamazaki, H. and Osborn, T. (1993). Direct estimation of heat flux in a seasonal thermocline. *J. Phys. Oceanogr.*, 23:503–515.